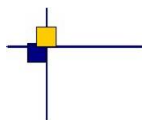


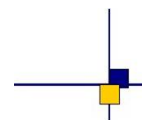


CalVal Jason-3



Jason-3 validation and cross calibration activities (Annual report 2019)

Contract No 160182-14026/00 Lot 1.6.3



Nomenclature : SALP-RP-MA-EA-23399-CLS

Issue : 1.1

Date : March 23, 2020

Chronology Issues:

Issue:	Date:	Reason for change:
1.0	2019-12-20	Creation
1.1	2020-03-23	taking into account CNES review

People involved in this issue :

	AUTHORS	COMPANY	DATE	INITIALS
Written by:	H. Roinard L. Michaud	CLS		
Checked by:		CLS		
Approved by:		CLS CLS		
Application authorised by:				

Index Sheet :

Context:	
Keywords:	
Hyperlink:	

Distribution:

Company	Means of distribution	Names
CLS/DOS	electronic copy	V.ROSMORDUC
CNES	electronic copy	thierry.guinle@cnes.fr nicolas.picot@cnes.fr francois.bignalet-cazalet@cnes.fr gerald.dibarboue@cnes.fr aqgp_rs@cnes.fr dominique.chermain@cnes.fr delphine.vergnoux@cnes.fr

List of tables and figures

List of Tables

1	<i>Events on Jason-3 mission</i>	12
2	<i>Acquisition mode</i>	13
3	<i>List of GDR version "D" standard</i>	17
4	<i>List of missing Jason-3 passes</i>	25
5	<i>Editing criteria over cycles 1 to 132</i>	30
6	<i>Seasonal variations of Jason SLA (cm) for years 2016 to 2018</i>	66
7	<i>Seasonal variations of Jason SLA standard deviation (cm) for years 2016 to 2018</i>	68

List of Figures

1	<i>Acquisition mode for cycle 060 (identical to acquisition mode automatic switch for cycles 6, 9, 11-19, 21-56,58-140). 8 = autonomous acquisition / tracking, 9 = autonomous DIODE acquisition / tracking, 10 = DIODE + Digital Elevation Model tracking</i>	14
2	<i>Global GDRs data availability per cycle</i>	18
3	<i>Map of percentage of available measurements over land for Jason-3 (left) and for Jason-2 (right). Top: Jason-3 cycle 039 in DEM mode and Jason-2 cycle 320 in median mode. Bottom: Jason-3 cycle 031 in DEM mode and Jason-2 cycle 311 in DEM mode</i>	19
4	<i>Jason-2 and Jason-3 GDR data availability over ocean (per cycle)</i>	26
5	<i>Jason-3 data editing average by cycle.</i>	27
6	<i>Cycle per cycle monitoring of the percentage of edited measurements by ice flag criterion.</i>	28
7	<i>Top: Percentage of edited measurements by altimeter rain flag criterion. Bottom left: Map of global edited measurements without considering the rain flag. Bottom right: Map of global edited measurements using all criteria and considering the rain flag. All figures are computed over ocean and from cycle 96 to 132.</i>	29
8	<i>Jason-3 data editing by thresholds average by cycle.</i>	31
9	<i>Percentage of edited measurements by 20Hz range measurements threshold criterion (top) and by 20Hz range measurements standard deviation threshold criteria (bottom). Cycle per cycle monitoring compared with Jason-2 (left) and Jason-3 averaged map from cycle 96 to 132 (right).</i>	32
10	<i>Percentage of edited measurements by SWH threshold criterion. Left: Cycle per cycle monitoring compared with Jason-2 (Jason-2 DEM cycle in cyan. Jason-3 median tracker cycles in purple.) Right: Jason-3 averaged map from cycle 96 to 132.</i>	33
11	<i>Percentage of edited measurements by backscatter coefficient threshold criterion (top) and by 20Hz backscatter coefficient standard deviation threshold criteria (bottom). Cycle per cycle monitoring compared with Jason-2 (left, Jason-2 DEM cycle in cyan. Jason-3 median tracker cycles in purple) and Jason-3 averaged map from cycle 96 to 132 (right).</i>	34
12	<i>Percentage of edited measurements by radiometer wet troposphere correction threshold criterion. Left: Cycle per cycle monitoring compared with Jason-2. Right: Jason-3 averaged map from cycle 96 to 132.</i>	35
13	<i>Percentage of edited measurements by ionospheric correction threshold criterion. Left: Cycle per cycle monitoring compared with Jason-2. Right: Jason-3 averaged map from cycle 96 to 132.</i>	35
14	<i>Percentage of edited measurements by wind speed threshold criterion. Left: Cycle per cycle monitoring compared with Jason-2. Right: Jason-3 averaged map from cycle 96 to 132.</i>	36
15	<i>Percentage of edited measurements by sea state bias threshold criterion. Left: Cycle per cycle monitoring compared with Jason-2. Right: Jason-3 averaged map from cycle 96 to 132.</i>	37

16	Percentage of edited measurements by ocean tide threshold criterion. Cycle per cycle monitoring compared with Jason-2.	38
17	Percentage of edited measurements by square off nadir angle threshold criterion. Left: Cycle per cycle monitoring compared with Jason-2. Right: Jason-3 averaged map from cycle 96 to 132.	38
18	Percentage of edited measurements by sea surface height threshold criterion. Left: Cycle per cycle monitoring compared with Jason-2. Right: Jason-3 averaged map from cycle 96 to 132.	39
19	Percentage of edited measurements by sea level anomaly threshold criterion. Left: Cycle per cycle monitoring compared with Jason-2. Right: Jason-3 averaged map from cycle 96 to 132.	40
20	Top: Cyclic monitoring of number of elementary 20 Hz range measurements for Jason-2 and Jason-2 for Ku-band and C-band. Bottom: Jason-2 - Jason-3 difference daily monitoring of elementary 20 Hz range measurements number (until september 2017).	42
21	Map of number of 20 Hz range measurements for Jason-3 averaged over cycles 96 to 132, in Ku-band (left) and in C-band (right).	43
22	Top: Cyclic monitoring of elementary 20 Hz range measurements standard deviation for Jason-2 and Jason-3 for Ku-band and C-band. Bottom: Jason-2 - Jason-3 difference daily monitoring of elementary 20 Hz range measurements standard deviation.	44
23	Map of 20 Hz range measurements standard deviation for Jason-3 averaged over cycles 96 to 132, in Ku-band (left) and in C-band (right).	44
24	Left: Cyclic monitoring of the square off-nadir angle for Jason-2 and Jason-3 for GDRs (blue and red curves) and Jason-3 IGDRs (product IGDR for cycles 1 to 41, and IGDR L2P from cycle 25 to 132 in green). Right: Jason-2 - Jason-3 difference daily monitoring of the square off-nadir angle (GDR data).	45
25	Map of the square off-nadir angle for Jason-3 averaged over cycles 96 to 132.	46
26	Left: Mean per day of mispointing for Jason-3 from cycle 4. Right: Square off nadir angle against swl.	46
27	Top: Cyclic monitoring of backscatter coefficient for Jason-3 (Ku-band) OGDR/IGDR/GDR. Bottom: difference of atmospheric attenuation applied to sigma0 between IGDR and GDR products.	47
28	Top: Cyclic monitoring of backscatter coefficient for Jason-2 and Jason-3 for Ku-band (left) C-band (right). Bottom: daily monitoring of Jason-2 - Jason-3 GDR difference of the backscatter coefficient.	48
29	Map of backscatter coefficient for Jason-3 averaged over cycles 96 to 132, in Ku-band (left) and in C-band (right).	48
30	Cyclic monitoring of significant wave height for Jason-3 (Ku-band) OGDR/IGDR/GDR.	49
31	Cyclic monitoring of significant wave height for Jason-2 and Jason-3 for Ku-band (left) and for C-band (right). Jason-2 - Jason-3 difference daily monitoring of significant wave height (bottom).	49
32	Map of significant wave height for Jason-3 averaged over cycles 96 to 132, in Ku-band (left) and in C-band (right).	50
33	Cyclic monitoring of ionospheric correction for Jason-2 and Jason-3. (left). Cyclic monitoring of Jason-3 ionospheric correction for IGDR and GDR data (right). Jason-2 - Jason-3 difference daily monitoring of ionospheric correction (bottom).	51
34	Left: Map of ionospheric correction for Jason-3 averaged over cycles 96 to 132. Right: Map of dual-frequency minus GIM ionospheric correction solutions.	51
35	Cyclic monitoring of GIM ionosphere correction minus filtered altimeter ionosphere correction for Jason-2 and Jason-3. Left: mean, right: standard deviation.	52
36	Map of Jason-3 brightness temperatures averaged over cycles 96 to 132: 18.7 Ghz channel (top left), 23.8 Ghz channel (top right) and 34.0 Ghz channel (bottom left). Map of AMR wet troposphere correction for Jason-3 averaged over cycles 96 to 132 (bottom right)	53
37	Daily monitoring of AMR minus ECMWF model wet tropospheric correction. mean (left) and standard deviation (right)	54

38	<i>Cyclic monitoring of altimeter wind speed mean (left) and standard deviation (right). Top: for Jason-2 and Jason-3. Bottom: for Jason-3 GDR, IGDR and OGDR data.</i>	55
39	<i>Jason-2 - Jason-3 difference daily monitoring of altimeter wind speed mean (left) and standard deviation (right).</i>	55
40	<i>Cyclic monitoring of the sea state bias mean and standard deviation for Jason-2 and Jason-3</i>	56
41	<i>Jason-2 - Jason-3 difference daily monitoring of the sea state bias mean (left) and standard deviation (right).</i>	56
42	<i>Monitoring of mean of Jason-3 SSH crossover differences for OGDRs, IGDRs and GDRs. Only data with $latitude < 50^\circ$, bathymetry $< -1000m$ and low oceanic variability were selected. (ocean_tide_sol1 = GOT is used in SSH computation)</i>	59
43	<i>Map of SSH crossovers differences mean for Jason-3 cycle 0 to 132(left) and for Jason-2 cycle 281 to 506 (right)</i>	59
44	<i>Cyclic monitoring of Jason-2 - Jason-3 SSH crossover differences mean (left) and map over cycle 1 to 58 (right). Only data with $latitude < 50^\circ$, bathymetry $< -1000m$ and low oceanic variability were selected.</i>	60
45	<i>Cycle by cycle standard deviation of SSH crossover differences for Jason-2 and Jason-3 (left), and for Jason-3 using OGDRs, IGDRs and GDRs (right). Only data with $latitude < 50^\circ$, bathymetry $< -1000m$ and low oceanic variability were selected.</i>	61
46	<i>Monitoring (left) and periodogram (right) of pseudo time-tag bias estimated cycle by cycle from GDR products for Jason-2 and Jason-3</i>	61
47	<i>Daily monitoring of SSH bias between Jason-2 and Jason-3 before Jason-2 moved to interleaved ground-track in October 2016: SSH bias without applying geophysical corrections (black) and with corrections using radiometer wet troposphere correction (blue) or using ECMWF model wet troposphere correction (cyan).</i>	62
48	<i>GDR data. Caution: color map ranges are different between the two figures. Left: Map of SLA difference between Jason-2 and Jason-3 over tandem phase Right: Map of Jason-2 and Jason-3 SLA differences for Jason-3 cycles 025 to 058</i>	63
49	<i>Cyclic monitoring of along-track SLA standard deviation. Jason-3 OGDRs, IGDRs and GDRs (left). Jason-2 and Jason-3 GDRs (right)</i>	64
50	<i>Global (right) and regional (left) MSL trends from 1993 onwards.</i>	69
51	<i>Evolution of the GMSL differences between the altimeter mission Jason-3 and the GLOSS/CLIVAR tide gauges network. Annual and semi-annual signals have been removed beforehand from each individual timeseries, and a 2-months filter have been applied on the differences (thin blue line). The slope (blue dashed line) is obtained from a generalized least square method applied on the 2-months filtered timeseries. The thick blue line is the 6-months filtered timeseries.</i>	70
52	<i>Rejected measurement on IGDR data for Jason-3 cycle 112 before SHM event for altimeter criteria (left) and radiometer wet troposphere correction threshold criterion (right)</i>	72

List of items to be defined or to be confirmed

Applicable documents / reference documents

Contents

1. Introduction	2
2. Processing status	8
2.1. Data Used	8
2.2. List of events	8
2.3. Tracking and acquisition mode	12
2.4. Models and standards	15
2.5. Processing versions	17
3. Data coverage and edited measurements	18
3.1. Missing measurements	18
3.1.1. Over land and ocean	18
3.1.2. Over ocean	25
3.2. Edited measurements	26
3.2.1. Global editing	26
3.2.2. Flagging quality criterion: Ice flag	27
3.2.3. Flagging quality criterion: Rain flag	28
3.2.4. Editing on thresholds criteria	29
3.2.4.1. Threshold criteria: 20-Hz range measurements number and standard deviation	31
3.2.4.2. Threshold criteria: Significant wave height (swh)	32
3.2.4.3. Threshold criteria: Backscatter coefficient (sigma0)	33
3.2.4.4. Threshold criteria: Radiometer wet troposphere correction	34
3.2.4.5. Threshold criteria: Ionospheric correction	35
3.2.4.6. Threshold criteria: Altimeter wind speed	36
3.2.4.7. Threshold criteria: Sea State Bias	37
3.2.4.8. Threshold criteria: Ocean tide	38
3.2.4.9. Threshold criteria: Square off nadir angle	38
3.2.4.10. Threshold criteria: Sea surface height	39
3.2.4.11. Threshold criteria: Sea Level Anomaly	39
4. Monitoring of altimeter and radiometer parameters	41
4.1. Methodology	41
4.2. 20Hz range measurements	41
4.2.1. 20 Hz range measurements number in Ku-Band and C-Band	42
4.2.2. 20 Hz range measurements standard deviation in Ku-Band and C-Band	43
4.3. Off-Nadir Angle from waveforms	45
4.4. Backscatter coefficient	47
4.5. Significant wave height	49
4.6. Dual-frequency ionosphere correction	50
4.7. AMR Wet Troposphere Correction	53
4.7.1. Overview	53
4.7.2. Comparison with the ECMWF model	54
4.8. Altimeter wind speed	55
4.9. Sea state bias	56

.....	
5. SSH crossover analysis	58
5.1. Overview	58
5.2. Mean of SSH crossover differences	59
5.3. Standard deviation of SSH crossover differences	61
5.4. Estimation of pseudo time-tag bias	61
6. Sea Level Anomalies (SLA) Along-track analysis	62
6.1. Overview	62
6.2. Mean of SLA differences between Jason-3 and Jason-2	62
6.3. Standard deviation of SLA differences between Jason-3 and Jason-2	63
6.4. Sea level seasonal variations	65
7. Mean Sea Level (MSL) calculation	69
7.1. Mean sea level (MSL) calculation of reference time serie and regional MSL trends	69
7.2. External data comparisons with tide gauges	70
8. Particular points and investigations	71
8.1. Focus on 2019 Safe Hold Modes [SHM]	71
8.1.1. 2019 February SHM: cycles 112 and 113	71
8.1.2. 2019 April SHM: cycle 116	73
8.2. Poster on Jason-3 mission performance towards GDR-F at OSTST	74
8.3. Poster on Improving Conventional Altimetry Innovative LRM retracking at OSTST	76
9. References	78

Glossary

AMR Advanced Microwave Radiometer

CLS Collecte Localisation Satellites

CNES Centre National d'Etudes Spatiales

CNG Consigne Numerique de Gain (= Automatic Gain Control)

DEM Digital Elevation Model

DIODE Détermination Immédiate d'Orbite par Doris Embarqué

ECMWF European Centre for Medium-range Weather Forecasting

GDR Geophysical Data Record

GIM Global Ionosphere Maps

GOT Global Ocean Tide

IGDR Interim Geophysical Data Record

JPL Jet Propulsion Laboratory (Nasa)

MLE Maximum Likelihood Estimator

MOE Medium Orbit Ephemeris

MQE Mean Quadratic Error

MSS Mean Sea Surface

PLTM PayLoad TeleMetry

POE Precise Orbit Ephemeris

OGDR Operational Geophysical Data Record

SALP Service d'Altimétrie et de Localisation Précise

SSH Sea Surface Height

SLA Sea Level Anomaly

SLR Satellite Laser Ranging

SSB Sea State Bias

SWH Significant Wave Height

TM TeleMetry

1. Introduction

This document presents the synthesis report concerning validation activities of Jason-3 data (Geophysical Data Records (GDRs), as well as Interim and Operational Data Records (O/IGDR)) under SALP contract (N° 160182/Lot 1.6.3) supported by CNES at the CLS Space Oceanography Division.

History

Jason-3 satellite was successfully launched on the 17th of January 2016. Since February 12th, Jason-3 is on its operational orbit to continue the long term climate data record on the primary TOPEX, Jason-1, and OSTM/Jason-2 ground track. Until October 2nd, 2016, Jason-3 and Jason-2 were in tandem flight, with only 80 seconds delay, before Jason-2 was moved to the same interleaved orbit that was used by TOPEX from 2002-2005 and Jason-1 from 2009-2012. Jason-2 was on its repetitive interleaved position until May 17th 2017, then was moved on a first Long Repeat Orbit from July 11th 2017 to July 18th 2017, and finally was on a second interleaved long repeat orbit from July 25th 2018 to the end of the mission on October 1st 2019. After tandem phase with Jason-2, Jason-3 has become the reference mission in DUACS system from mid-september 2016 onwards. On February 24th 2019 at 09:57:16, Jason-3 entered in Safe Hold Mode (SHM). This first SHM ended 10 days after on March 6th 2019 at 08:44:21. On April 6th 2019 at 23:17:22, second SHM occurred. This SHM lasted around 7 days and ended on April 12th 2019 at 02:20:01. (see details in part 8.1.).

CalVal activities

Since the beginning of the mission, Jason-3 data have been analyzed and monitored in order to assess the quality of Jason-3 products. Cycle per cycle reports summarizing mission performance are generated and made available through the AVISO web page ¹. This encompasses several points, which are either part of Cal/Val routine activities or following mission events:

- mono-mission validation and monitoring,
- Jason-3/Jason-2 cross-calibration,
- accuracy and stability of SLA measurements check,
- specific studies and investigations.

Overview

The present document assesses Jason-3 data quality and mission performance. After an executive summary, dedicated sections of this report deal with:

- description of data processing,
- data coverage / availability,
- monitoring of rejected spurious data,
- analysis of relevant parameters derived from instrumental measurements and geophysical corrections.
- system performance via analyses at crossover points,
- system performance via along-track Sea Level Anomalies monitoring,
- long-term monitoring and contribution to climat surveys.

¹<http://www.aviso.altimetry.fr/en/data/calval/systematic-calval/validation-reports.html>

Over all these parts , the document also focuses on Jason-3/Jason-2 cross-calibration:

- During the tandem flight (February, 12th to October 2nd 2016) both satellites were on the same ground track, which is a unique opportunity to precisely assess parameter discrepancies between both missions and detect geographically correlated biases, jumps or drifts.
- But even after Jason-2 move to interleaved orbit (formation flight phase, after the end of the tandem phase and until move to LRO),
- and also during Jason-2 flight on LRO, comparisons were still possible while Jason-2 data are available.

The difference at crossovers, SLA performances and consistency with Jason-2 are described. *Please note that in this document, only Jason-2 cycles 281 to 506 - corresponding to February 2016 to mid September 2017 - are used to compute Jason-2 GDR statistics.*

By succeeding to TOPEX/Poseidon, Jason-1 and Jason-2 on their primary ground track, Jason-3 has extended the high-precision ocean altimetry data record [1]. It was launched on January 17th 2016. During the tandem phase with Jason-2 (February 12th to October 2nd 2016), both satellites were on the same ground-track (with only 80 seconds delay), which is a unique opportunity to precisely assess parameter discrepancies between both missions and detect geographically correlated biases, jumps or drifts. OGDR and IGDR products have been publicly available since June 30th 2016. OGDRs were generated in version “T” until cycle 18/pass 137, and then turned into “D” version. Concerning IGDRs, they turned from “T” to “D” version at cycle 14/pass 143 on June 27th. GDR products have been available in version “T” since early October 2016 (more details on products versions on Jason-3 handbook [2]). During each cycle, missing measurements were monitored, spurious data were edited and relevant parameters derived from instrumental measurements and geophysical corrections were analysed for OGDR, IGDR and GDR.

Jason-3 can use two on-board tracking modes: Diode/DEM (open loop) and median tracker (more details in complete annual report). In addition, a tracking automatic transition is possible, which means that when authorized: acquisition mode switches automatically from autonomous DIODE acquisition mode over land to Diode/DEM over ocean and referenced inland water. During 2017, an update of DEM (Digital Elevation Model) was uploaded on August (cycle 057). It aims at adding new hydrologic targets such as rivers and lakes: 110 lakes and more than 2700 virtual stations over lakes and rivers have been added (from 1644 virtual stations up to 4366). **Please note the change in orbit standard solution available in the products:**

- until Jason-3 cycle 094, POE-E (MOE-E) orbit standard is available in GDR (IGDR) products
- from Jason-3 cycle 095 onwards, orbit standard “F” is used for both POE and MOE.
- from Jason-3 cycle 113 onwards, MOE orbit standard uses both DORIS and GPS data.

Data availability

Data availability is excellent for Jason-3. Jason-3 presents 100% of data availability over ocean after removing specific events (99.98% for Jason-2, see figure 1). Such events occurred by only four times over Jason-3 full period:

- during cycle 3, where 21.02% of measurements are missing due to the GPS platform upload,
- during cycle 57, where 1.76% of measurements are missing due to the DEM-onboard upload.
- during cycle 112/113, where 79.89% (for cycle 112) and 24.21% (for cycle 113) of measurements are missing due to SHM from 24/02/2019 09:57:16 until 06/03/2019 08:44:21.
- during cycle 116, where 53.19% of measurements are missing due to SHM from 06/04/2019 23:17:22 until 12/04/2019 02:20:01.

¹<https://www.avisio.altimetry.fr/?id=601&L=0>

²https://www.avisio.altimetry.fr/fileadmin/documents/data/tools/hdbk_j3.pdf

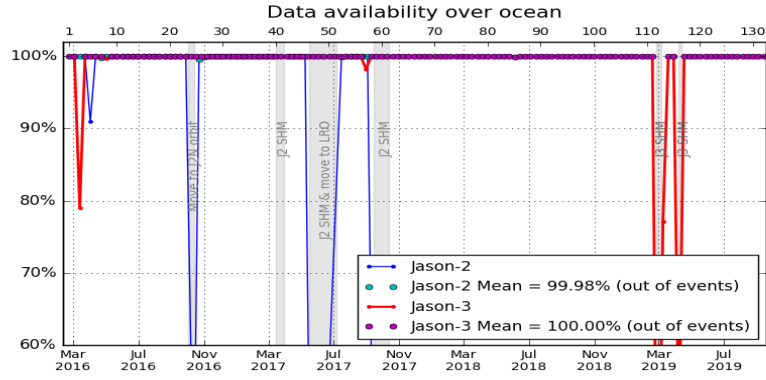


Figure 1 – Jason-2 and Jason-3 GDR data availability over ocean (per cycle)

Sea Level Anomalies

Over the tandem phase, mean SLA differences between Jason-2 and Jason-3 data is stable in time with variations close to 1 mm rms (left of figure 2) and shows no drift. It presents only a weak hemispheric bias as both satellites measure the same oceanic features only 1'20" apart (figure 2) that corresponds to orbital signatures observed on sea surface height. The global average SSH bias is close to 2.98 cm using SSH corrections (2.84 cm when using ECMWF instead of radiometer wet troposphere correction) and 2.23 cm without.

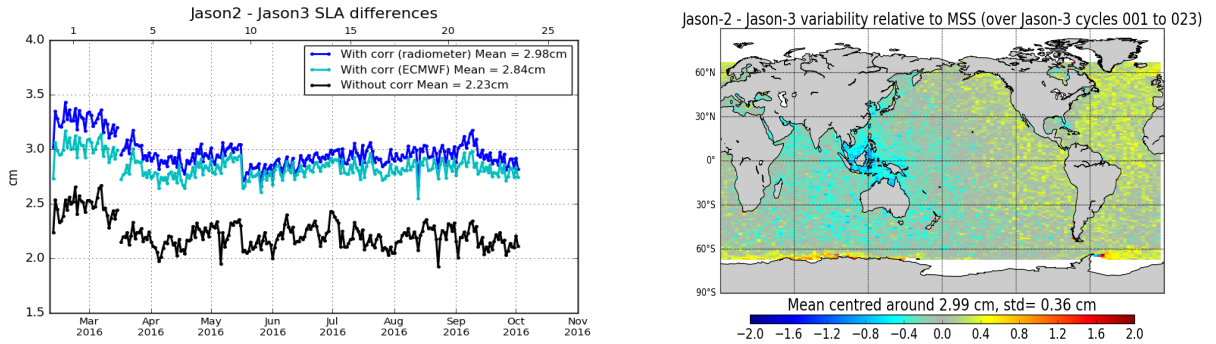


Figure 2 – Jason-3/Jason-2 tandem phase: until 02-10-2016. **Left:** Daily monitoring of SSH bias between Jason-2 and Jason-3 before Jason-2 moved to interleaved ground-track in October 2016: SSH bias without applying geophysical corrections (**black**) and with corrections using radiometer wet troposphere correction (**blue**) or using ECMWF model wet troposphere correction (**cyan**). **Right:** Map of SLA difference between Jason-2 and Jason-3 over tandem phase

During the formation flight (i.e. over cycles 25 to 46 from 12-10-2016 to 17-05-2017) and over Jason-2 LRO phase (until Jason-3 cycle 58, on 14-09-2017), average difference of gridded SLA for Jason-2 and Jason-3 shows high variability regions as Gulf Stream and Antarctic circumpolar currents are visible (figure 3). This difference is quite noisy as both satellites are shifted in time and sea state changes especially in regions of high ocean variability.

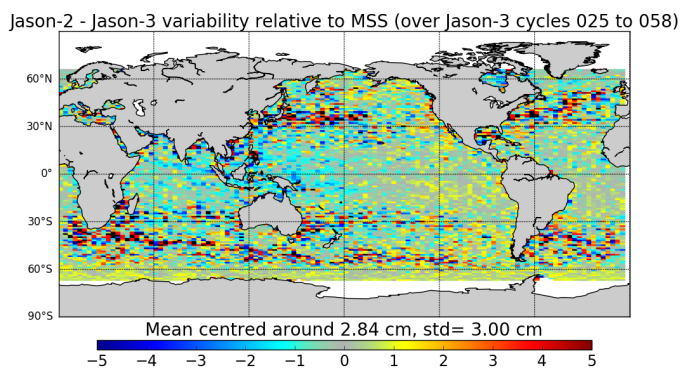


Figure 3 – GDR data. Map of Jason-2 and Jason-3 SLA differences for Jason-3 cycles 025 to 058

Performances at crossover points

Looking at SSH difference at crossovers (figure 4), a 120 day signal is visible on the mean for Jason-3 GDR data until move to orbit standard-F.

Concerning SSH error at crossover points ($standard\ deviation / \sqrt{2}$), Jason-3 missions show very good and stable performances with an error of 3.46 cm (3.47cm for Jason-2).

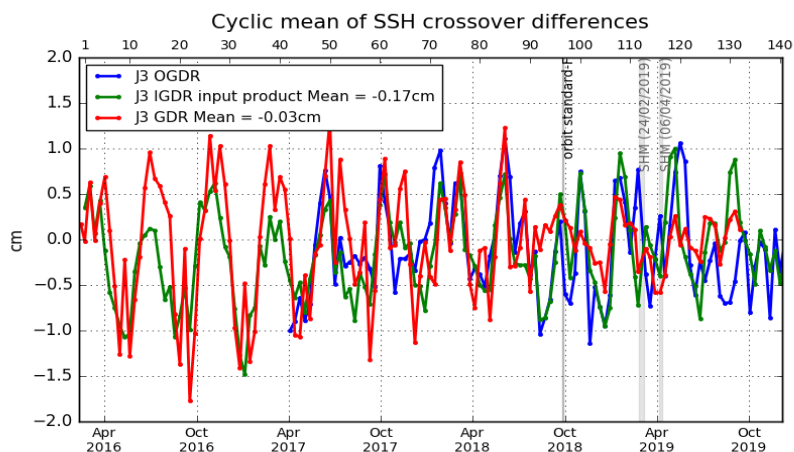


Figure 4 – Monitoring of mean of Jason-3 SSH crossover differences for OGDRs, IGDRs and GDRs. Only data with $|latitude| < 50^\circ$, bathymetry $< -1000m$ and low oceanic variability were selected. (ocean_tide_sol1 = GOT is used in SSH computation)

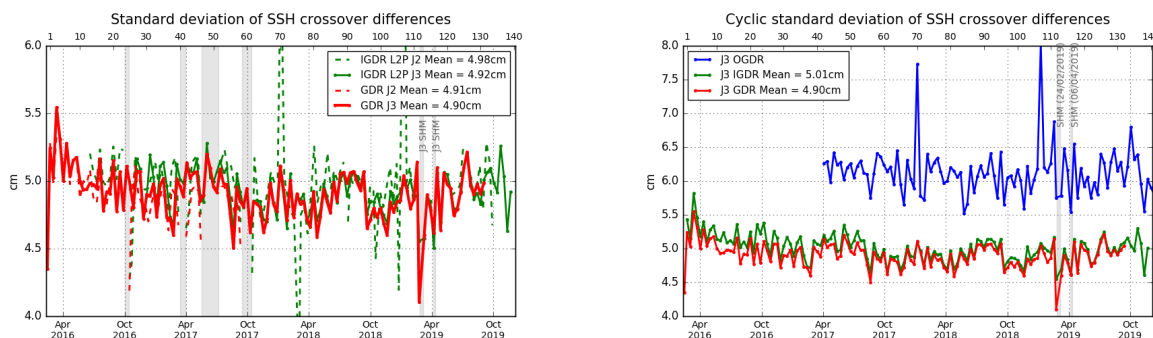


Figure 5 – Cycle by cycle standard deviation of SSH crossover differences for Jason-2 and Jason-3 (left), and for Jason-3 using OGDRs, IGDRs and GDRs (right). Only data with $|latitude| < 50^\circ$, bathymetry $< -1000m$ and low oceanic variability were selected.

Mean SSH differences at Jason 3/Jason 2 crossovers is quite stable and around 3cm in average (figure 6, left). The geographical pattern indicates some hemispheric biases: positive to the west, negative to the east (figure 6, right). It corresponds to orbital signatures observed on sea surface height.

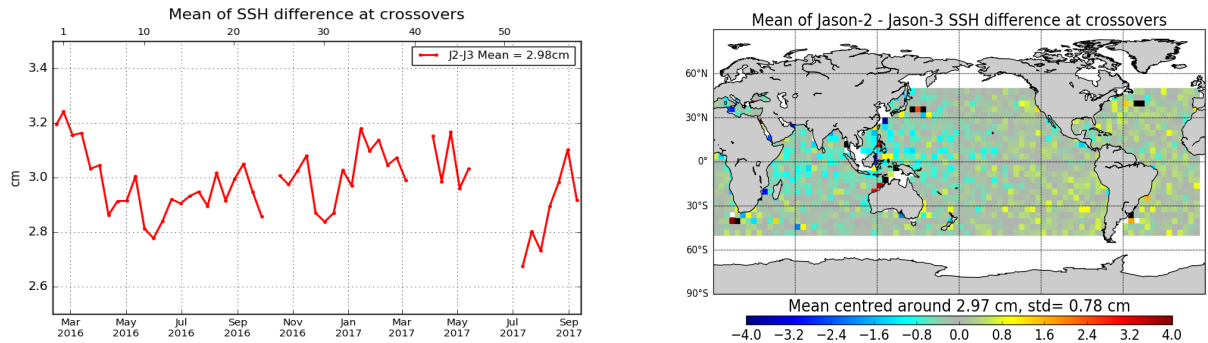


Figure 6 – Cyclic monitoring of Jason-2 - Jason-3 SSH crossover differences mean (left) and map over cycle 1 to 58 (right). Only data with $|\text{latitude}| < 50^\circ$, bathymetry $< -1000\text{m}$ and low oceanic variability were selected.

Contribution to Global Mean Sea Level

Since May 2016 (Jason-3 cycle 11), Jason-3 has been the reference altimetry mission to estimate the Global Mean Sea Level (GMSL), replacing Jason-2. Regional and global biases between missions have to be precisely estimated in order to ensure the quality of the reference GMSL serie. For more precisions, see the dedicated section on AVISO+ website [3].

³<https://www.aviso.altimetry.fr/en/data/products/ocean-indicators-products/mean-sea-level.html>

2. Processing status

2.1. Data Used

Metrics provided in this document are based on Jason-3 dataset from cycle 0 to 132 for GDR products (corresponding to February 12th 2016 to September 18th 2019). This period extends until cycle 140 (December 6th 2019) when IGDR data are considered. Cycle 0 is not included in many statistics because of its available data covering only 5 days.

After tandem phase with Jason-2, Jason-3 has become the reference mission in *DUACS* system from mid-september 2016 onwards. Note that in order to improve their product quality (and also to use as possible same corrections for multimission products), *DUACS* system applies some updates to IGDR data. If no precision is done, IGDR results that are presented in this document contains *DUACS* updates (also called here IGDR-L2P).

2.2. List of events

The following table shows the major events during the Jason-3 mission.

Start time → End time	Cycle	Event
15/02/2016 08:00:00 → 18:04:28	0	First calibration in DIODE + DEM mode
16/02/2016 16:07:00 → 16:38:59	0	Poseidon3B instrument CNG calibration
08/03/2016 20:00:00 → 09/03/2016 00:00:01	3	Gyro calibration
11/03/2016 05:14:00 → 05:34:00	3	AMR Cold Sky calibration maneuver
15/03/2016 → 17/03/2016	3	Platform GPS upload
25/03/2016 09:30:15	4	AMR OFF / ON
06/04/2016 06:05:00 → 06:36:59	5	Poseidon3B instrument CNG calibration
07/04/2016 00:21:27 → 22:19:56	6	DIODE DEM mode
08/04/2016 04:44:30 → 05:00:46 05:11:00 → 05:28:21	6	Poseidon3B instrument CAL2 calibration
27/04/2016 11:38:21 → 12:05:55	8	OPS error
		.../...

Start time → End time	Cycle	Event
02/05/2016 14:34:23 → 14:37:28	8	DEM patch upload.
06/05/2016 18:16:59 → 16/05/2016 16:15:29	9	DIODE DEM mode
12/05/2016 22:44:59 → 22:52:23	9	AMR Cold Sky calibration maneuver
16/05/2016 10:00:00 → 10:16:15	9	Poseidon3B instrument CAL2 calibration
17/05/2016 02:34:00 → 19/05/2016 03:34:16	10	Poseidon3B instrument CAL2 calibration (5 sequences)
25/06/2016 08:09:39 → 05/07/2016 06:08:10	14	DIODE DEM mode
07/07/2016 15:04:44 → 15:11:15	15	AMR internal error
12/07/2016 04:26:36 → 04:34:00	15	AMR Cold Sky calibration maneuver
05/09/2016 04:24:44 → 04:32:08	21	AMR Cold Sky calibration maneuver
10/2016	24	OSTM/Jason 2 moved to the interleaved orbit, end of the verification phase for Jason 3
07/11/2016 22:21:30 → 22:28:54	27	AMR Cold Sky calibration maneuver
27/11/2016 06:15:00 → 06:46:59	29	Poseidon3B instrument CNG calibration
08/12/2016 04:36:34 → 09/12/2016 12:58:47	30	AMR anomaly
10/01/2017 16:37:35 → 16:44:59	34	AMR Cold Sky calibration maneuver
23/02/2017 11:35:00 → 12:06:59	38	Poseidon3B instrument CNG calibration
26/02/2017 17:13:07 → 17:20:31	38	AMR Cold Sky calibration maneuver
27/04/2017 04:13:16 → 04:20:40	44	AMR Cold Sky calibration maneuver
.../...		

Start time → End time	Cycle	Event
03/06/2017 15:46:00 → 16:17:59	48	Poseidon3B instrument CNG calibration
28/06/2017 05:10:04 → 05:17:28	51	AMR Cold Sky calibration maneuver
14/08/2017 05:57:05 → 06:04:29	55	AMR Cold Sky calibration maneuver
29/08/2017 13:41:14 → 31/08/2017 16:24:07	57	DEM onboard upload
31/08/2017 21:33:00 → 22:04:59	57	Poseidon3B instrument CNG calibration
04/09/2017 17:32:09 → 17:39:33	58	AMR Cold Sky calibration maneuver
14/09/2017 16:54:56 → 17:52:18	59	Gyro calibration
14/10/2017 15:30:11 → 15:37:35	62	AMR Cold Sky calibration maneuver
02/11/2017 02:05:23 → 02:12:47	63	AMR Cold Sky calibration maneuver
02/12/2017 02:30:00 → 03:01:59	66	Poseidon3B instrument CNG calibration
16/12/2017 02:03:45 → 02:11:09	68	AMR Cold Sky calibration maneuver
05/01/2018 20:45:36 → 20:53:00	70	AMR Cold Sky calibration maneuver
04/02/2018 16:46:42 → 16:54:06	73	AMR Cold Sky calibration maneuver
26/02/2018 02:36:17 → 02:43:41	75	AMR Cold Sky calibration maneuver
01/03/2018 08:17:00 → 08:48:59	75	Poseidon3B instrument CNG calibration
07/04/2018 23:25:16 → 23:32:40	79	AMR Cold Sky calibration maneuver
25/04/2018 20:34:10 → 20:41:34	81	AMR Cold Sky calibration maneuver
.../...		

Start time → End time	Cycle	Event
29/05/2018 14:05:00 → 14:36:59	84	Poseidon3B instrument CNG calibration
30/05/2018 13:08:34 → 13:17:02 14:41:24 → 14:42:47	85	Poseidon BDR update (2 sequences)
10/06/2018 00:41:29 → 00:48:53	86	AMR Cold Sky calibration maneuver
07/07/2018 19:27:47 → 19:35:10	88	AMR Cold Sky calibration maneuver
31/07/2018 01:05:47 → 01:13:11	91	AMR Cold Sky calibration maneuver
22/08/2018 01:25:28 → 01:32:52	93	AMR Cold Sky calibration maneuver
29/08/2018 19:00:00 → 19:31:59	94	Poseidon3B instrument CNG calibration
02/10/2018 18:53:50 → 19:01:14	97	AMR Cold Sky calibration maneuver
21/10/2018 14:32:55 → 14:40:19	99	AMR Cold Sky calibration maneuver
01/12/2018 00:25:00 → 00:59:59	103	Poseidon3B instrument CNG calibration
04/12/2018 01:36:39 → 01:44:03	103	AMR Cold Sky calibration maneuver
25/12/2018 18:48:13 → 18:55:37	106	AMR Cold Sky calibration maneuver
22/01/2019 15:56:15 → 16:03:39	108	AMR Cold Sky calibration maneuver
28/01/2019 21:50:00	109	AMR Reset
12/02/2019 22:04:38 → 22:12:02	111	AMR Cold Sky calibration maneuver
24/02/2019 09:57:16 → 06/03/2019 08:44:21	112- 113	Safe Hold Mode (SHM)
27/02/2019	112	Doris Software patch update (during recovery)
.../...		

Start time → End time	Cycle	Event
28/02/2019	112	Upload of the GPS software (version N) on PMB (during recovery)
27/03/2019 02:53:30 → 03:00:54	115	AMR Cold Sky calibration maneuver
06/04/2019 23:17:22 → 12/04/2019 02:20:01	116	Safe Hold Mode (SHM)
29/05/2019 05:50:23 → 05:57:47	121	AMR Cold Sky calibration maneuver
31/05/2019 11:10:00 → 11:41:59	121	Poseidon3B instrument CNG calibration
18/06/2019 18:36:47 → 18:44:11	123	AMR Cold Sky calibration maneuver
18/07/2019 00:15:34 → 00:22:58	126	AMR Cold Sky calibration maneuver
08/08/2019 21:00:06 → 21:07:30	128	AMR Cold Sky calibration maneuver
18/08/2019 11:10:00 → 11:41:59	129	Poseidon3B instrument CNG calibration
20/09/2019 20:18:57 → 20:26:21	133	AMR Cold Sky calibration maneuver
09/10/2019 15:58:18 → 16:05:42	135	AMR Cold Sky calibration maneuver
21/11/2019 19:38:16 → 19:45:40	139	AMR Cold Sky calibration maneuver
25/11/2019 22:42:00 → 23:13:59	139	Poseidon3B instrument CNG calibration

Table 1 – Events on Jason-3 mission

2.3. Tracking and acquisition mode

Jason-3 can use two on-board tracking modes: Diode/DEM (open loop) and median tracker. In addition, a tracking automatic transition is possible, which means that when authorized: acquisition mode switches automatically from autonomous DIODE acquisition mode over land to Diode/DEM over ocean and referenced inland water. The status of tracking and acquisition modes are detailed in table 2.

Cycle	Acquisition Mode over land	Acquisition Mode over ocean and all referenced inland waters	Comment
Cycle 000	Median tracker + autonomous acquisition / tracking + DEM	Median tracker + autonomous acquisition / tracking + DEM	tracking automatic transition inhibited except for 7 passes
Cycles 001 to 005	Median tracker	Median tracker	tracking automatic transition inhibited.
Cycles 006	see dedicated point below	see dedicated point below	
Cycles 007	Median tracker	Median tracker	tracking automatic transition inhibited everywhere.
Cycles 008	mainly Median tracker	mainly Median tracker	autonomous acquisition / tracking for passes 144 to 148 (DEM patch upload on 2016-05-02) . tracking automatic transition inhibited everywhere.
Cycle 009 Pass 001 to mid-248	Median tracker	DEM	mid-pass 248 = CAL2 event on 2016-05-16 10:00)
Cycle 009 Pass mid-248 to 254	Median tracker	Median tracker	mid-pass 248 = CAL2 event on 2016-05-16 10:00)
Cycle 010	Median tracker	Median tracker	tracking automatic transition inhibited
Cycles 011 to 019	Median tracker	DEM	tracking automatic transition authorized
Cycle 020	Median tracker	Median tracker	tracking automatic transition inhibited
Cycles 021 to 056	Median tracker	DEM	tracking automatic transition authorized
Cycle 057			DEM upload
Cycles 058 onwards	Median tracker	DEM	tracking automatic transition authorized

Table 2 – Acquisition mode

- About cycle 006: Altimeter state flag for tracking mode is set to 1 by three times (=0 everywhere else):

- for passes 018 to 029 from 2016-04-07 16:32:57 to 2016-04-08 03:13:59 :
>DIODE Acquisition/Autonomous mode (Altimeter state flag for acquisition mode is set to 9) due to operation error after transponder calibration : back to DIODE DEM mode after the next routine calibration.
 - for passes 065 to 070, from 2016-04-09 12:46:05 to 2016-04-09 17:25:10 :
>Auto Acquisition/Autonomous tracking mode (Altimeter state flag for acquisition mode is set to 8) due to automatic reinitialisation in POS3B default mode, triggered on-board by GPS reinit : back to DIODE DEM mode after the next routine calibration
 - for passes 113 to 116, from 2016-04-11 10:03:37 to 2016-04-11 12:20:28 :
>Auto Acquisition/Autonomous tracking mode (Altimeter state flag for acquisition mode is set to 8) due to automatic reinitialisation in POS3B default mode, triggered on-board by GPS OFF-ON : back to DIODE DEM mode after the next routine calibration
- From cycle 21 onwards, except during DEM upload on cycle 057, tracking automatic transition is activated.

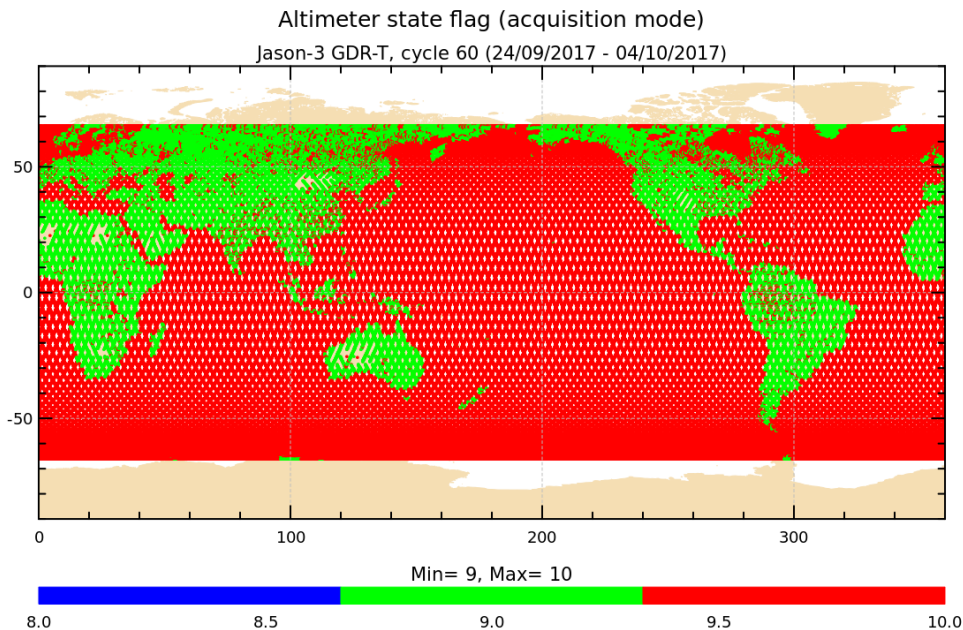


Figure 1 – Acquisition mode for cycle 060 (identical to acquisition mode automatic switch for cycles 6, 9, 11-19, 21-56,58-140). 8 = autonomous acquisition / tracking, 9 = autonomous DIODE acquisition / tracking, 10 = DIODE + Digital Elevation Model tracking

- About cycle 057, some passes are entirely autonomous acquisition / tracking, and some passes entirely median tracker. DEM upload during this cycle is detailed in [22].

2.4. Models and standards

The standards used for version “D” are listed in Table 3.

The main differences between the O/IGDRs versions “T” and “D” are summarized hereafter:

- CAL-2 calibration processing are based on typical ocean AGC values, correcting the negative squared-attitude values that were observed from the start of the mission.
- Backscatter (σ_0) values are adjusted internally during ground processing. A calibration bias of +0.14 dB and +0.109 dB is added to the measured (and reported) MLE-4 and MLE-3 Ku-band σ_0 , respectively, prior to wind speed computation; a calibration bias of -0.231 dB and -0.012 dB is added to the measured (and reported) MLE-3 Ku- and C-band σ_0 , respectively, prior to rain flag computation and rain flag values. This ensure that they are properly aligned with the adopted algorithms, so that rain flagging and wind speed values are in-line with those from Jason-2.

Model	Product version “D”
Orbit	<p>Based on Doris onboard navigator solution for OGDRs.</p> <p>DORIS tracking data for IGDRs (orbit standard MOE-E until cycle 094 and MOE-F from cycle 095 onwards).</p> <p>From Feb.2019 onwards, a DORIS+GPS solution is used for MOE computation</p> <p>DORIS and/or GPS tracking data for GDRs (orbit standard POE-E until cycle 094 and POE-F from cycle 095 onwards).</p>
Altimeter Retracking	<p>OceanMLE4 retracking: MLE4 fit from 2nd order Brown model: MLE4 simultaneously retrieves the following 4 parameters from the altimeter waveforms:</p> <ul style="list-style-type: none"> • Epoch (tracker range offset) → altimeter range • Composite Sigma → SWH • Amplitude → Sigma0 • Trailing Edge slope → Square of mispointing angle (Ku band only, a null value is used in input of the C band retracking algorithm) <p>OceanMLE3 retracking: MLE3 fit from first order Brown analytical model: MLE3 simultaneously retrieves the 3 parameters that can be inverted from the altimeter waveforms:</p> <ul style="list-style-type: none"> • Epoch (tracker range offset) → altimeter range • Composite Sigma → SWH • Amplitude → Sigma0

.../...

Model	Product version "D"
	<p>"Ice" retracking: Geometrical analysis of the altimeter waveforms, which retrieves the following parameters:</p> <ul style="list-style-type: none"> • Epoch (tracker range offset) → altimeter range • Amplitude → Sigma0
Altimeter Instrument Corrections	Two sets: one set consistent with MLE4 retracking and one set consistent with MLE3 retracking
Jason3 Advanced Microwave Radiometer (AMR) Parameters	Using parameters derived from long term calibration tool developed and operated by NASA/JPL
Dry Troposphere Range Correction	From ECMWF atmospheric pressures and model for S1 and S2 atmospheric tides
Wet Troposphere Range Correction from Model	From ECMWF model
Ionosphere correction from model	Based on Global Ionosphere TEC Maps from JPL
Sea State Bias Model	<p>Two empirical models:</p> <ul style="list-style-type: none"> • MLE4 version derived from 1 year of MLE4 Jason-2 altimeter data with version "D" geophysical models • MLE3 version derived from 1 year of MLE3 Jason-2 altimeter data with version "D" geophysical models
Mean Sea Surface Model	MSS_CNES-CLS11 (reference 7 years)
Mean Dynamic Topography Model	MDT_CNES-CLS09
Geoid	EGM96
Bathymetry Model	DTM2000.1
Inverse Barometer Correction	Computed from ECMWF atmospheric pressures after removing S1 and S2 atmospheric tides
Non-tidal High-frequency De-aliasing Correction	Mog2D high resolution ocean model on I/GDRs. None on OGDRs. Ocean model forced by ECMWF atmospheric pressures after removing S1 and S2 atmospheric tides.
Tide Solution 1	GOT4.8 + S1 ocean tide. S1 load tide ignored
Tide Solution 2	FES2004 + S1 and M4 ocean tides. S1 and M4 load tides ignored
Equilibrium long-period ocean tide model.	From Cartwright and Taylor tidal potential.
Non-equilibrium long-period ocean tide model.	Mm, Mf, Mtm, and Msqm from FES2004
Solid Earth Tide Model	From Cartwright and Taylor tidal potential.
Pole Tide Model	Equilibrium model
	.../...

Model	Product version "D"
Wind Speed from Model	ECMWF model
Rain Flag	Derived from comparisons to thresholds of the radiometer-derived integrated liquid water content and of the difference between the measured and the expected Ku-band backscatter coefficient
Ice Flag	Derived from comparison of the model wet tropospheric correction to a dual-frequency wet tropospheric correction retrieved from radiometer brightness temperatures, with a default value issued from a climatology table

Table 3 – List of GDR version "D" standard

2.5. Processing versions

OGDR and IGDR products are publicly available since June 30th 2016. OGDRs were generated in version "T" until cycle 18/pass 137, and then turned in "D" version.

→ The first OGDR "D" file is: *JA3.OPN_2PdS018.137_20160809_080914_20160809_100739.nc*

Concerning IGDRs, they turned from "T" to "D" version a few days before OGDRs on June 27th(cycle 14/pass 143).

→ The first IGDR "D" file is: *JA3_IPN_2PdP014.043_20160626_233040_20160627_002653.nc*

GDRs were generated in version "T" until cycle 021/pass 254, and then turned in "D" version.

→ The first GDR "D" file is: *JA3_GPN_2PdP022.001_20160912_155750_20160912_165403.nc*

Caution (see part "Caution about qual inst corr 1hz sig0 ku" in [23]):

Natural evolution of PTR has resulted in gradual increase in Ku-band sigma0 instrument correction which has exceeded thresholds for flagging from cycle 72 onwards. The flag 'qual_inst_corr_1hz_sig0_ku' parameter has abnormally number of points with value set to 1 over ocean and should not be used then. This has no impact on data quality or system performance.

Note that from cycle 99 onwards, the threshold used to set the flag qual_inst_corr_1hz_sig0_ku has been adjusted in the processing chain. As a consequence the flag qual_inst_corr_1hz_sig0_ku is back ok for a standard use from cycle 99 onwards.

3. Data coverage and edited measurements

3.1. Missing measurements

3.1.1. Over land and ocean

Determination of missing measurements relative to the theoretically expected orbit ground pattern is an essential tool to detect missing telemetry or satellite events for instance. Applying the same procedure for Jason-2 and Jason-3, the comparison of the percentage of missing measurements has been performed.

Figure 2 shows the percentage of available measurements for Jason-3 and Jason-2 for all kind of surfaces observed, computed with respect to a theoretical possible number of measurements. In average Jason-3 provides 99.06% of measurements over 132 cycles (without taking into accounts cycles with explained anomalies or safe hold mode), which shows an improvement compared to Jason-2 tracking capabilities.

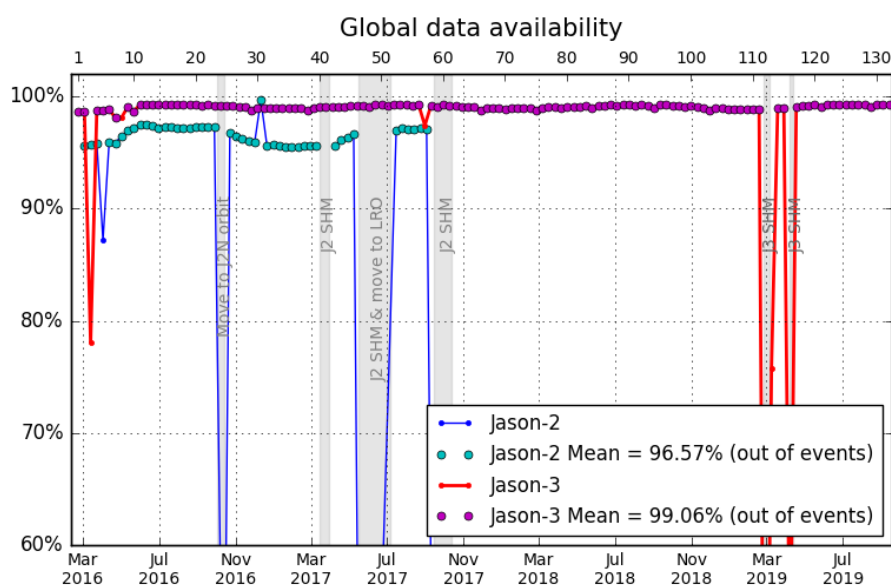


Figure 2 – Global GDRs data availability per cycle

Out of Jason-2 SHM or move of orbit, missing measurements on Jason-2 and Jason-3 since the beginning of Jason-3 mission are:

- **Jason-3 Cycle 3**: GPS platform upload interrupted the data production for two days.
- **Jason-3 Cycle 57**: DEM onboard upload interrupted the data production for few passes.
- **Jason-3 Cycles 112-113**: First Jason-3 SHM (Safe Hold Mode) occurred from 24/02/2019 09:57:16 until 06/03/2019 08:44:21. Over this SHM event, missing data rate is 79.89% for cycle 112 and 24.21% for cycle 113.
- **Jason-3 Cycle 116**: Second SHM occurred from 06/04/2019 23:17:22 until 12/04/2019 02:20:01. Over this SHM event, missing data rate is 53.19% for cycle 116.

- **Jason-2 Cycle 285**: Data are missing in 2016 between April, 5 at 13:35:10 and April, 6 at 12:02:40. No scientific products have been processed during this period to allow the upload of new GPS On Board software.

Jason-2 in median tracker mode and Jason-3 in DEM mode: For almost all cycles, available data percentage is greater for Jason-3 than for Jason-2. This is due to differences in tracking and acquisition modes (Jason-3 uses DEM mode over ocean and inland waters and Jason-2 uses median tracker everywhere): Jason-3 data coverage over land surface can be slightly different regarding to Jason-2 (as shown on top of figure 3).

Jason-2 and Jason-3 both in median tracker: Available data percentage is greater for Jason-3 than for Jason-2 even over cycles where median tracker is used on Jason-2 (all except Jason-2 cycle 311) and only median tracker is used on Jason-3 (cycles 1 to 5, 7-8, 10 and 20: see 2.3.). This difference is probably due to a limitation imposed on Jason-2 tracking to avoid ghost echoes.

Jason-2 and Jason-3 both in DEM mode: Note that Jason-2 cycle 311 (partly over Jason-3 cycles 30 and 31) is in DEM mode, so that availability of measurements over this cycle is quite 100% (but more data are rejected). Bottom part of figure 3 shows that these additional measurements for Jason-2 (right) compared to Jason-3 (left) are mainly located over Asia.

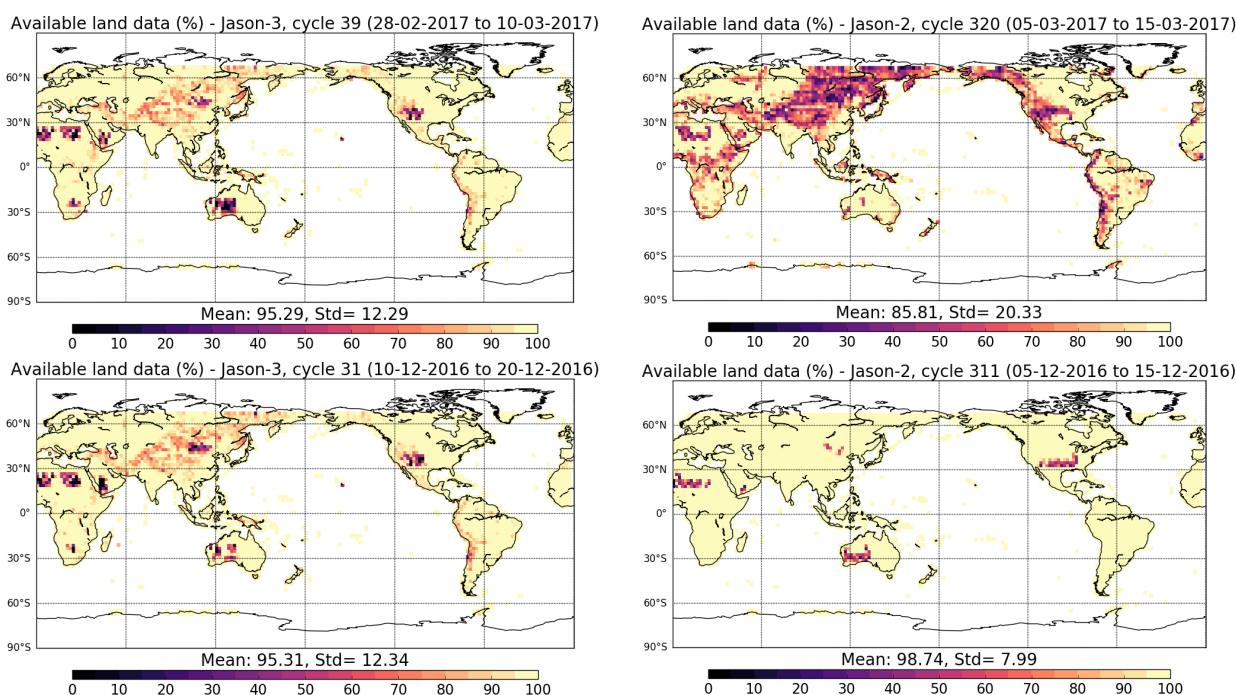


Figure 3 – Map of percentage of available measurements over land for Jason-3 (left) and for Jason-2 (right). **Top**: Jason-3 cycle 039 in DEM mode and Jason-2 cycle 320 in median mode. **Bottom**: Jason-3 cycle 031 in DEM mode and Jason-2 cycle 311 in DEM mode

Table 4 gives an overview of missing passes and reasons for Jason-3.

Date	Jason-3 Cycle/Pass	Reason
Before 12/02/2016 01:11:09	C000 / P001-116	Final ground-track reached on 12-02-2016 01:11:09
	C000 / P201, 203, 236	Due to calibration events, passes 201 (~10%), 203 (~12%) and 236 (~8%) partly missing
08/03/2016 20:00:00 → 09/03/2016 00:00:01	C003	Due to Gyro calibration , data gap on pass 018.
11/03/2016 05:14:00 → 05:34:00	C003	AMR Cold Sky calibration maneuver
15/03/2016 07:15:04 to 17/03/2016 08:06:13	C003 / P181-233	Due to platform GPS software upload, passes 182 to 232 are entirely missing, as well as part of passes 181 and 233
06/04/2016 06:05:00 → 06:36:59	C005 / P235	Due to Poseidon3B instrument CNG calibra- tion, data gap on pass 235, that mainly con- cerns land data acquisition and a portion of Red Sea.
26/04/2016 20:18:29 → 2016-05-06 18:16:59	C008	Due to Poseidon3B instrument CAL2 calibra- tions , data gaps over land on passes 55, 53, 27, 5, 38, 12 and 29
27/04/2016 11:38:11 to 12:05:55	C008 / P017	Due to OPS error, pass 017 has 49.39% of missing measurements (42.44% over ocean)
08/04/2016 04:44:30 → 05:00:46 05:11:00 → 05:28:21	C006	Due to Poseidon3B instrument CAL2 calibra- tion, data gaps over land
02/05/2016 10:17:04 to 10:28:14 and 14:34:22 to 14:37:28	C008 / P144,148	Due to DEM upload: <ul style="list-style-type: none"> • Pass 144 has 20.33% of missing mea- surements (13.27% over ocean, Nor- wegian Sea) • Pass 148 has 6.60% of missing mea- surements over ocean (western african coast)
12/05/2016 22:44:59 → 22:52:23	C009	AMR Cold Sky calibration maneuver
16/05/2016 10:00:00 → 10:16:15	C009	Due to Poseidon3B instrument CAL2 calibra- tion, data gap over land on pass 248
.../...		

Date	Jason-3 Cycle/Pass	Reason
17/05/2016 02:34:00 → 19/05/2016 03:34:16	C010	Due to Poseidon3B instrument CAL2 calibration (5 sequences), data gaps over land on passes 31, 64, 38, 12, and 44
12/07/2016 04:26:36 → 04:34:00	C015	AMR Cold Sky calibration maneuver
05/09/2016 04:24:44 → 04:32:08	C021	AMR Cold Sky calibration maneuver
07/11/2016 22:21:30 → 22:28:54	C027	AMR Cold Sky calibration maneuver
27/11/2016 06:15:00 to 06:46:58	C029 / P159, 160	Due to CNG calibration, parts of passes 159 and 160 are missing (mostly over land). Pass 159 has 54.73% of missing measurements (10.54% over ocean).
10/01/2017 16:37:35 → 16:44:59	C034	AMR Cold Sky calibration maneuver
23/02/2017 11:35:00 → 12:06:59	C038	Poseidon3B instrument CNG calibration
26/02/2017 17:13:07 → 17:20:31	C038	AMR Cold Sky calibration maneuver
27/04/2017 04:13:16 → 04:20:40	C044	AMR Cold Sky calibration maneuver
03/06/2017 from 15:46:00 to 16:17:59	C048 / P159	Due to CNG calibration, pass 159 has 56.55% of missing data mostly over land (10.54% over ocean)
28/06/2017 05:10:04 → 05:17:28	C051	AMR Cold Sky calibration maneuver
14/08/2017 05:57:05 → 06:04:29	C055	AMR Cold Sky calibration maneuver
30/08/2017 12:07:15 to 14:10:33	C057 / P123-125	Due to DEM upload: <ul style="list-style-type: none"> • Pass 123 has 23.91% of missing measurement (15.44% over ocean). • Pass 124 is missing • Pass 125 has 96.16% of missing measurement (100% over ocean).
.../...		

Date	Jason-3 Cycle/Pass	Reason
31/08/2017 14:22:58 to 16:26:10	C057 / P151-153	Due to DEM upload: <ul style="list-style-type: none"> • Pass 151 has 12.40% of missing measurement (8.57% over ocean). • Pass 152 has 100% of missing measurement over ocean • Pass 153 has 98.40% of missing measurement (100% over ocean).
31/08/2017 21:33:00 to 22:04:59	C057 / P159	Due to CNG calibration, pass 159 has 56.17% of missing measurement (10.54% over ocean).
04/09/2017 17:32:09 → 17:39:33	C058	AMR Cold Sky calibration maneuver
14/09/2017 from 16:54:56 to 17:52:18	C059 / P005	Due to Gyro calibration, pass 5 has 47.22% of missing measurements (0.07% over ocean)
14/10/2017 15:30:11 → 15:37:35	C062	AMR Cold Sky calibration maneuver
02/11/2017 02:05:23 → 02:12:47	C063	AMR Cold Sky calibration maneuver
02/12/2017 02:30:00 → 03:01:59	C066 / P235	Due to CNG calibration, pass 235 has 57.16% of missing measurement (8.33% over ocean).
16/12/2017 02:03:45 → 02:11:09	C068	AMR Cold Sky calibration maneuver
26/12/2017 23:03:32 → 23:06:25	C069	Pass 110 has 5.88% of missing measurement (5.66% over ocean) probably due to connection to Usingen anomaly.
05/01/2018 20:45:36 → 20:53:00	C070	AMR Cold Sky calibration maneuver
04/02/2018 16:46:42 → 16:54:06	C073	AMR Cold Sky calibration maneuver
26/02/2018 02:36:17 → 02:43:41	C075	AMR Cold Sky calibration maneuver
01/03/2018 08:17:00 → 08:48:59	C075 / P235	Due to CNG calibration, pass 235 has 57.03% of missing measurement (8.33% over ocean).
.../...		

Date	Jason-3 Cycle/Pass	Reason
07/04/2018 23:25:16 → 23:32:40	C079	AMR Cold Sky calibration maneuver
25/04/2018 20:34:10 → 20:41:34	C081	AMR Cold Sky calibration maneuver
29/05/2018 14:05:00 → 14:36:59	C084 / P235	Due to CNG calibration, pass 235 has 57.00% of missing measurement (8.33% over ocean).
30/05/2018 13:08:34 → 13:17:02 14:41:24 → 14:42:47	C085 / P006-007	Due to BDR update: <ul style="list-style-type: none"> • Pass 6 has 15.31% of missing measurement (10.80% over ocean). • Pass 7 has 2.84% of missing measurement (4.86% over ocean).
10/06/2018 00:41:29 → 00:48:53	C086	AMR Cold Sky calibration maneuver
07/07/2018 19:27:47 → 19:35:10	C088	AMR Cold Sky calibration maneuver
31/07/2018 01:05:47 → 01:13:11	C091	AMR Cold Sky calibration maneuver
22/08/2018 01:25:28 → 01:32:52	C093	AMR Cold Sky calibration maneuver
29/08/2018 19:00:00 → 19:31:59	C094 / P057	Due to CNG calibration, pass 057 has 57.00% of missing measurement (12.67% over ocean).
02/10/2018 18:53:50 → 19:01:14	C097	AMR Cold Sky calibration maneuver
21/10/2018 14:35:37 → 14:40:19	C099	AMR Cold Sky calibration maneuver
01/12/2018 00:25:00 → 00:56:59	C103 / P159	Due to CNG calibration, pass 159 has 56.43% of missing measurement (10.54% over ocean).
04/12/2018 01:36:39 → 01:44:03	C103	AMR Cold Sky calibration maneuver
25/12/2018 18:48:13 → 18:55:37	C106	AMR Cold Sky calibration maneuver
.../...		

Date	Jason-3 Cycle/Pass	Reason
22/01/2019 15:56:15 → 16:03:39	C108	AMR Cold Sky calibration maneuver
12/02/2019 22:04:38 → 22:12:02	C111	AMR Cold Sky calibration maneuver
24/02/2019 09:57:16→ 06/03/2019 08:44:21	C112 P050 / C113 P061	Safe Hold Mode. Passes 050 to 254 of cycle 112 and passes 001 to 060 of cycle 113 are missing.
07/03/2019 14:30:00 → 15:25:00	C113 / P093 and 094	Due to Gyro calibration, passes 093 and 094 have respectively 19.2% and 23.9% of missing measurements (all over ocean)
27/03/2019 02:53:30 → 03:00:54	C115	AMR Cold Sky calibration maneuver
06/04/2019 23:17:22→ 12/04/2019 02:20:01	C116	Safe Hold Mode. Passes 108 to 245 are completely missing and pass 246 has 16.37% of missing measurement (15,46% over ocean).
30/04/2019 07:43:45 → 07:47:01	C118	Due to PLTM gaps, pass 199 has 26 non-continuous missing points over ocean.
29/05/2019 05:50:23 → 05:57:47	C121	AMR Cold Sky calibration maneuver
31/05/2019 11:10:00 → 11:41:59	C121 / P235	Due to CNG calibration, pass 235 has 59.96% of missing measurement (8.00% over ocean).
11/06/2019 → 13/06/2019	C123	Due to PLTM gaps, passes 021 and 071 have 47 and 33 non-continuous missing points over ocean.
18/06/2019 18:36:47 → 18:44:11	C123	AMR Cold Sky calibration maneuver
18/07/2019 00:15:34 → 00:22:58	C126	AMR Cold Sky calibration maneuver
08/08/2019 21:00:06 → 21:07:30	C128	AMR Cold Sky calibration maneuver
18/08/2018 18:58:00 → 19:29:59	C129 / P235	Due to CNG calibration, pass 235 has 55.42% of missing measurement (7.98% over ocean).
20/09/2019 20:18:57 → 20:26:21	C133	AMR Cold Sky calibration maneuver
.../...		

Date	Jason-3 Cycle/Pass	Reason
09/10/2019 15:58:18 → 16:05:42	C135	AMR Cold Sky calibration maneuver
04/11/2019 22:08:50 and 22:14:46	C137	Due to PLTM gaps, pass 204 has 2.63% of missing points over ocean.
21/11/2019 19:38:16 → 19:45:40	C139	AMR Cold Sky calibration maneuver
25/11/2019 22:42:00 → 23:13:59	C139 / P235	Due to CNG calibration, pass 235 has 57.19% of missing measurement (8.40% over ocean).

Table 4 – List of missing Jason-3 passes

3.1.2. Over ocean

The behaviour of Jason-3 over ocean is excellent and conform to what is observed with Jason-2 during tandem phase (on the same ground track, with 80 seconds of difference), and even after on interleaved groundtrack.

Looking at data over ocean, Jason-3 is always available (ocean is fully covered) out of specific events (see figure 4)

- 21.03% of missing measurements due to GPS platform upload during cycle 3,
- 0.3% of missing measurements over cycle 8 due to operator error,
- 1.74% of missing measurements due to the DEM-onboard upload during cycle 57.
- 79.82% of missing measurements due to safe hold mode during cycle 112.
- 22.92% of missing measurements due to safe hold mode during cycle 113.
- 53.16% of missing measurements due to safe hold mode during cycle 116.

Jason-2 missing measurements reason until end of 2017 is detailed in Jason-2 2017 Annual report [115].

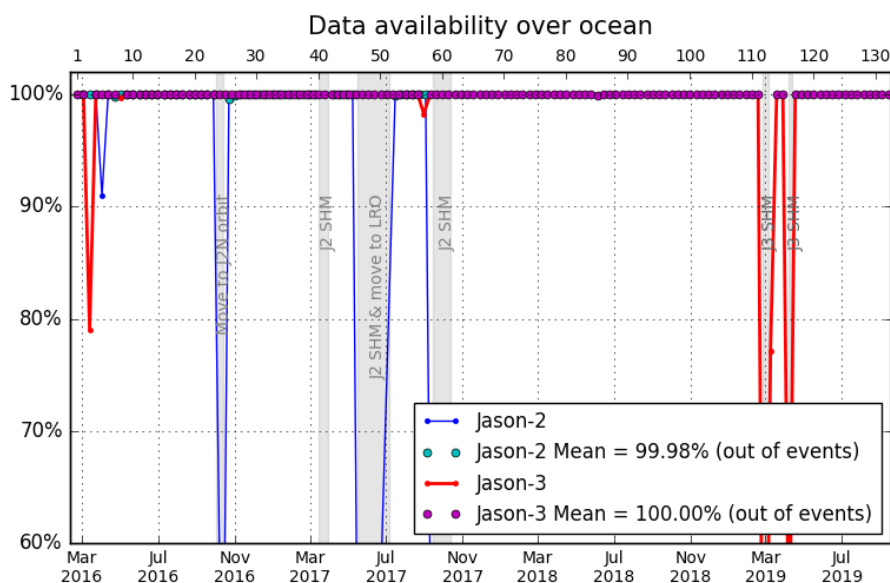


Figure 4 – Jason-2 and Jason-3 GDR data availability over ocean (per cycle)

3.2. Edited measurements

Editing criteria allow to select only measurements considered as valid over ocean. This editing process is structured in 4 main steps:

1. Measurements over land are removed, only measurements over ocean and lakes are kept
2. Measurements over ice are removed
3. Threshold criteria are applied on altimeter, radiometer and geophysical parameters as described in the following table 5. Except for the dual frequency ionosphere correction, only Ku-band measurements are used in this editing procedure, as they mainly represent the end user dataset.
4. A spline criterion is applied to remove the remaining spurious data.

3.2.1. Global editing

The percentage of total edited measurements is monitored on a cyclic basis. The average of total edited measurements is 37.6% (see Figure 5). A small annual cycle is visible due to ice coverage signal (see dedicated part 3.2.2.): the total percentage is slightly lower during March/April/May (30-35%), then increasing during May to July and remains around 38-42%, and start to slowly decrease in mid-September. This expected behaviour is related to sea ice coverage, and was already observed on previous altimetry missions such as OSTM/Jason 2. The peak detected on cycle 30 is due to an AMR anomaly that occurred from 08/12/2016 04:36:34 to 09/12/2016 12:58:47. The second peak visible on cycle 112 is due to edited data before SHM (see details about SHM in 8.1.1.).

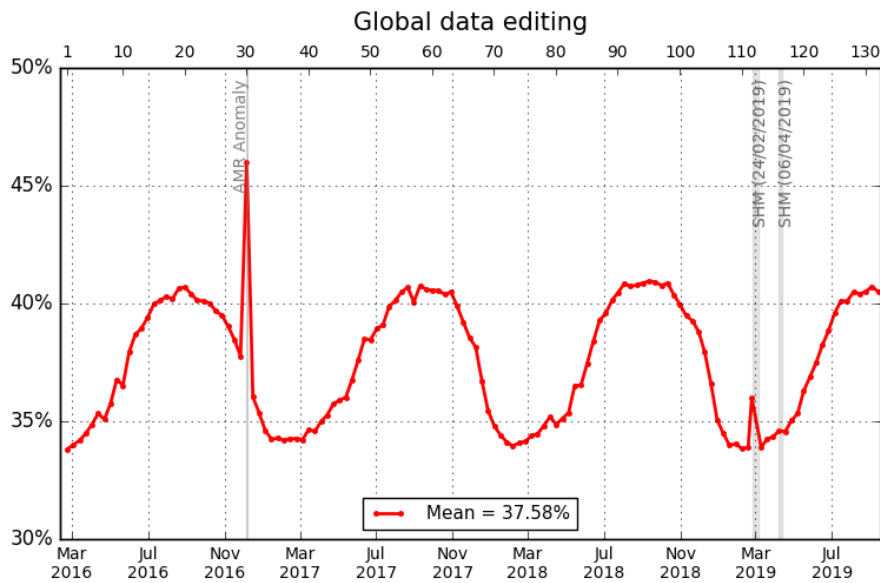


Figure 5 – Jason-3 data editing average by cycle.

3.2.2. Flagging quality criterion: Ice flag

The ice flag (from GDR) is used to remove the ice and sea ice data. Figure 6 shows cycle per cycle percentage of measurements edited by this criterion in comparison with Jason-2 (only ocean and big lakes measurements are kept). Jason-2 and Jason-3 ice flag show similar features while on repetitive orbit. A small bias ($< 0.2\%$) is visible since Jason-2 has been on its drifting orbit. This difference is due to the change in global number of ocean points for Jason-2 (that increased globally and everywhere from repetitive phase to LRO), so that ice flagged points percentage relatively to global number of points decreased.

Over the shown period, no anomalous trend is detected but the nominal annual cycle is visible. Indeed, the maximum number of points over ice is reached during the southern winter (i.e. July - September). As Jason-3 takes measurements between 66° north and south, it does not detect thawing of sea ice (due to global warming), which takes place especially in northern hemisphere over 66°N .

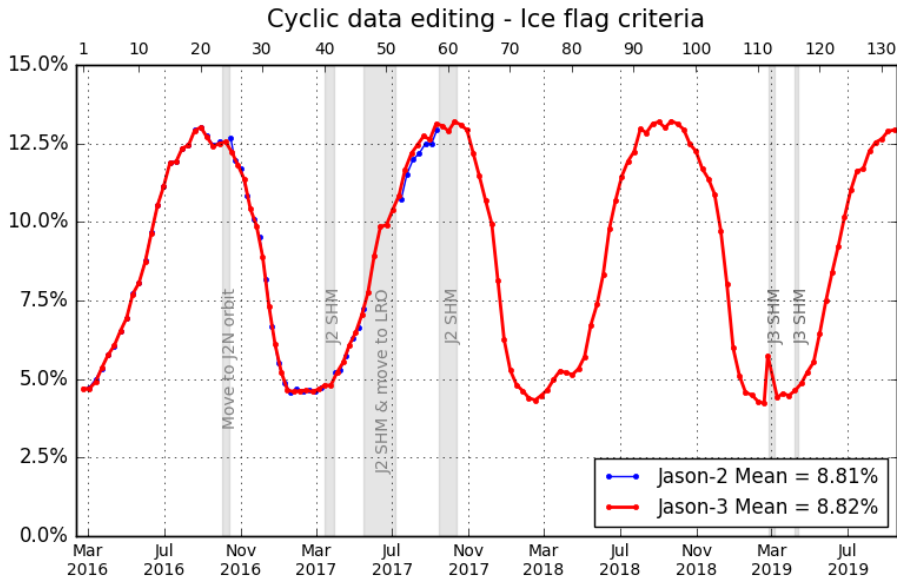


Figure 6 – Cycle per cycle monitoring of the percentage of edited measurements by ice flag criterion.

3.2.3. Flagging quality criterion: Rain flag

Though the altimeter rain flag is available in GDR, it is not used hereafter during the editing procedure. The percentage of measurements where rain flag is set to 1 is plotted in figure 7 top panel. Using the altimeter rain flag would lead to edit 6.1% of additional measurements compared to recommended editing procedure (see figure 7 bottom panels for comparison).

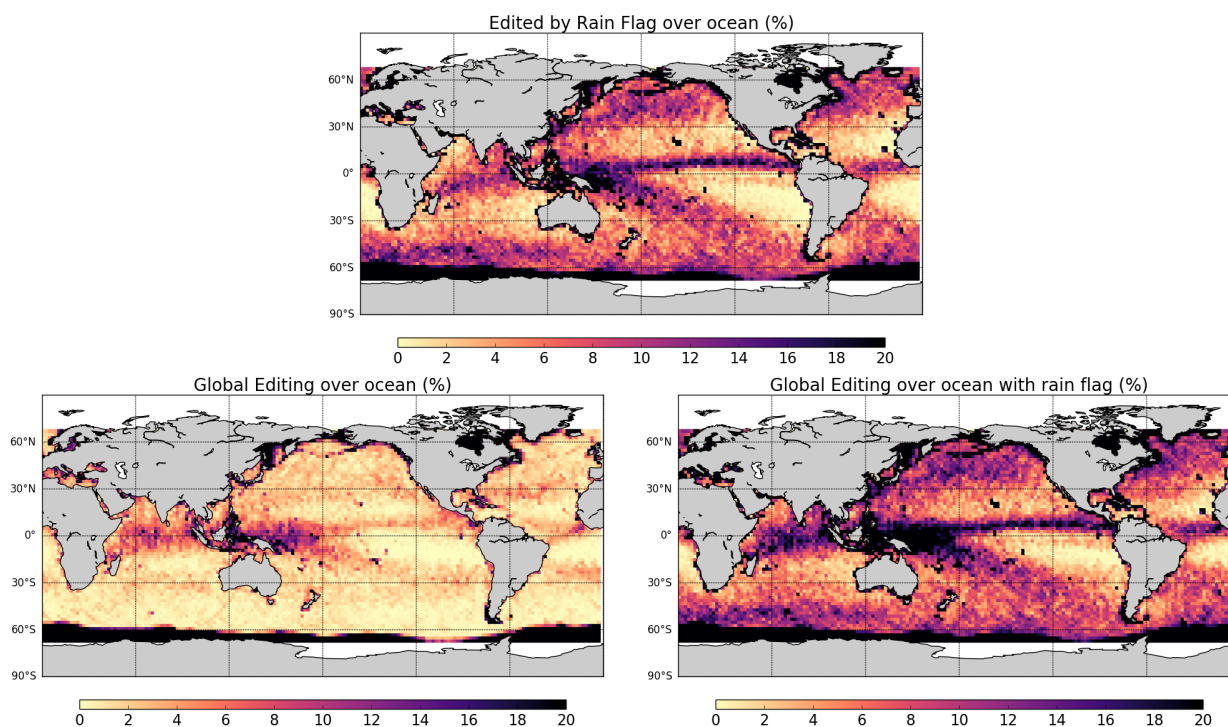


Figure 7 – Top: Percentage of edited measurements by altimeter rain flag criterion. Bottom left: Map of global edited measurements without considering the rain flag. Bottom right: Map of global edited measurements using all criteria and considering the rain flag. All figures are computed over ocean and from cycle 96 to 132.

3.2.4. Editing on thresholds criteria

After quality flag analysis, instrumental parameters have also been analyzed from comparison with thresholds. The average of total edited measurements following threshold criterion is around 3.2% (Figure 8). For each criterion, cycle percentage of edited measurements is monitored (detailed from part 3.2.4.1. to 3.2.4.11.). This allows detection of anomalies in the number of removed data, which could have instrumental, geophysical or algorithmic origins. In particular, note that no measurement is edited by the following corrections (these parameters are only verified in order to detect data at default values, which might happen during a processing anomaly):

- dry troposphere correction,
- inverted barometer correction (including DAC),
- equilibrium tide,
- earth tide,
- pole tide.

Threshold criteria applied on altimeter, radiometer and geophysical parameters are described in the following table 5. The last column represents the mean of rejected data on each criterion over GDR cycles 1 to 132.

Parameter	Min thresholds	Max thresholds	Mean edited
Sea surface height	-130 m	100 m	0.74%
Sea level anomaly	-2.0 m	2.0 m	0.93%
Number measurements of range	10	<i>Not applicable</i>	1.02%
Standard deviation of range	0	0.2 m	1.33%
Squared off-nadir angle	-0.2 deg ²	0.64 deg ²	0.58%
Dry troposphere correction	-2.5 m	-1.9 m	0.00%
Inverted barometer correction	-2.0 m	2.0 m	0.00%
AMR wet troposphere correction	-0.5m	-0.001 m	0.19%
Ionosphere correction	-0.4 m	0.04 m	1.15%
Significant wave height	0.0 m	11.0 m	0.58%
Sea State Bias	-0.5 m	0.0 m	0.51%
Number measurements of Ku-band Sigma0	10	<i>Not applicable</i>	1.00%
Standard deviation of Ku-band Sigma0	0	1.0 dB	2.06%
Ku-band Sigma0 ²	7.0 dB	30.0 dB	0.55%
Ocean tide	-5.0 m	5.0 m	0.01%
Equilibrium tide	-0.5 m	0.5 m	0.00%
Earth tide	-1.0 m	1.0 m	0.00%
Pole tide	-15.0 m	15.0 m	0.00%
Altimeter wind speed	0 m.s ⁻¹	30.0 m.s ⁻¹	1.03%
All together	-	-	3.24%

Table 5 – Editing criteria over cycles 1 to 132

The peak detected on cycle 30 (Figure 8) is due to an AMR anomaly that occurred from 08/12/2016 04:36:34 to 09/12/2016 12:58:47. The second peak is located on cycle 112, where occurred Safe Hold Mode. Before going into safe hold mode, data is rejected by several parameters out of threshold (square off nadir angle, rms of range, backscattering coefficient, significant wave height, altimeter ionosphere, sea state bias, wind speed, sea surface height, sea level anomaly). Except those anomalies the rate of rejected by thresholds data is quite stable.

²A bias of -2.38 dB is subtracting in order to be in agreement with TOPEX thresholds.

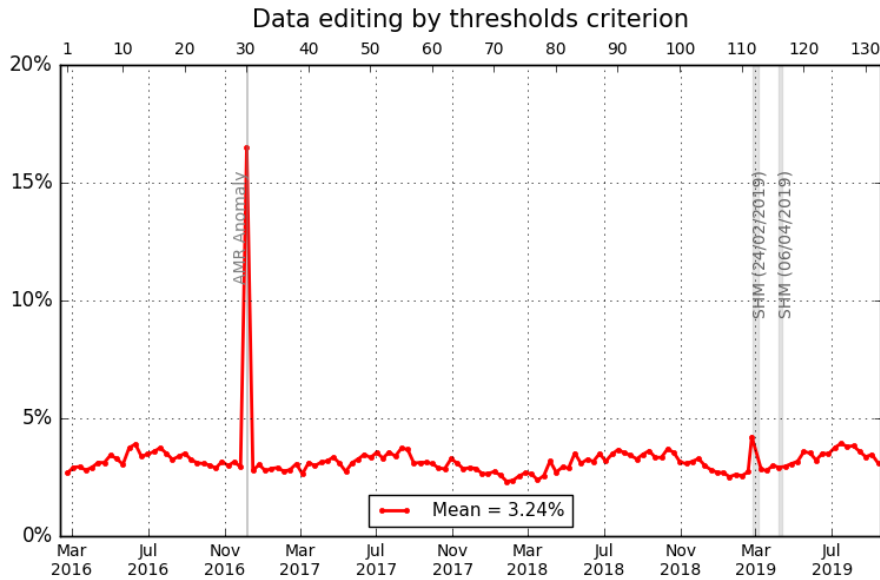


Figure 8 – Jason-3 data editing by thresholds average by cycle.

3.2.4.1. Threshold criteria: 20-Hz range measurements number and standard deviation

1Hz range measurements computed with less than 10 full resolutions (20Hz, 20 measurements/seconds) are removed. Indeed they are considered as not consistent to compute 1Hz resolution range. Such situation usually occurs in regions with disturbed sea state or heavy rain, as shown on Figure 9 top right. Indeed waveforms are distorted by rain cells, which makes them often meaningless for SSH calculation. As a consequence, edited measurements due to several altimetric criteria are often correlated with wet areas.

For Jason-3, the average percentage of removed measurements using this criterion is 1.02% whereas it is 1.04% for Jason-2. The two missions provide very closed values (Figure 9 top right).

Using the threshold editing on 20Hz measurements standard deviation (Figure 9 bottom), 1.33% of data are removed in average for Jason-3, which is very close to Jason-2 (1.41%). An annual signal appears here for both missions. As for 20Hz range measurements number, edited measurements are correlated with wet areas.

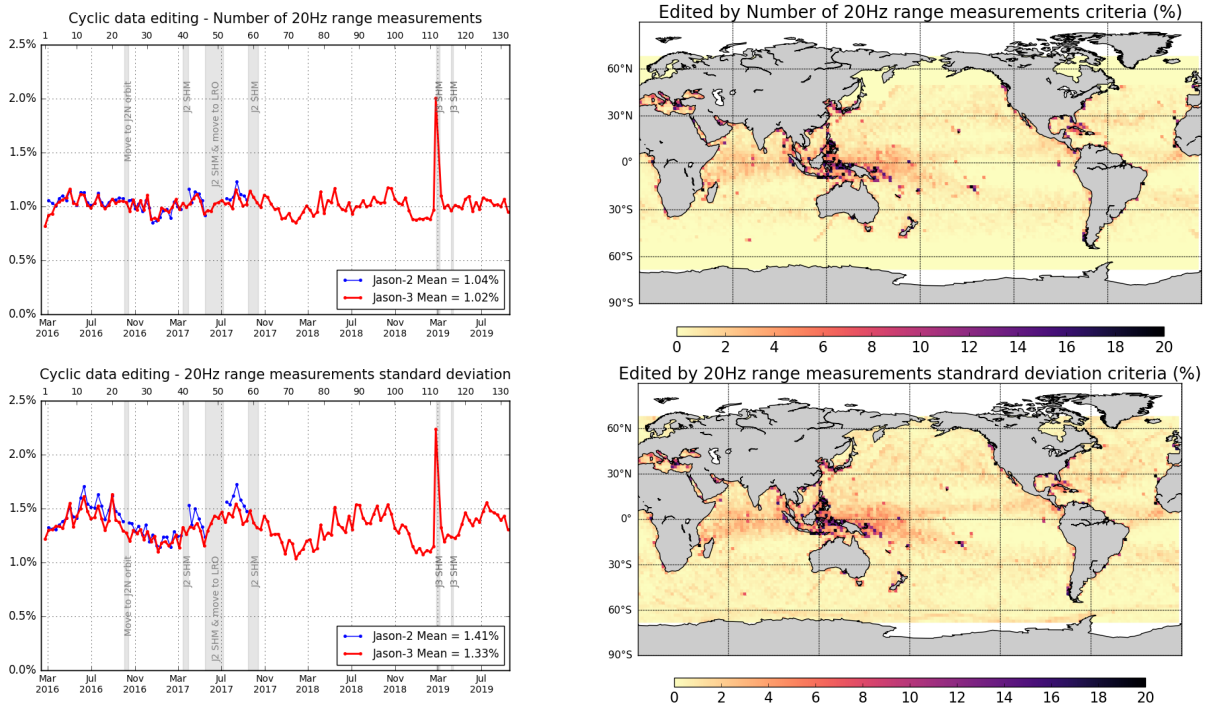


Figure 9 – Percentage of edited measurements by 20Hz range measurements threshold criterion (top) and by 20Hz range measurements standard deviation threshold criteria (bottom). Cycle per cycle monitoring compared with Jason-2 (left) and Jason-3 averaged map from cycle 96 to 132 (right).

3.2.4.2. Threshold criteria: Significant wave height (swh)

The percentage of edited measurements due to significant wave heights criterion is represented on Figure 10, and is about 0.58%. They are mostly due to set to default values data, and are located near coasts, in the equatorial regions and in circumpolar areas. Compared to Jason-2, the former removes globally more SWH data (0.64%), which seems to be linked to acquisition modes:

- For Jason-3 cycles 1 to 5, 7-8, 10, and 20, both missions are using median tracker: rejected data rate on this criterion are equivalent for both missions.
- For almost all cycles, Jason-2 uses median tracker and Jason-3 uses Diode/DEM automatic switch: there are less data removed for Jason-3 than for Jason-2.
- For Jason-2 cycle 311 (over Jason-3 cycles 30 and 31), both missions are in Diode/DEM mode: there are quite equivalent, with slightly less data removed on Jason-2.

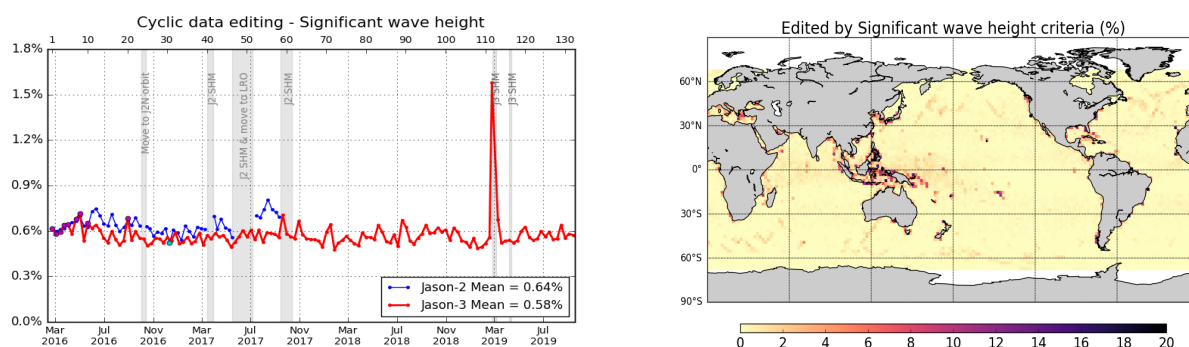


Figure 10 – Percentage of edited measurements by SWH threshold criterion. Left: Cycle per cycle monitoring compared with Jason-2 (Jason-2 DEM cycle in cyan. Jason-3 median tracker cycles in purple.) Right: Jason-3 averaged map from cycle 96 to 132 .

3.2.4.3. Threshold criteria: Backscatter coefficient (σ_0)

The percentage of edited measurements due to backscatter coefficient criterion is represented on top of Figure 11. It is about 0.55%, compared to 0.61% for Jason-2. The bottom part of Figure 11 shows again close values between the two missions for the 20Hz σ_0 standard deviation criterion. However, there are slightly more rejected measurements with this criterion on Jason-3 (2.06%) than Jason-2 (1.95%). Edited measurements are especially found in regions with disturbed waveforms, as shown on the maps. As for SWH criterion (3.2.4.2.), differences seem to be linked to acquisition modes:

- For Jason-3 cycles 1 to 5, 7-8, 10, and 20, both missions are using median tracker: rejected data rate on this criterion are equivalent for both missions.
- For almost all cycles, Jason-2 uses median tracker and Jason-3 uses Diode/DEM automatic switch: there are less data removed for Jason-2 than for Jason-3.
- For Jason-2 cycle 311 (over Jason-3 cycles 30 and 31), both missions are in Diode/DEM mode: there are quite equivalent.

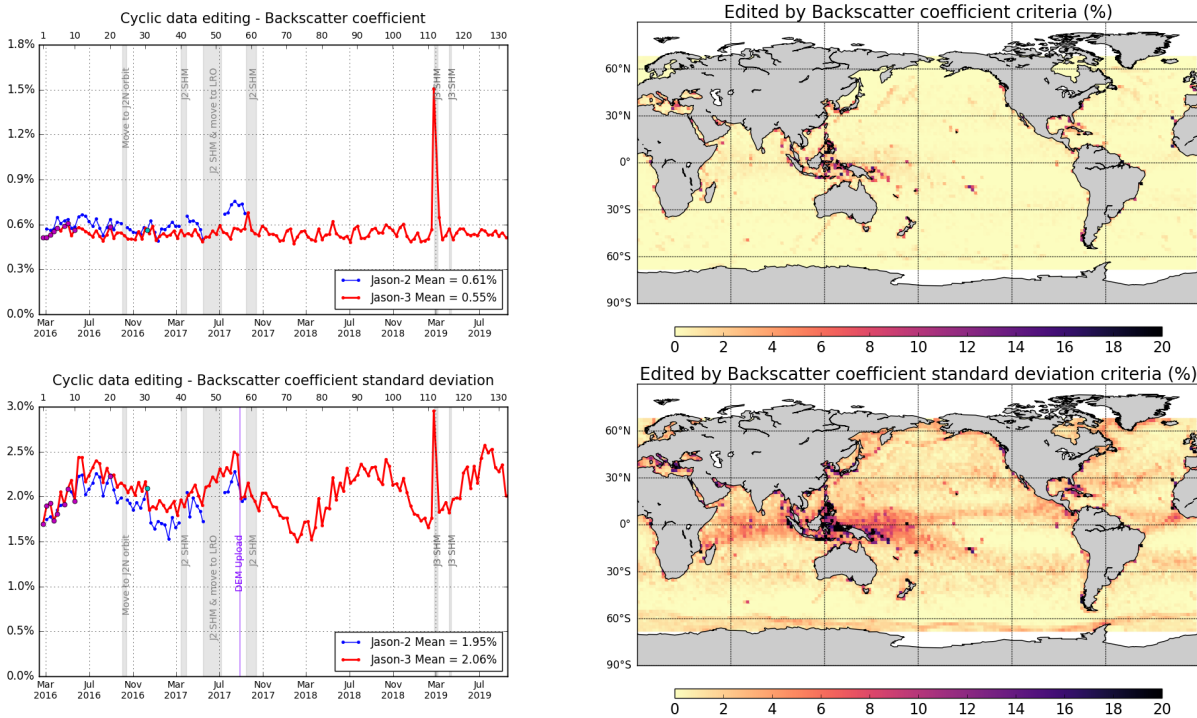


Figure 11 – Percentage of edited measurements by backscatter coefficient threshold criterion (top) and by 20Hz backscatter coefficient standard deviation threshold criteria (bottom). Cycle per cycle monitoring compared with Jason-2 (left, Jason-2 DEM cycle in cyan. Jason-3 median tracker cycles in purple) and Jason-3 averaged map from cycle 96 to 132 (right).

3.2.4.4. Threshold criteria: Radiometer wet troposphere correction

The percentage of edited measurements due to radiometer wet troposphere correction criterion is represented in figure 12. It is about 0.19%. When removing cycles which experienced problems, percentage of edited measurements drops to 0.08%. For some cycles, the percentage of edited measurements is higher than usual. For cycle 30, this unusual value (13.85%) is due to an AMR anomaly. Compared to Jason-2 values, they are within the same order of magnitude, except specific events or anomalies (Jason-2 AMR anomalies during cycle 285 and cycle 326, that correspond respectively to Jason-3 cycle 5 and cycle 45 datation).

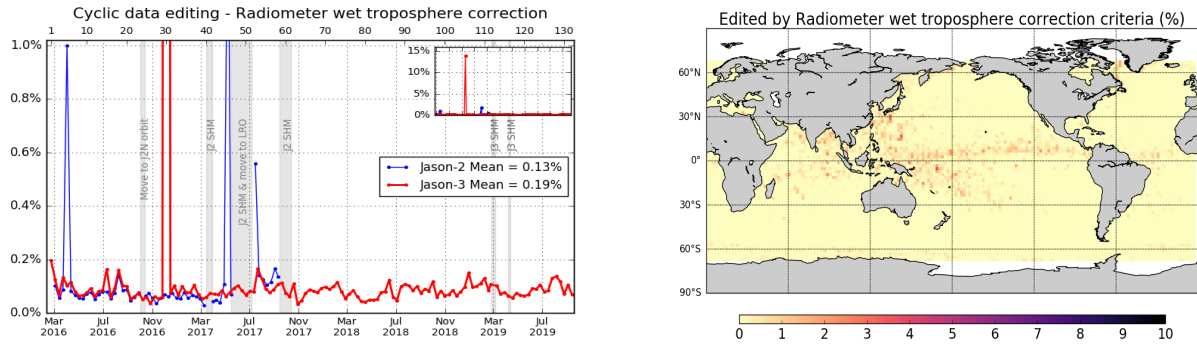


Figure 12 – Percentage of edited measurements by radiometer wet troposphere correction threshold criterion. Left: Cycle per cycle monitoring compared with Jason-2. Right: Jason-3 averaged map from cycle 96 to 132.

3.2.4.5. Threshold criteria: Ionospheric correction

The mean percentage of edited data by threshold criterion on ionospheric correction is 1.15% and is close to Jason-2 mean (1.18%). The map on figure 13 shows that measurements edited by dual frequency ionosphere correction are mostly found in equatorial regions.

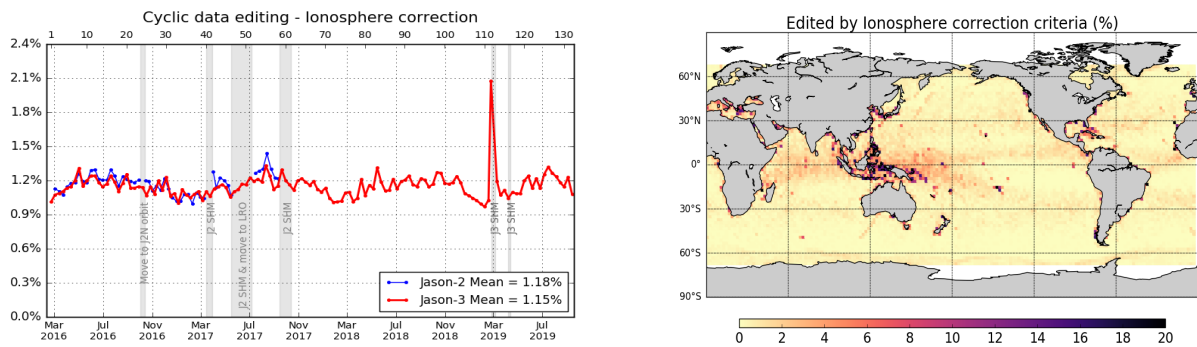


Figure 13 – Percentage of edited measurements by ionospheric correction threshold criterion. Left: Cycle per cycle monitoring compared with Jason-2. Right: Jason-3 averaged map from cycle 96 to 132.

3.2.4.6. Threshold criteria: Altimeter wind speed

The percentage of edited measurements due to altimeter wind speed criterion is represented on figure 14. It is about 1.03%, and in accordance with Jason-2. Measurements are usually edited because of default values. This is the case when sigma0 itself is at default value, or when it shows very high values (higher than 25 dB), which occurs during sigma bloom situations and also over sea ice. Indeed, the wind speed algorithm (which uses backscatter coefficient and significant wave height) can not retrieve values for sigma0 higher than 25 dB.

Wind speed is also edited when it includes negative values, which can occur in GDR products. Nevertheless, sea state bias is available even for negative wind speed values. Therefore, the percentage of edited altimeter wind speed data is higher than the percentage of edited sea state bias data (see 3.2.4.7.).

The map 14 showing percentage of measurements edited by altimeter wind speed criterion is correlated with maps 10 (swh) and 15 (ssb).

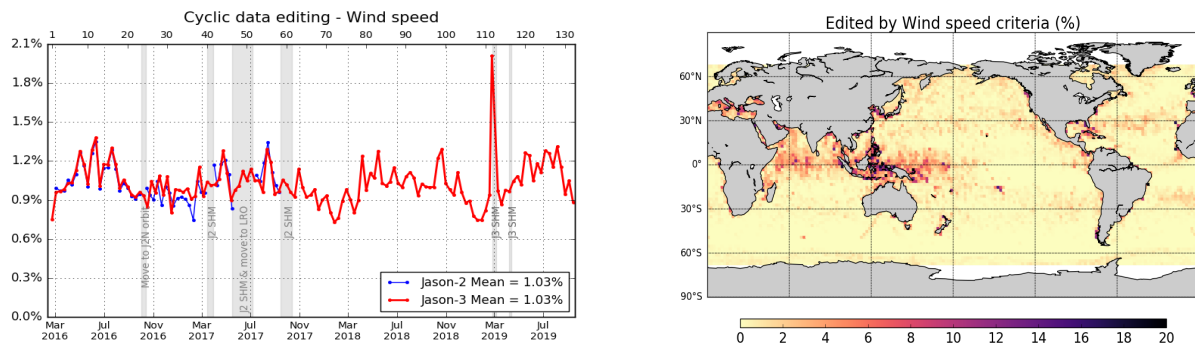


Figure 14 – Percentage of edited measurements by wind speed threshold criterion. Left: Cycle per cycle monitoring compared with Jason-2. Right: Jason-3 averaged map from cycle 96 to 132.

3.2.4.7. Threshold criteria: Sea State Bias

Regarding the sea state bias criterion, the percentage of Jason-3 edited measurements is about 0.51% and 0.63% for Jason-2. The difference can also be observed on the sigma0 and the significant wave height threshold criteria (which are both used for SSB computation).

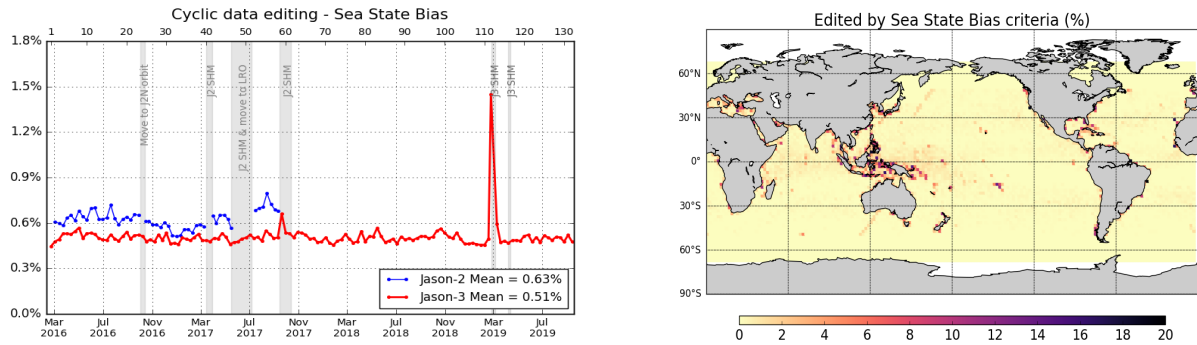


Figure 15 – Percentage of edited measurements by sea state bias threshold criterion. Left: Cycle per cycle monitoring compared with Jason-2. Right: Jason-3 averaged map from cycle 96 to 132.

3.2.4.8. Threshold criteria: Ocean tide

The percentage of edited measurements due to ocean tide is 0.01% for both missions. The ocean tide correction is a model output, there should therefore be no edited measurement. Indeed there are no measurements edited in open ocean areas, but only very few near coasts (Alaska, Kamchatka, Labrador). These measurements are mostly at default values. The level of edited measurements decreases or increases with move of orbit for Jason-2 : this is related to the new ground track, which no longer overflows the same areas.

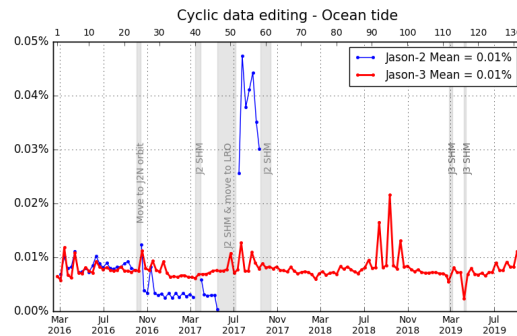


Figure 16 – Percentage of edited measurements by ocean tide threshold criterion. Cycle per cycle monitoring compared with Jason-2.

3.2.4.9. Threshold criteria: Square off nadir angle

The percentage of edited data for both missions is similar (0.58% for both missions). An increase in Jason-2 edited measurements is observed from July 2017 after Jason-2 move to drifting orbit.

The map 17 shows that edited measurements are mostly found in coastal regions and regions with disturbed waveforms.

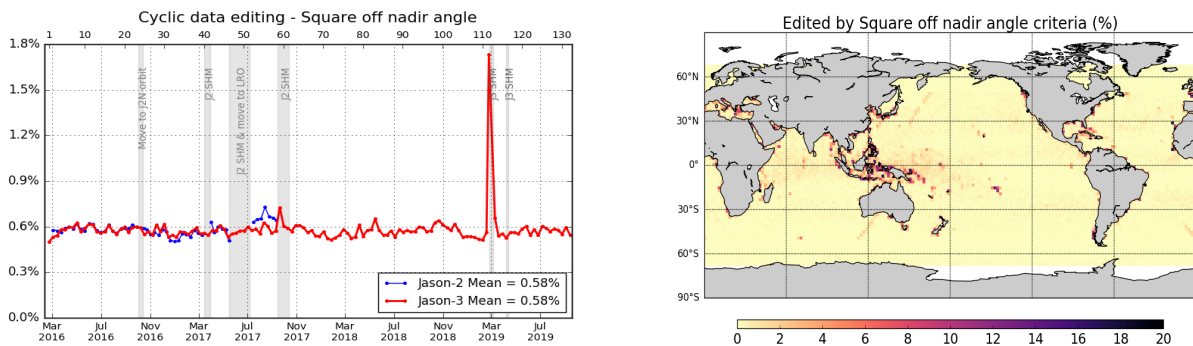


Figure 17 – Percentage of edited measurements by square off nadir angle threshold criterion. Left: Cycle per cycle monitoring compared with Jason-2. Right: Jason-3 averaged map from cycle 96 to 132.

3.2.4.10. Threshold criteria: Sea surface height

Sea surface height represents the difference between the orbit and the altimeter range in Ku band. Figure 18 summarizes the editing resulting from the sea surface height threshold criterion. It removes in average 0.74% of data for Jason 3 whereas it removes 0.77% of data for Jason 2. The editing is usually due to range measurements at default values near coast in equatorial and mid-latitude regions, as well as regions with low significant wave heights.

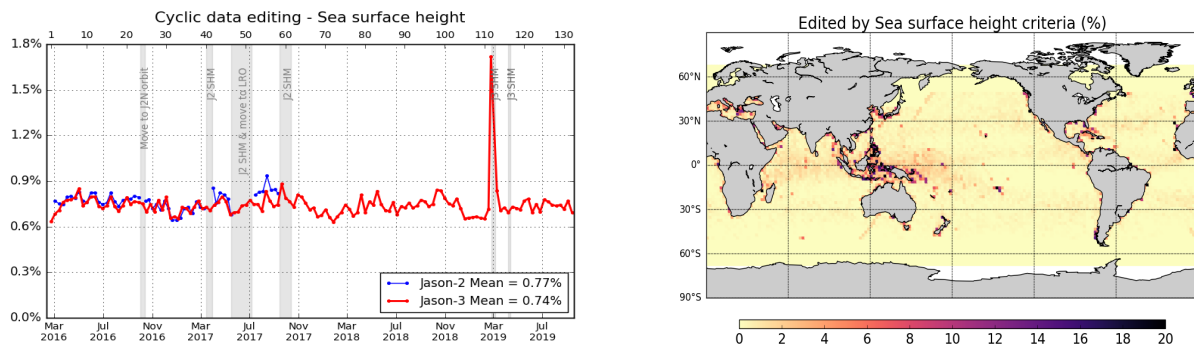


Figure 18 – Percentage of edited measurements by sea surface height threshold criterion. Left: Cycle per cycle monitoring compared with Jason-2. Right: Jason-3 averaged map from cycle 96 to 132.

3.2.4.11. Threshold criteria: Sea Level Anomaly

The percentage of edited data by threshold criterion is 0.93% for Jason-3. As the wet tropospheric correction is used in the SLA computation, percentage of edited SLA measurement presents the same peak on cycle 30. In the same way edited data due to derived from altimeter corrections before SHM at cycle 112 are rejected for this criterion (second peak in february 2019). When removing these cycles, percentage of edited measurements drops to 0.82%. The rate of rejected data for Jason-3 is quite equivalent as for Jason-2 (0.93%). As in case of Jason-3, higher points on Jason-2 monitoring are mainly due to Jason-2 wet troposphere contribution, where AMR was unavailable during cycle 285 (Jason-3 cycle 5), cycle 326 (Jason-3 cycle 45), and for restart after SHM, leading to an increase of the quantity of edited data (point out of plot scale).

Otherwise the overall performance of Jason-3 system is in excellent agreement with Jason-2, and shows very close results in terms of edited data.

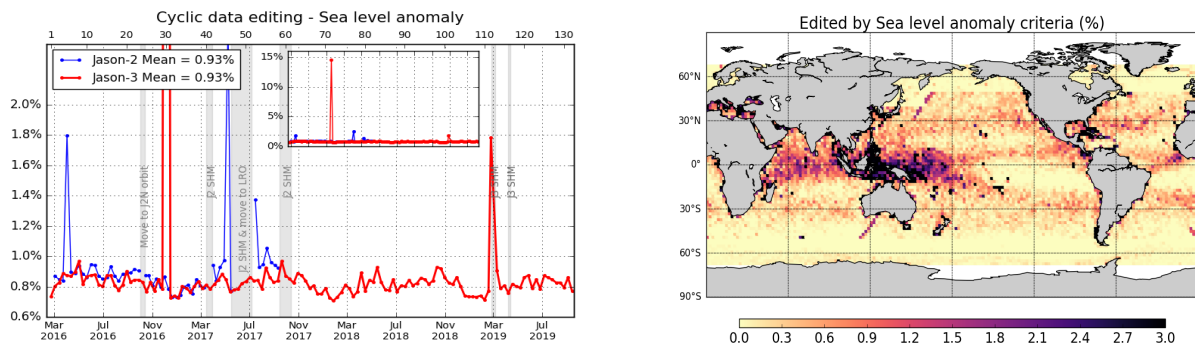


Figure 19 – Percentage of edited measurements by sea level anomaly threshold criterion. Left: Cycle per cycle monitoring compared with Jason-2. Right: Jason-3 averaged map from cycle 96 to 132.

4. Monitoring of altimeter and radiometer parameters

4.1. Methodology

Mean and standard deviation of Jason-3 main parameters have both been monitored since the beginning of the mission. Moreover, a comparison with Jason-2 parameters has been performed: it allows to monitor the bias between the parameters of the 2 missions.

- Till Jason-3 cycle 23, Jason-3 and Jason-2 are on the same ground track and are spaced out about 80 seconds apart (tandem phase), the mean of the Jason-2 - Jason-3 differences can be computed using a point by point repeat track analysis (referred as 'residuals' in plots).
- From Jason-3 cycle 24, a maneuver sequence was conducted (from end of Jason-2 cycle 303) to move Jason-2 to the new formation flight mission orbit. Jason-2 has a repeat ground-track which is interleaved with Jason-3. It is the same ground-track as already used by Topex/Poseidon during its formation flight phase with Jason-1, and Jason-1 with Jason-2. Because of a time shift of 5 days, geographical variations are then too strong to directly compare Jason-3 and Jason-2 parameters on a point by point basis. Therefore day per day global differences have been carried out to monitor differences between the two missions. A filter over 11 days was applied. Nevertheless the differences are still quite noisy, especially for corrections which vary rapidly in time and space. Therefore occasional small jumps might be covered by the noise of the differences. Nevertheless it should be possible to detect drifts and permanent jumps. Jason-3 and Jason-2 were in this formation flight phase from Jason-3 cycles 25 to 46 (Jason-2 cycles 305 to 327).

In March and May 2017, Jason-2 experienced several safe holds caused by gyro anomalies. It was decided to move Jason-2 to an End-of-Life (EOL) Long Repeat Orbit (LRO). Jason-2 mission phase is detailed in [115]. Science data on the first LRO are available from 11th of July 2017 to 16th of July 2018. Note that the first cycle on the new orbit starts with cycle 500 (this corresponds to mid-Jason-3 cycle 52) and this first interleaved ground track ends on cycle 537 (end of Jason-3 cycle 89). Note that after this first LRO, Jason-2 was moved to a second interleaved ground track (iLRO) on 18th of July 2018. Science data restart on 25th of July 2018 with cycle 600. Jason-2 mission ended on October 1st 2019 during cycle 644.

As during the formation flight phase, day per day global differences of the parameters have been carried out to monitor differences between the two missions (only until Jason-2 cycle 506 (14th of September 2017)): differences are done over Jason-3 cycles 1 to 58, corresponding to Jason-2 cycles 281 to 506.

4.2. 20Hz range measurements

The monitoring of the number and standard deviation of 20 Hz elementary range measurements used to derive 1 Hz data is presented here. These two parameters are computed during the altimeter ground processing. For both Jason-2 and Jason-3, before performing a regression to derive the 1 Hz range from 20 Hz data, a MQE (mean quadratic error) criterion is used to select valid 20 Hz measurements. This first step of selection consists in verifying that the 20 Hz waveforms can be approximated by a Brown echo model (Brown, 1977 [49]) (Thibaut et al. 2002 [101]).

Then, through an iterative regression process, elementary ranges too far from the regression line are discarded until convergence is reached. Thus, monitoring the number of 20 Hz range measurements and the standard deviation computed among them is likely to reveal changes at instrumental level.

4.2.1. 20 Hz range measurements number in Ku-Band and C-Band

Jason-3 number of elementary 20 Hz range measurements starts with values slightly higher than Jason-2 until cycle 3. During cycle 3, new calibration (CAL2) filter turned the square off-nadir angle to zero, which implies the absence of waveform mispointing, a higher MQE and a smaller number of elementary measurements. Then from cycle 4 onwards, Jason-3 number of elementary 20 Hz range measurements is very similar to Jason-2 with an average of 19.61 versus 19.60 in Ku-band (left of figure 20) and 19.24 versus 19.25 in C-band (right of figure 20).

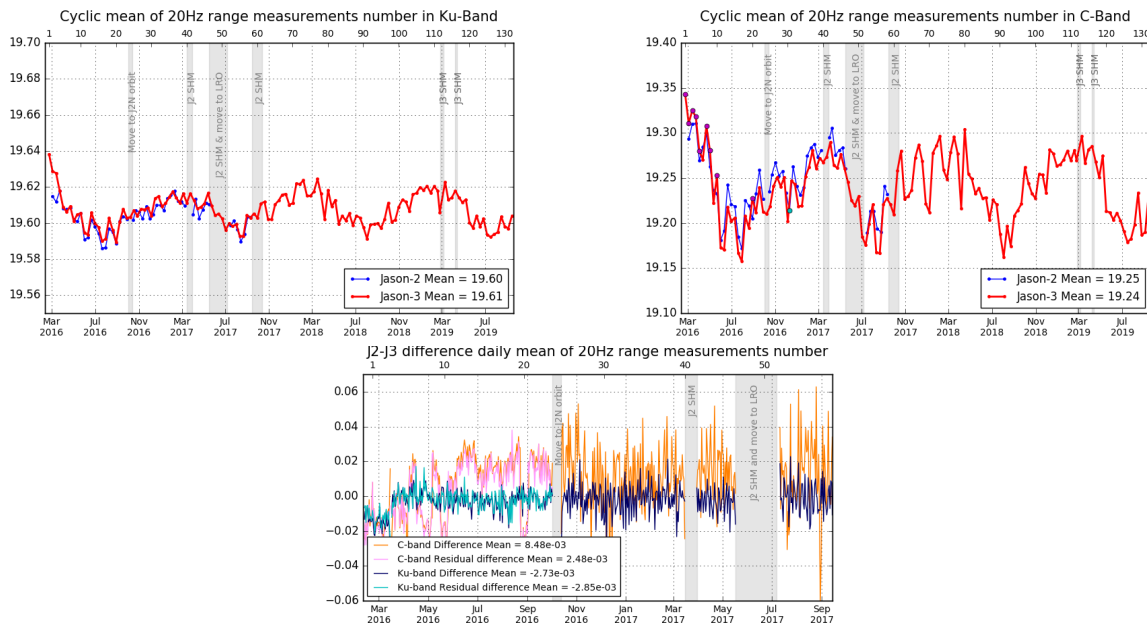


Figure 20 – **Top:** Cyclic monitoring of number of elementary 20 Hz range measurements for Jason-2 and Jason-3 for Ku-band and C-band. **Bottom:** Jason-2 - Jason-3 difference daily monitoring of elementary 20 Hz range measurements number (until september 2017).

Elementary number of measurements used to compute a 1Hz measurement is correlated to significant wave height (4.5.): figure 21 shows less elementary range measurements around Indonesia, the Mediterranean Sea and close to coasts, which are all regions of low significant wave heights.

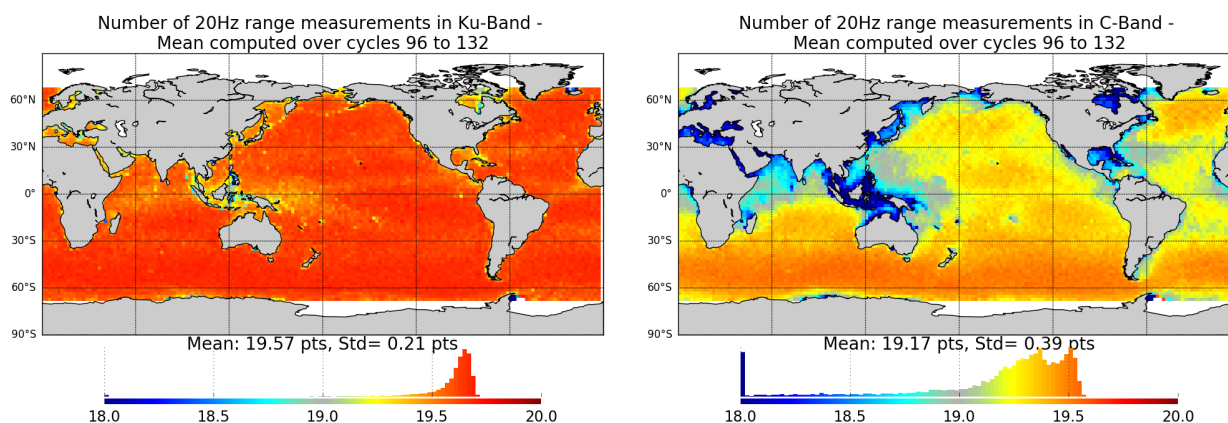


Figure 21 – Map of number of 20 Hz range measurements for Jason-3 averaged over cycles 96 to 132, in Ku-band (left) and in C-band (right).

4.2.2. 20 Hz range measurements standard deviation in Ku-Band and C-Band

Figure 22 shows the monitoring of Jason-3 and Jason-2 20 Hz range measurements standard deviation, in Ku-band (left) and C-band (right). Jason-3 standard deviation of the 20 Hz measurements is 7.99 cm for Ku-Band and 17.56 cm for C-Band. It is similar to Jason-2 data (8.00 cm in Ku-Band and 17.43 cm in C-Band). 20 Hz range measurements standard deviation is higher on C-band than on Ku-band due to the onboard averaging that is performed over less waveforms (onboard averaging of 90 measurements for each 20Hz Ku-band value, against 15 in case of C-band), which leads to an increased noise.

Standard deviation of measurements is correlated to significant wave height (swh dedicated part: 4.5.).

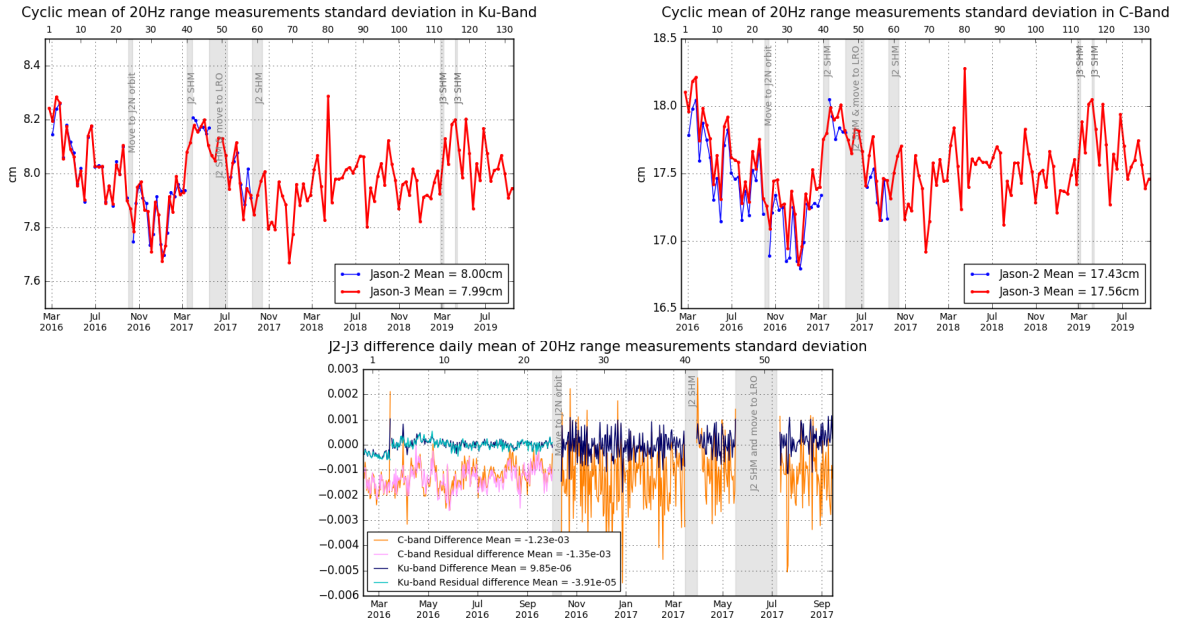


Figure 22 – **Top:** Cyclic monitoring of elementary 20 Hz range measurements standard deviation for Jason-2 and Jason-3 for Ku-band and C-band. **Bottom:** Jason-2 - Jason-3 difference daily monitoring of elementary 20 Hz range measurements standard deviation.

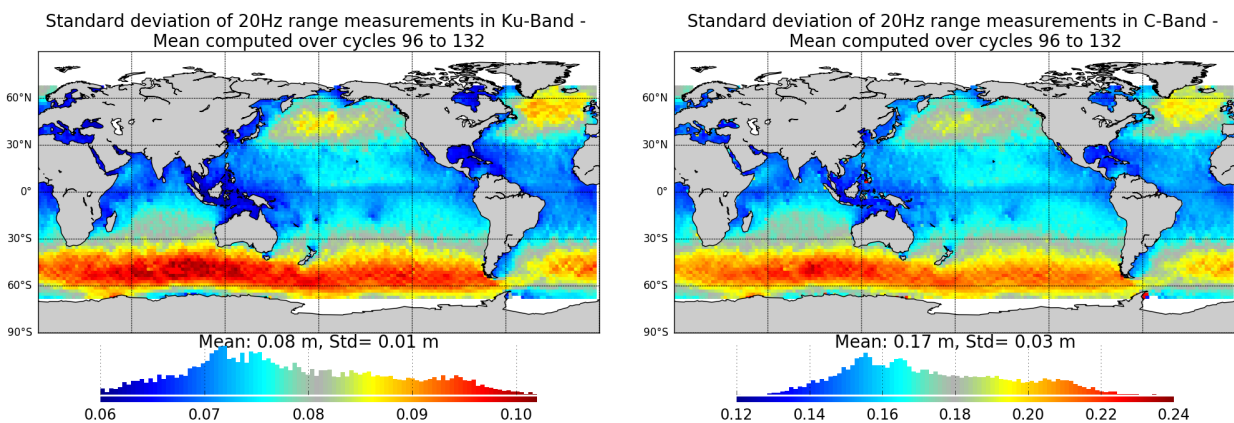


Figure 23 – Map of 20 Hz range measurements standard deviation for Jason-3 averaged over cycles 96 to 132, in Ku-band (left) and in C-band (right).

4.3. Off-Nadir Angle from waveforms

The off-nadir angle is derived from the slope of the trailing edge of the waveform during the altimeter processing: it can either be caused by real platform mispointing or by backscattering properties of the surface. The square of the off-nadir angle, averaged on a cyclic basis (taking into account valid measurements only), has been plotted for Jason-3 and Jason-2 on figure 24.

At the beginning of the mission, Jason-3 altimeter mispointing was deeply analysed to understand the negative values observed from cycle 3 after GPS upload. Mispointing is actually related to CAL2 filter shapes, which depends on automatic gain control settings for Jason-3. During the first cycles, the in-flight calibration (CAL2) filters were measured using a different Automatic Gain Control code than the one used during waveform acquisition over ocean, in order to optimize the CAL2 measurement numerical accuracy (quantification optimization). It has however an impact on the filter slope and fully explains the observed mispointing negative values. The filter slope was modified during cycle 14 (June 26th, 2016) and explains the jump to zero on the IGDR curve. This correction was applied during GDR production, which explains the difference between red and green curves between cycles 4 and 14, so that GDR mispointing has been close to zero from cycle 4.

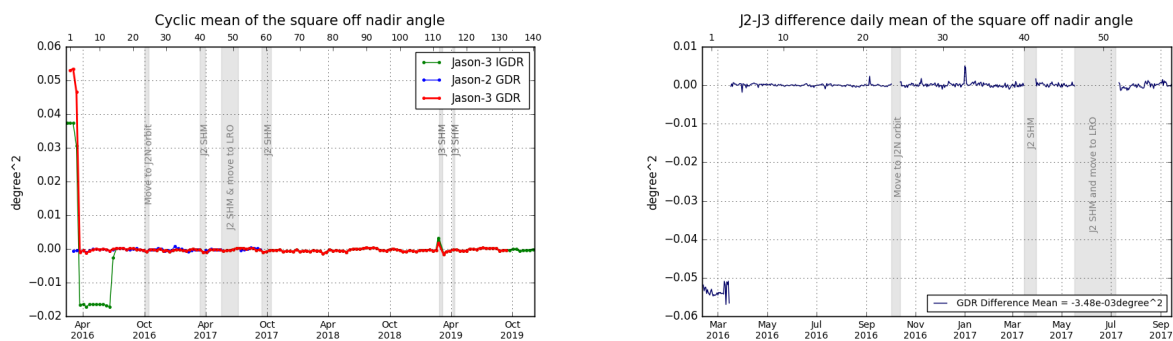


Figure 24 – **Left:** Cyclic monitoring of the square off-nadir angle for Jason-2 and Jason-3 for GDRs (blue and red curves) and Jason-3 IGDRs (product IGDR for cycles 1 to 41, and IGDR L2P from cycle 25 to 132 in green). **Right:** Jason-2 - Jason-3 difference daily monitoring of the square off-nadir angle (GDR data).

Except round SHM in early 2019, no mispointing event occurred on Jason-3 over the considered period. The map figure 25 is generally slightly negative, except for regions around Indonesia, and close to coasts.

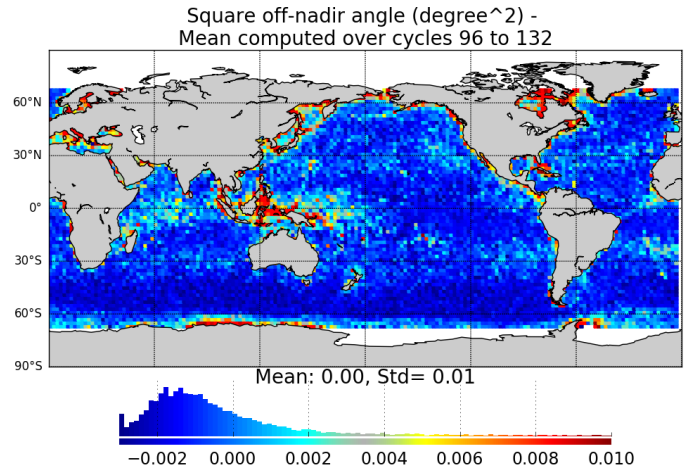


Figure 25 – Map of the square off-nadir angle for Jason-3 averaged over cycles 96 to 132.

Without taking into account the three first cycles, square off-nadir angle is monitored year by year on the left part of figure 26, highlighting a small annual signal (global mean is higher during summer). Also, a small higher value of square off-nadir angle is visible before SHM at cycle 112 . Square off-nadir angle slightly depends on significant wave height as shown on right part of figure 26: considering this monitoring for swh between 2m and 6m, slope is $-0.0004\text{deg}^2/\text{m}$.

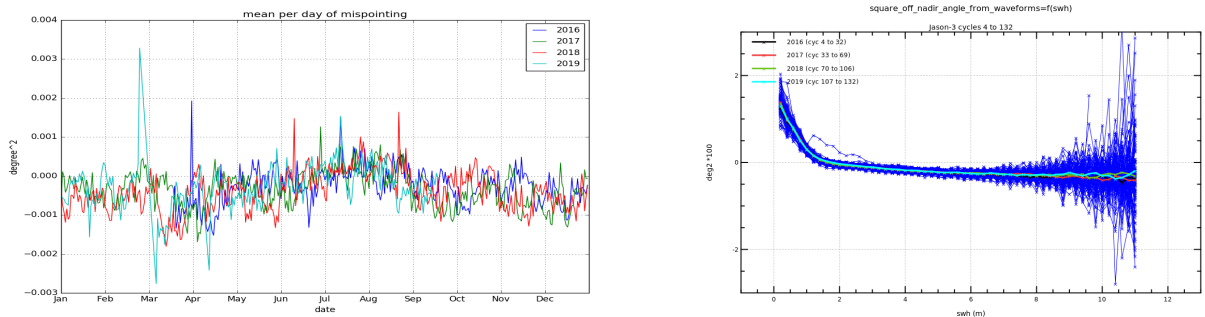


Figure 26 – **Left:** Mean per day of mispointing for Jason-3 from cycle 4. **Right:** Square off nadir angle against swh.

4.4. Backscatter coefficient

The Jason-3 Ku-band and C-band backscatter coefficients show good agreement with Jason-2 as visible on cyclic monitoring (figure 28). Jason-3 backscatter coefficient is about 13.75 dB for Ku-band (15.50 dB for C-band) while for Jason-2 it is about 13.51 dB (15.40 dB). The difference between the two missions is about -0.24 dB (-0.10 dB) and present a good stability. However, this was different from cycle 0 to cycle 4, where slight mispointing on Jason-3 caused higher differences of σ_0 between missions.

During the tandem flight, Jason-3 σ_0 was modified with a new altimeter characterization file, an update of the look up tables (Patch 6) and a new CAL2 filter (cycle 14, June 26th, 2016). All of them were applied on all GDR cycles. As a consequence, there is a bias between backscatter coefficient in GDR and IGDR products until cycle 14. In addition, a new AMR calibration file is applied for IGDR cycle 17 (see part 4.7.), so that IGDR and GDR σ_0 are slightly different until cycle 17 due to atmospheric attenuation applied to σ_0 (as the atmospheric attenuation is derived from radiometer parameters).

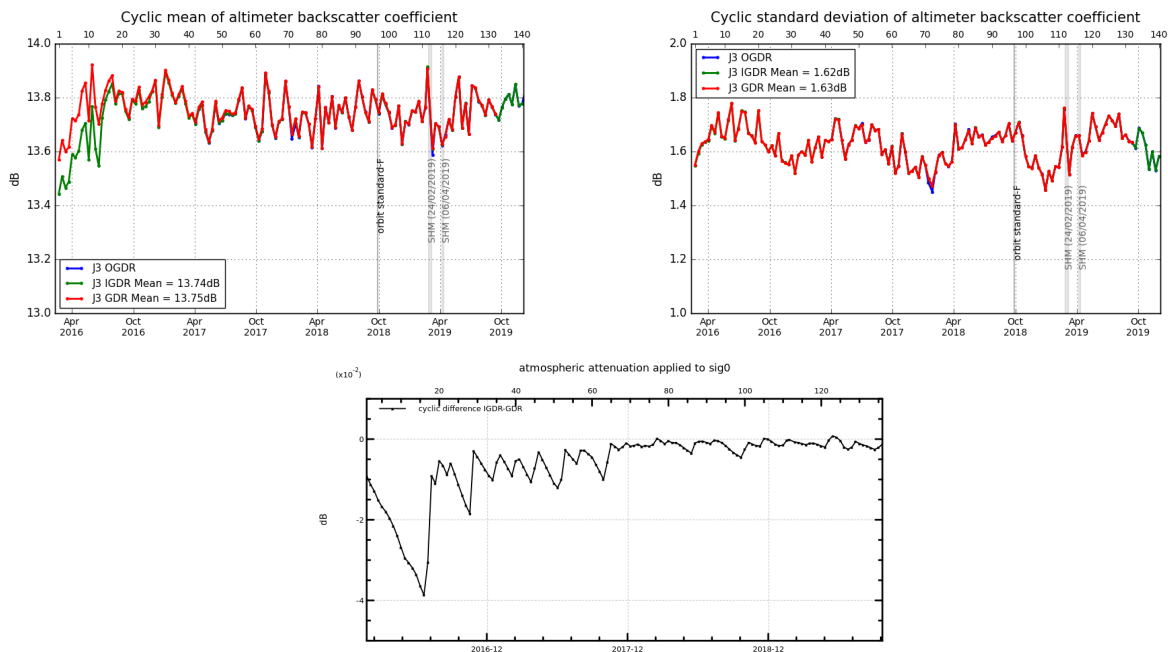


Figure 27 – **Top:** Cyclic monitoring of backscatter coefficient for Jason-3 (Ku-band) **OGDR/IGDR/GDR**. **Bottom:** difference of atmospheric attenuation applied to σ_0 between IGDR and GDR products.

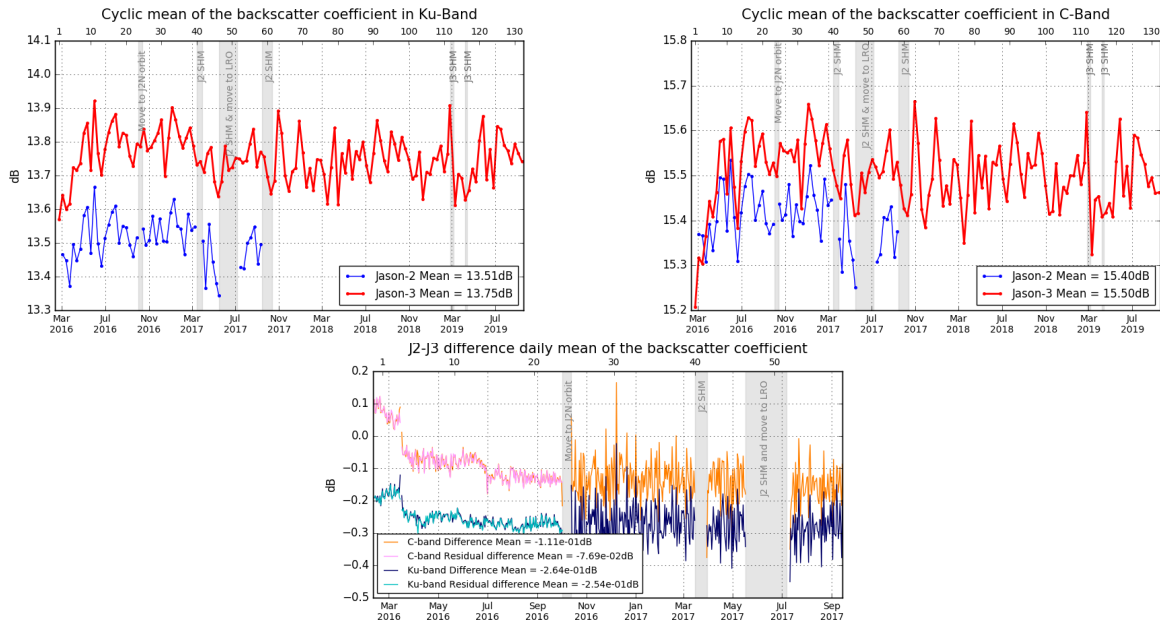


Figure 28 – **Top:** Cyclic monitoring of backscatter coefficient for Jason-2 and Jason-3 for Ku-band (left) C-band (right). **Bottom:** daily monitoring of Jason-2 - Jason-3 GDR difference of the backscatter coefficient.

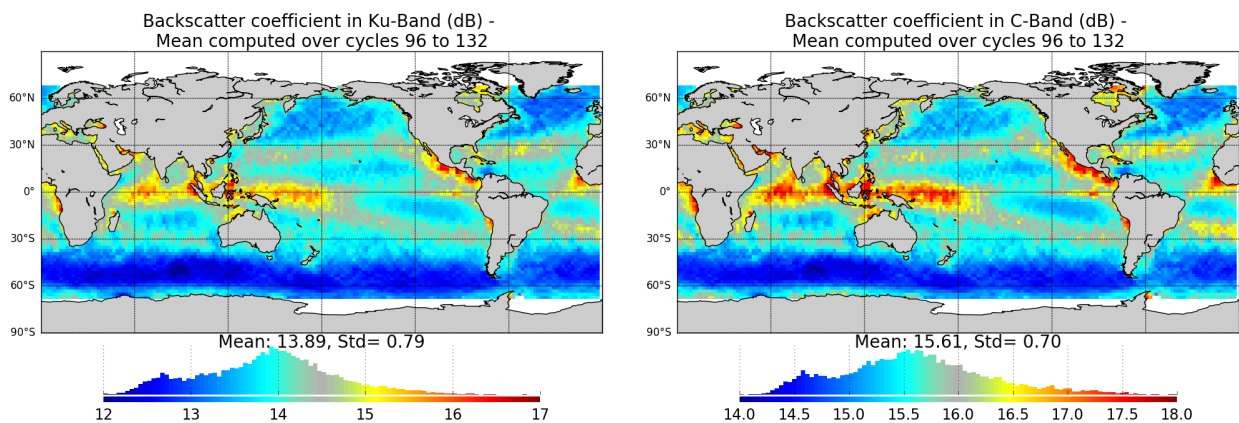


Figure 29 – Map of backscatter coefficient for Jason-3 averaged over cycles 96 to 132, in Ku-band (left) and in C-band (right).

4.5. Significant wave height

As for sigma0 parameter, a very good consistency between both Jason-2 and Jason-3 significant wave height is shown (see figure 31). In addition, until Jason-3 cycle 23 (tandem phase, observing the same ocean with only 1'20" apart), Jason-2 and Jason-3 measurements are identical. After Jason-2 move to interleaved orbit, the two missions are not as close as during tandem phase and measured swh are slightly different, but there is still no bias between Jason-2 and Jason-3 measured wave height in average (see bottom of figure 31).

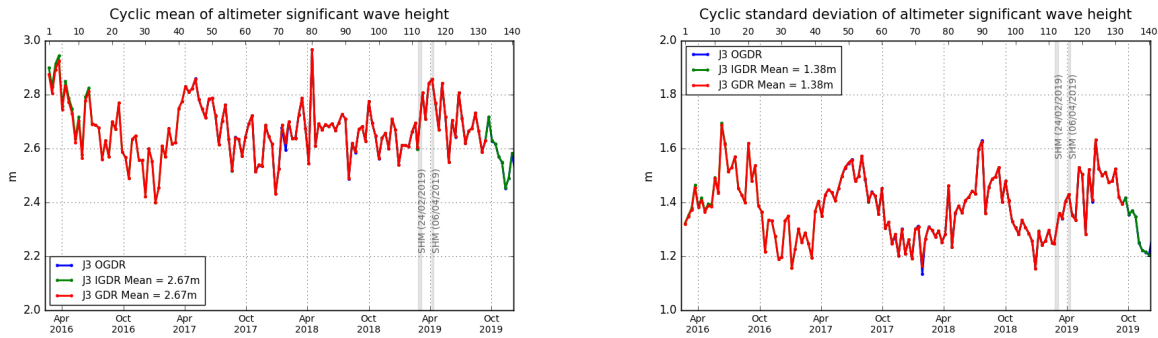


Figure 30 – Cyclic monitoring of significant wave height for Jason-3 (Ku-band) OGDR/IGDR/GDR.

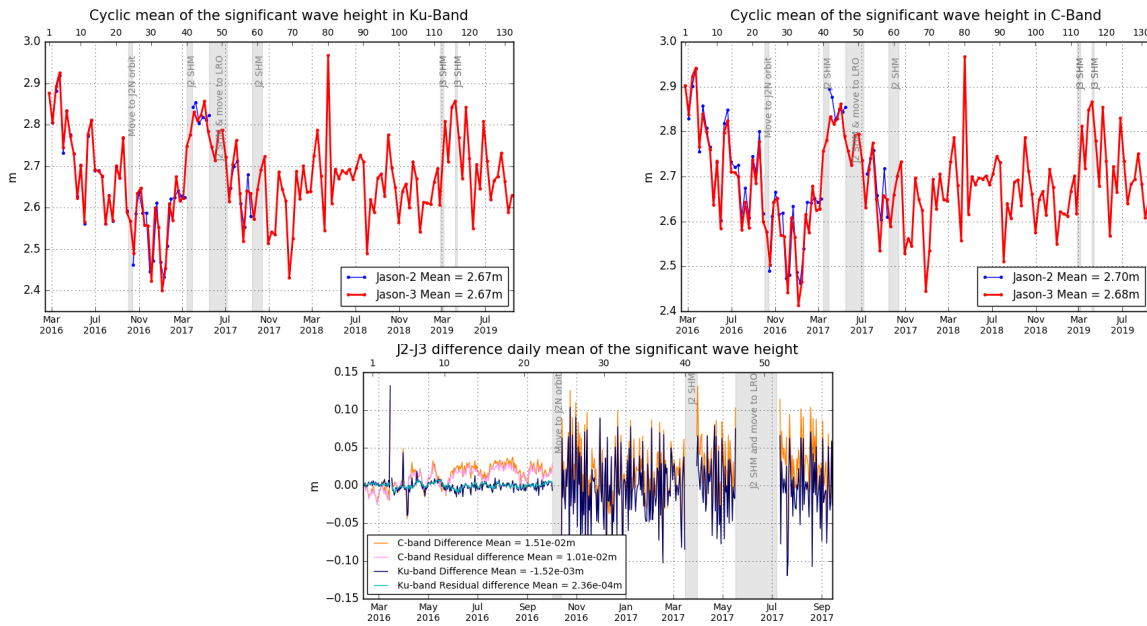


Figure 31 – Cyclic monitoring of significant wave height for Jason-2 and Jason-3 for Ku-band (left) and for C-band (right). Jason-2 - Jason-3 difference daily monitoring of significant wave height (bottom).

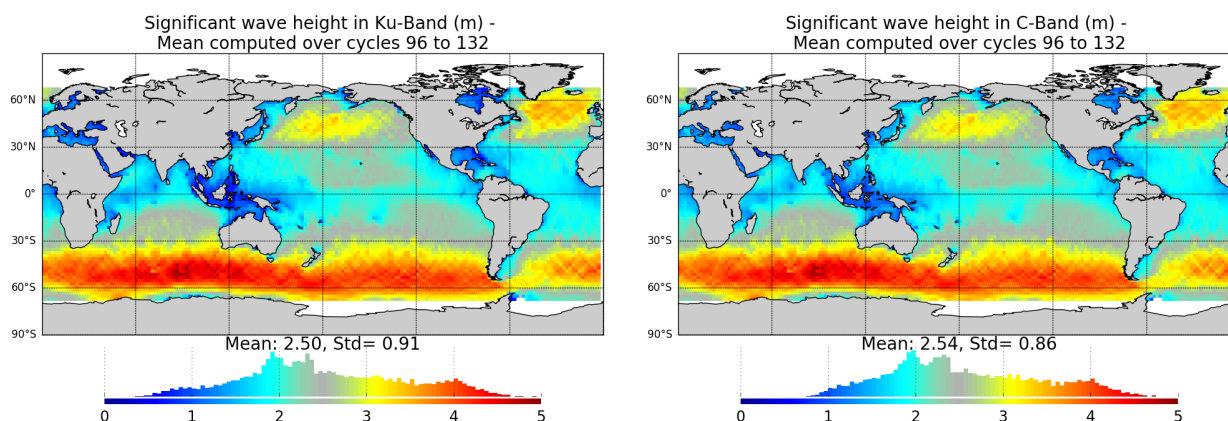


Figure 32 – Map of significant wave height for Jason-3 averaged over cycles 96 to 132, in Ku-band (left) and in C-band (right).

4.6. Dual-frequency ionosphere correction

The dual frequency ionosphere corrections derived from the Jason-3 and Jason-2 altimeters show a mean difference of about 0.87 cm (figure 33), with cycle to cycle variations lower than 1 mm.

Until the LUT changes that occurred during cycle 14 (for O/IGDRs), the mean bias between the two missions was 1 cm (for O/IGDRs). It turns then to 0.55 cm following “jumps” of Ku range (5 mm), C Range (1.5 cm) and sea state bias (0.1 mm). This event has an impact on Sea Level Anomalies retrieved from OGDRs and IGDRs products. For GDR products, the same LUT was used for the whole mission period, hence the absence of jump (see bottom and right of figure 33).

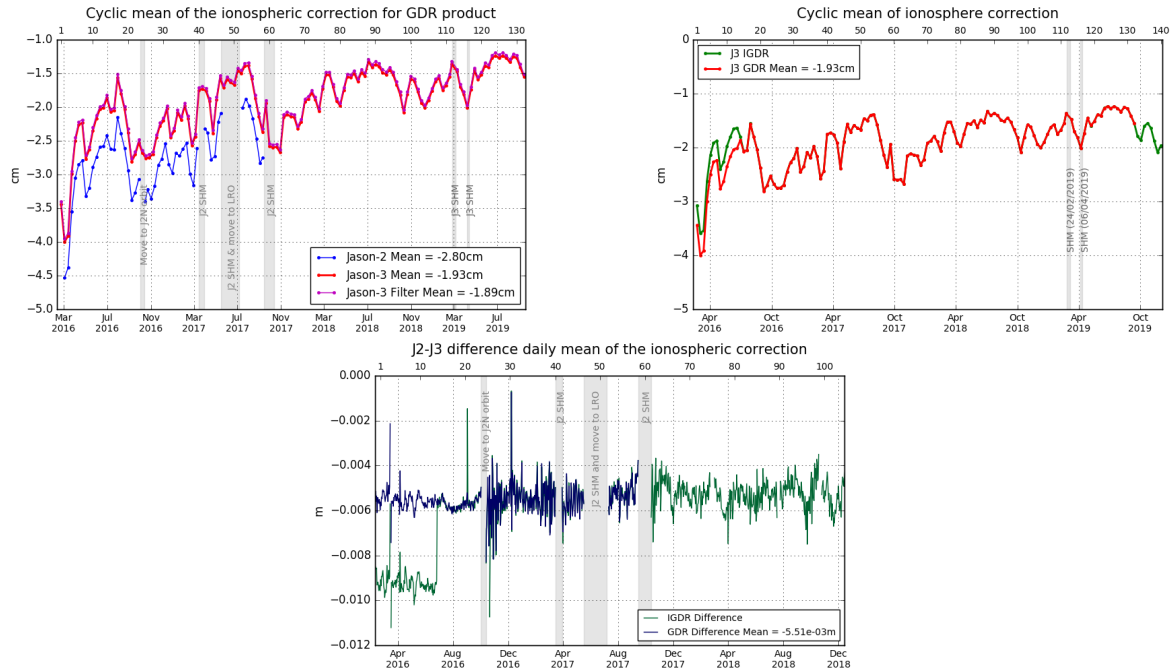


Figure 33 – Cyclic monitoring of ionospheric correction for Jason-2 and Jason-3. (left). Cyclic monitoring of Jason-3 ionospheric correction for IGDR and GDR data (right). Jason-2 - Jason-3 difference daily monitoring of ionospheric correction (bottom).

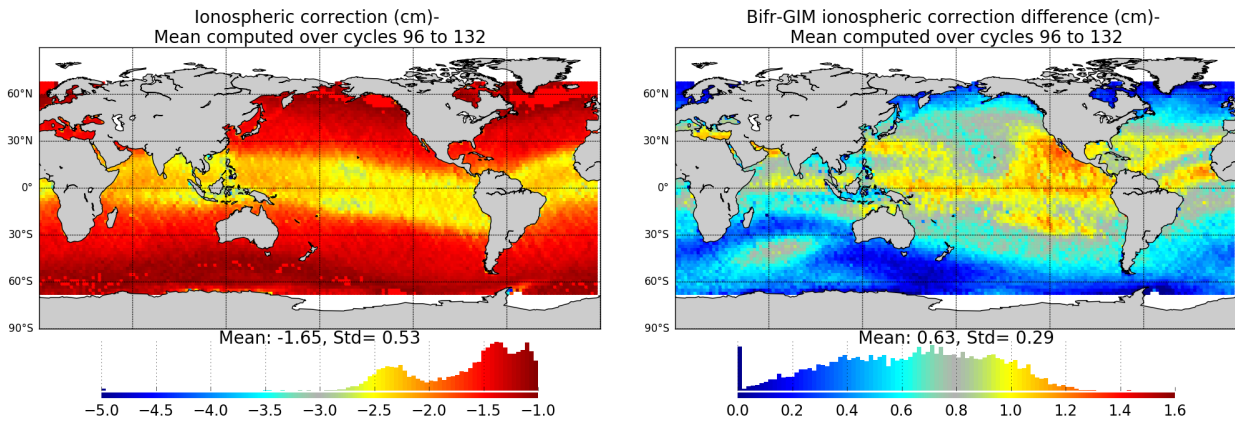


Figure 34 – Left: Map of ionospheric correction for Jason-3 averaged over cycles 96 to 132. Right: Map of dual-frequency minus GIM ionospheric correction solutions.

When comparing altimeter ionosphere correction to GIM correction (figure 35), mean as well as standard deviation of this difference present same variation for both missions.

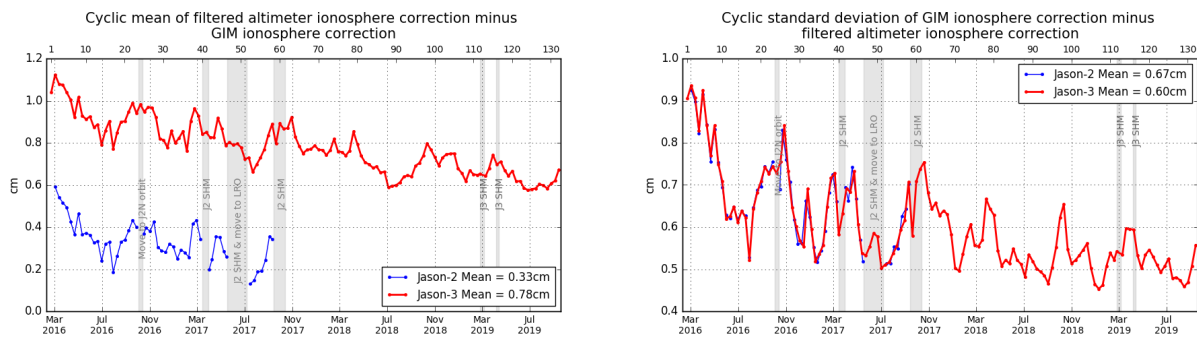


Figure 35 – Cyclic monitoring of GIM ionosphere correction minus filtered altimeter ionosphere correction for Jason-2 and Jason-3. Left: mean, right: standard deviation.

4.7. AMR Wet Troposphere Correction

4.7.1. Overview

In order to evaluate radiometer wet troposphere correction, liquid water content, water vapour content and atmospheric attenuation, Jason-3 uses a three-frequency AMR radiometer (18.7, 23.8 and 34.0 GHz), similar to the one used on Jason-2.

Note that the 23.8 GHz channel is the primary water vapor sensing channel, meaning higher water vapor concentrations leads to larger 23.8 GHz brightness temperature values. As a consequence, top right and bottom right parts of figure 36 are correlated. Moreover, the 34 GHz channel and the 18.7 GHz channel, which have less sensitivity to water vapor, facilitate the removal of the contributions from cloud liquid water and excess surface emissivity of the ocean surface due to wind, which also act to increase the 23.8 GHz brightness temperature.

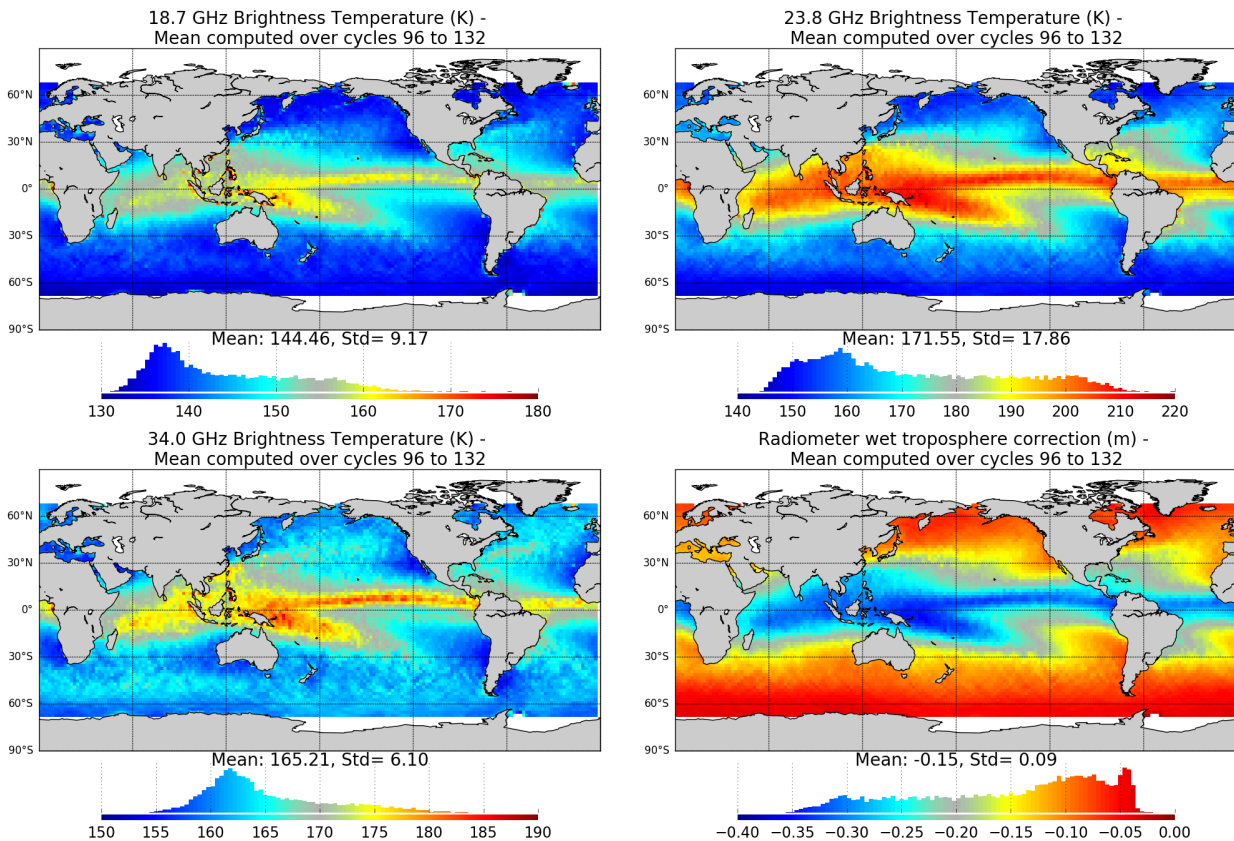


Figure 36 – Map of Jason-3 brightness temperatures averaged over cycles 96to 132: 18.7 Ghz channel (top left), 23.8 Ghz channel (top right) and 34.0 Ghz channel (bottom left). Map of AMR wet troposphere correction for Jason-3 averaged over cycles 96 to 132(bottom right)

4.7.2. Comparison with the ECMWF model

The wet troposphere correction computed from ECMWF model data has been used to check the Jason-2 and Jason-3 radiometer corrections. The cross-comparison between all radiometers and models available is necessary to analyze the stability of each wet troposphere correction. An overview of the wet troposphere correction importance for mean sea level is given in Obligis et al. [84]. The difference between AMR and model data is computed on a daily basis and is plotted on figure 37 for Jason-3 IGDR and GDR, and Jason-2 GDR for comparisons. As observed, Jason-3 AMR correction has a drift of more than half a millimetre per cycle for IGDRs (and OGDRs, not shown). Such behaviour is routinely monitored by JPL instrument expert team. Impact of drift is corrected through ground calibration (ARCS, Autonomous Radiometer Calibration System), also accounting for cold sky calibrations. The first ARCS calibration occurred at the end of cycle 17 and is visible on IGDR monitoring. As regards GDR data, AMR radiometer correction is calibrated at each cycle and the calibration coefficients are modified if necessary. It allows to correct the drift for GDR data (red curve on figure 37), nevertheless small drifts and jumps persist of up to 2 mm amplitude.

Due to an ECMWF model change of version on June 6th 2019, a jump is visible in the monitoring of radiometer minus model wet troposphere correction mid-2019.

In GDR, Jason-3 AMR-ECMWF model daily difference is about 6.6 mm and about 5.3 mm for Jason-2. Though Jason-3 radiometer wet troposphere correction is more stable for GDRs, Jason-3 and Jason-2 do not have exactly the same behaviour, with an inflexion point around cycle 13 and another one after Jason-2 moved to its new interleaved groundtrack on October 2016. With 2017 Safe Hold Modes, Jason-2 shows some jumps that are known to occur after restart.

Standard deviation of radiometer minus model wet troposphere correction is equivalent around 1.2 cm for both missions (right side of figure 37).

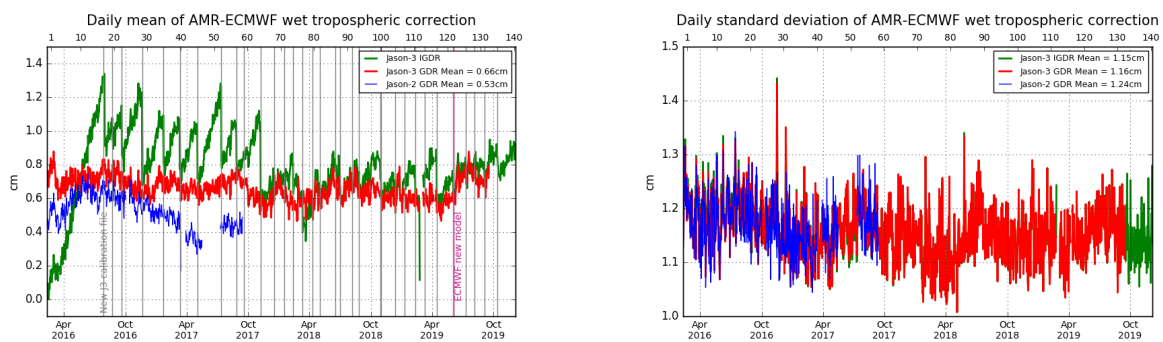


Figure 37 – Daily monitoring of AMR minus ECMWF model wet tropospheric correction. mean (left) and standard deviation (right)

4.8. Altimeter wind speed

Jason-3 and Jason-2 present very close results in terms of wind speed. Jason-2 provides higher wind values than Jason-3 (7.80 vs 7.56 m.s⁻¹, figure 38). The difference between the two missions is 0.24 m.s⁻¹ and can be separated in two phases: before and after 16-03-2016. The uploading of updated parameters for STR1 and gyros to correct misalignments occurred on March, 16th 2016 (Cycle 3) and corrected the square off nadir angle, i.e. the mispointing of the platform. Then from the restart of data production (March 18th) mispointing was set to value close to zero, which increases the sigma0 and decreases the wind speed.

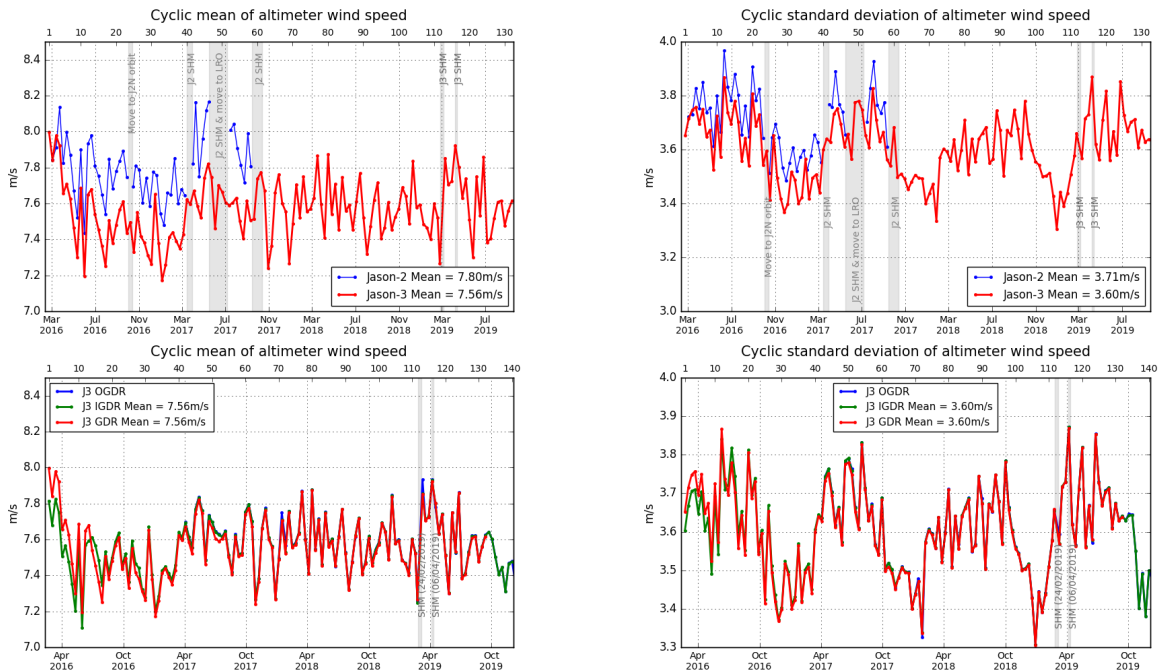


Figure 38 – Cyclic monitoring of altimeter wind speed mean (left) and standard deviation (right). **Top:** for Jason-2 and Jason-3. **Bottom:** for Jason-3 GDR, IGDR and OGDR data.

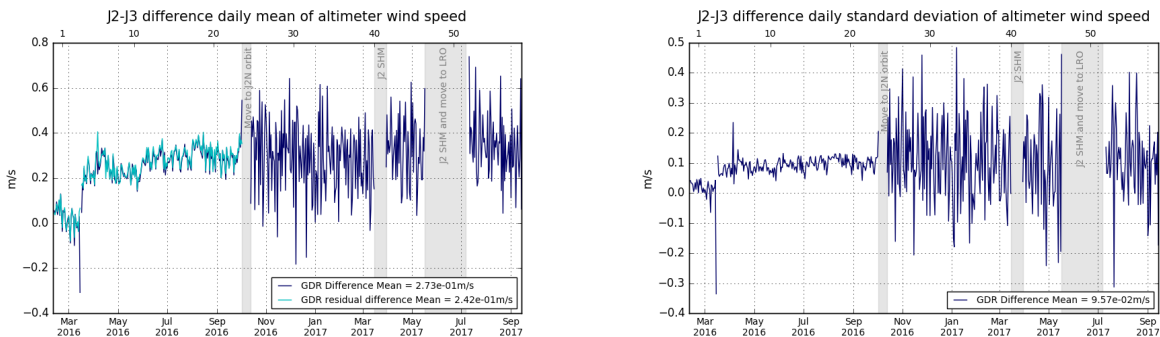


Figure 39 – Jason-2 - Jason-3 difference daily monitoring of altimeter wind speed mean (left) and standard deviation (right).

4.9. Sea state bias

GDR Sea state bias (SSB) in Ku band from Jason-3 (-8.40 cm) and Jason-2 (-8.44 cm) present an excellent agreement both in average and in standard deviation (4.62 cm vs 4.61 cm, respectively).

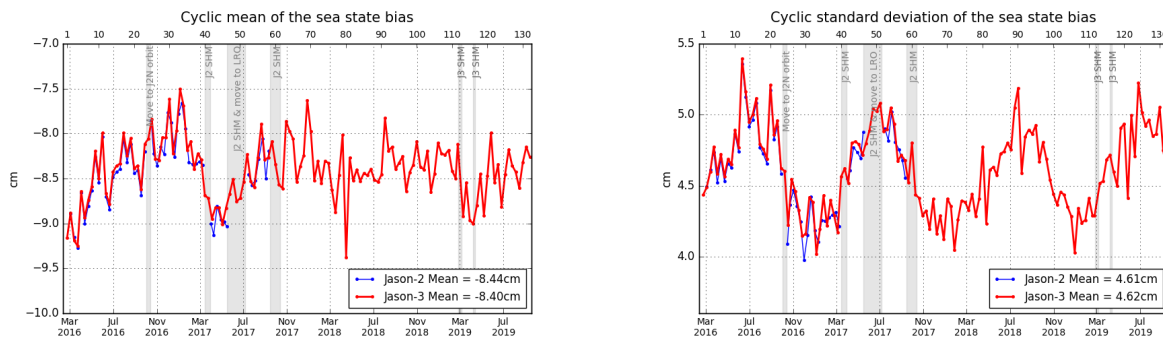


Figure 40 – Cyclic monitoring of the sea state bias mean and standard deviation for Jason-2 and Jason-3

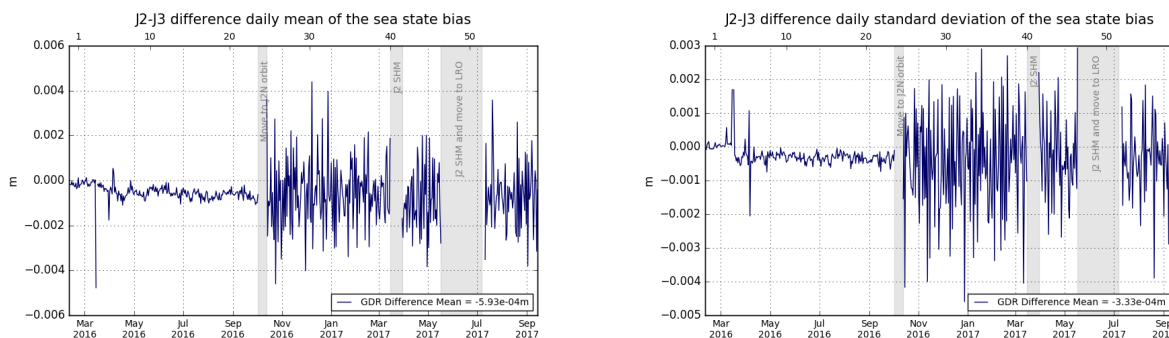


Figure 41 – Jason-2 - Jason-3 difference daily monitoring of the sea state bias mean (left) and standard deviation (right).

Improving the continuity of the Jason SSB time-series (Tran&al. work [120])

Most of the operational versions of the Sea State Bias (SSB) correction are computed empirically with the non parametric estimation technique based on kernel smoothing described in Gaspar et al [2002]. These solutions are derived from 10-day SSH differences (i.e. collinear analysis of repeat cycles of data or from crossover differences). Since only SSB differences are observed, the SSB solution can only be determined to within a constant when solving the equation system. This leads to potentially observe some solution shift related to the imposed constraint to have a SSB value equal to 0 for a flat surface between two versions of the SSB correction. This (constant) shift can reach a few centimeters when the SSB correction version is updated to consider SSH standard changes due to large uncertainty in data-poor region close to (SWH=0, WS=0) to correctly constrain the estimation of SSB(0, 0). This causes annoying disturbances every time that SSB solutions are updated for the monitoring of multi-mission altimeter biases at in-situ Cal/Val sites or for the intermission bias alignment needed to tie up the different global mean sea level time-series together. Tran &al. [120] propose changes in SSB model development to tackle/reduce the SSB constant shift issue that exists between different correction versions for a same altimetric mission or for different missions all operating at a same radar frequency and having the same data processing. The work focused on the Jason altimeters time-series, both Ku-band MLE4 and C-band data, to better connect the past and current missions. Tests with other data have also been performed (Sentinel-3A data) along with update of the 3D

SSB computation approach based on SSH differences data [Tran et al, 2016].
They concluded when the processing of the altimeter data is the same for different missions in Ku-band, the associated SSB solutions computed with the 2018 version of the non-parametric approach display very good agreement at the mm level.

5. SSH crossover analysis

5.1. Overview

SSH crossover differences are the main tool to estimate the whole altimetry system performances. They allow to analyze the SSH consistency between ascending and descending passes: it should not be significantly different from zero. More importantly, special care is given to the geographical homogeneity of the mean difference at crossovers. However in order to reduce the impact of oceanic variability, we select crossovers with a maximum time lag of 10 days. Mean and standard deviation of SSH crossover differences are computed from the valid dataset to perform maps or a cycle by cycle monitoring over all the altimeter period. In order to monitor the performances over stable surfaces, additional editing is applied to remove shallow waters (bathymetry above -1000m), areas of high ocean variability (variability above 20 cm rms) and high latitudes ($> |50|deg$). SSH performances are then always estimated with equivalent conditions. The main SSH calculation for Jason-3 (and Jason-2) are defined below.

$$SSH = Orbit - Altimeter Range - \sum_{i=1}^n Correction_i$$

with $Jason - 3 Orbit = CNES orbit$ for GDR products, and

$$\begin{aligned} \sum_{i=1}^n Correction_i &= \text{Dry troposphere correction} \\ &+ \text{Dynamical atmospheric correction} \\ &+ \text{Radiometer wet troposphere correction} \\ &+ \text{Dual frequency ionospheric correction} \\ &+ \text{Non parametric sea state bias correction} \\ &+ \text{Ocean tide correction (including loading tide)} \\ &+ \text{Earth tide height} \\ &+ \text{Pole tide height} \end{aligned}$$

In this part, performance indicators from IGDR input products or IGDR L2P (used in DUACS system) are presented. L2P updates that are then applied (ocean tide correction, mean sea surface model, mog2d dynamical atmospheric correction) are detailed in [123]. Note that comparisons between Jason-3 and Jason-2 have been done from Jason-3 cycle 1 to 58 only (Jason-2 cycles 281 to 506).

5.2. Mean of SSH crossover differences

The cycle by cycle mean of SSH differences is plotted in figure 42 for Jason-3 for OGDRs, IGDRs and GDRs. Mean of SSH differences at crossovers for Jason-3 IGDR products has noticeable negative values in average (-0.17cm for IGDR versus -0.04cm for GDR). A 120 days signal is visible for Jason-3 data, with a greater amplitude on GDR than IGDR (investigation in [23] dedicated to this topic): this signal is significantly reduced in GDR products after move to POE standard “F” in september 2018.

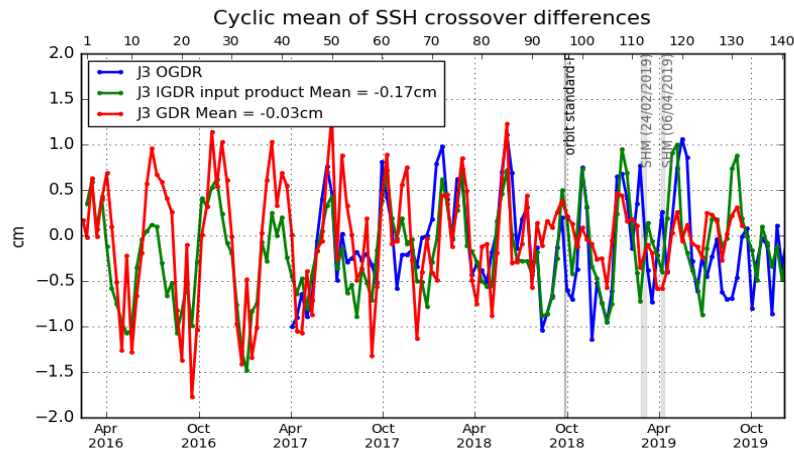


Figure 42 – Monitoring of mean of Jason-3 SSH crossover differences for OGDRs, IGDRs and GDRs. Only data with $|\text{latitude}| < 50^\circ$, bathymetry $< -1000\text{m}$ and low oceanic variability were selected. ($\text{ocean_tide_sol1} = \text{GOT}$ is used in SSH computation)

The maps of mean SSH crossover differences on figure 43 were calculated using GDR products for Jason-3 (left) and Jason-2 (right). These maps highlight equivalent small geographic patterns for Jason-3 and Jason-2.

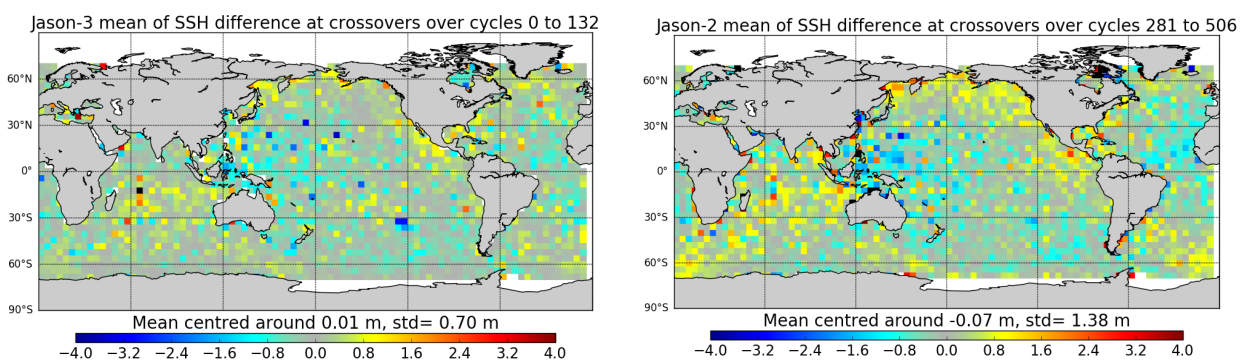


Figure 43 – Map of SSH crossovers differences mean for Jason-3 cycle 0 to 132(left) and for Jason-2 cycle 281 to 506 (right)

Dual-mission crossover performances are computed between Jason-3 and Jason-2 and presented figure 44. Mean SSH differences at Jason 3/Jason 2 crossovers is quite stable and around 3cm in average. The geographical pattern indicates some hemispheric biases, positive to the west, negative to the east. It corresponds to orbital signatures observed on sea surface height (right side of figure 44). Note that these 3 cm are due to processing differences as colocated Jason-2 minus Jason-3 non-corrected SLA (orbit - range - MSS) dif-

ferences averaged over the period of tandem phase (cycle 001 to 023) shows an equivalent bias (left side of figure 48).

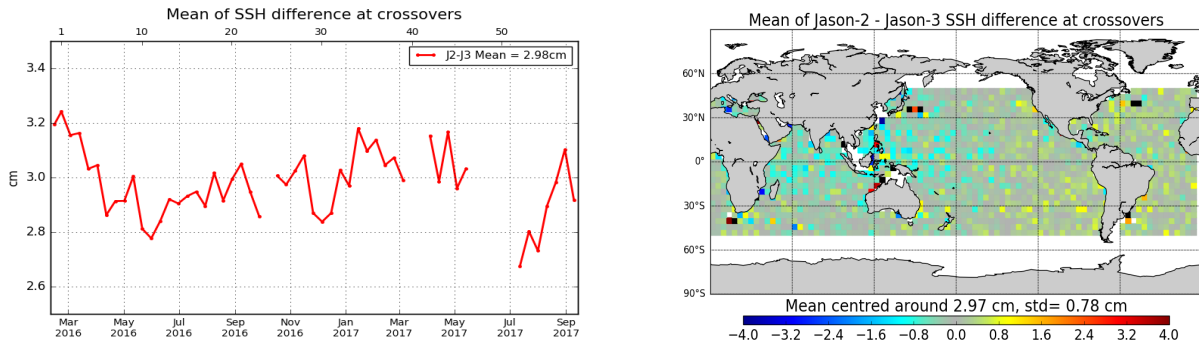


Figure 44 – Cyclic monitoring of Jason-2 - Jason-3 SSH crossover differences mean (left) and map over cycle 1 to 58 (right). Only data with $|latitude| < 50^\circ$, bathymetry $< -1000m$ and low oceanic variability were selected.

5.3. Standard deviation of SSH crossover differences

The cycle by cycle standard deviation of SSH crossovers differences are plotted for Jason-3 and Jason-2 in figure 45 after applying geographical criteria (bathymetry, latitude, oceanic variability). Both missions show very good performances, very similar and stable in time. No anomaly is detected. In GDR, the average figure is equivalent for both missions (4.90 cm rms for Jason-3, and 4.91 cm rms for Jason-2). This metric allows to estimate the system noise by dividing by $\sqrt{2}$ (3.48 cm).

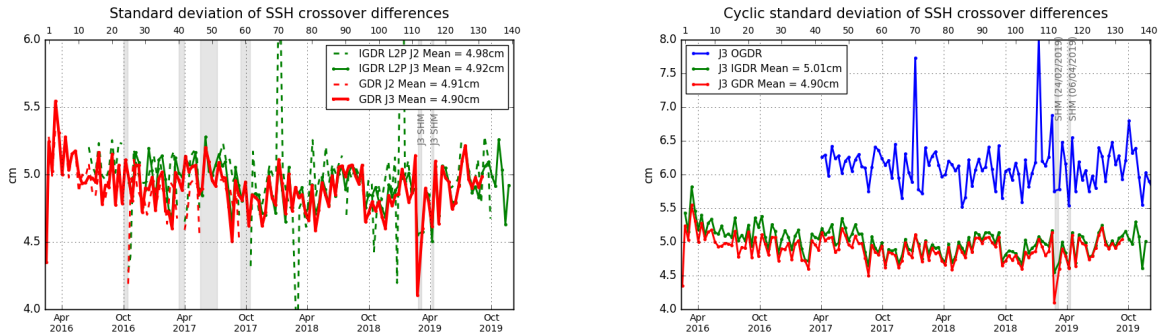


Figure 45 – Cycle by cycle standard deviation of SSH crossover differences for Jason-2 and Jason-3 (left), and for Jason-3 using OGDGs, IGDRs and GDRs (right). Only data with $|latitude| < 50^\circ$, bathymetry $< -1000m$ and low oceanic variability were selected.

5.4. Estimation of pseudo time-tag bias

The pseudo time tag bias (α) is found by computing at SSH crossovers a regression between SSH and orbital altitude rate (\dot{H}), also called satellite radial speed: $SSH = \alpha \dot{H}$.

This empirical method allows us to estimate the potential real time tag bias but it can also absorb other errors correlated with \dot{H} . Therefore it is called “pseudo” time tag bias. The monitoring of this coefficient estimated at each cycle is performed for Jason-2 and Jason-3 in figure 46. Both curves are very similar highlighting an almost 59-day signal with almost no bias (close to -0.03 ms for Jason-3). Both missions present 59 and 117 day signals. However, a near 90-day signal appears for Jason-3: using FES2014 ocean tide correction in SSH computation shows a reduction of 59-days signal and no 90-days signal (purple curve).

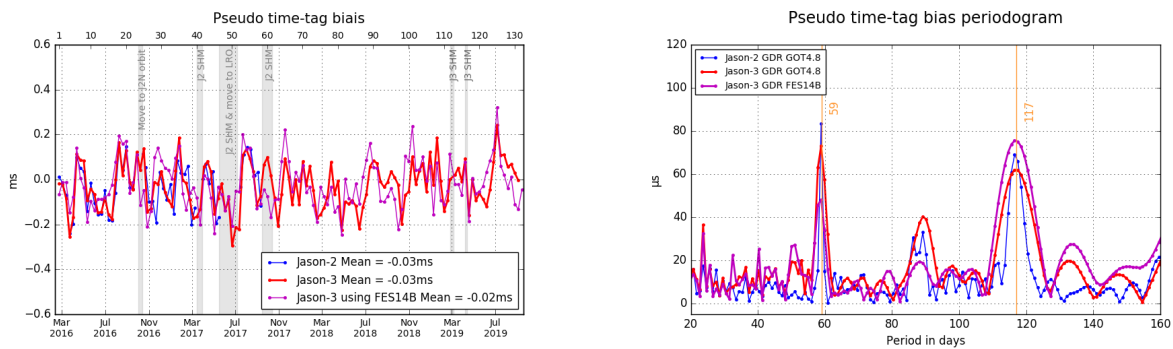


Figure 46 – Monitoring (left) and periodogram (right) of pseudo time-tag bias estimated cycle by cycle from GDR products for Jason-2 and Jason-3

6. Sea Level Anomalies (SLA) Along-track analysis

6.1. Overview

The Sea Level Anomalies (SLA) are computed along track from the subtraction of the mean sea surface to the SSH, with the SSH calculated as defined in previous section 5.1. : $SLA = SSH - MSS$. SLA analysis is a complementary indicator to estimate the altimetry system performances. It allows to study the evolution of SLA mean (detection of jump, abnormal trend or geographical correlated biases), and also the evolution of the SLA variance highlighting the long-term stability of the altimetry system performances. In order to take advantage of the Jason-3/Jason-2 tandem flight (cycles 1 to 23), we performed direct SLA comparisons between both missions during this period.

6.2. Mean of SLA differences between Jason-3 and Jason-2

The daily monitoring of mean SLA differences between Jason-2 and Jason-3 data over the tandem phase is plotted on figure 47, where this SSH bias is computed with and without the SSH corrections. During this period, both types of curves are very similar and stable in time with variations close to 1 mm rms, except that they are spaced out by a 0.75 cm bias (0.61 cm when using ECMWF model wet troposphere correction). This bias can result from differences between Jason-3 and Jason-2 sea state bias model used, and to a small amount due to ionosphere correction differences. The global average SSH bias is close to 2.98 cm using SSH corrections (2.84 cm when using ECMWF instead of radiometer wet troposphere correction) and 2.23 cm without. However, the more crucial point for scientific applications is to insure that there is no drift between both missions, since the global bias can be corrected a fortiori.

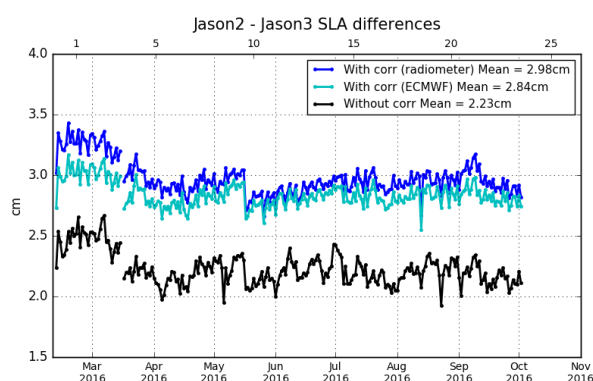


Figure 47 – Daily monitoring of SSH bias between Jason-2 and Jason-3 before Jason-2 moved to interleaved ground-track in October 2016: SSH bias without applying geophysical corrections (**black**) and with corrections using radiometer wet troposphere correction (**blue**) or using ECMWF model wet troposphere correction (**cyan**).

Colocated Jason-2 minus Jason-3 SLA differences averaged over the period of tandem phase (cycle 001 to 023) are shown on left side of figure 48. As both satellites measure the same oceanic features only 1'20" apart, only a weak hemispheric bias is visible (likely due to differences in orbit processing). Since Jason-2 has moved to its new interleaved orbit, maps of direct Jason-2 minus Jason-3 SLA measurements are no longer available. But differences of gridded SLA for Jason-2 and Jason-3 can be made. This difference is quite noisy for one cycle, especially as both satellites are shifted in time and sea state changes especially

in regions of high ocean variability. Therefore figure 48 shows an average over SLA grid differences from Jason-3 cycles 025 to 058. High variability regions as Gulf Stream and Antarctic circumpolar current are visible.

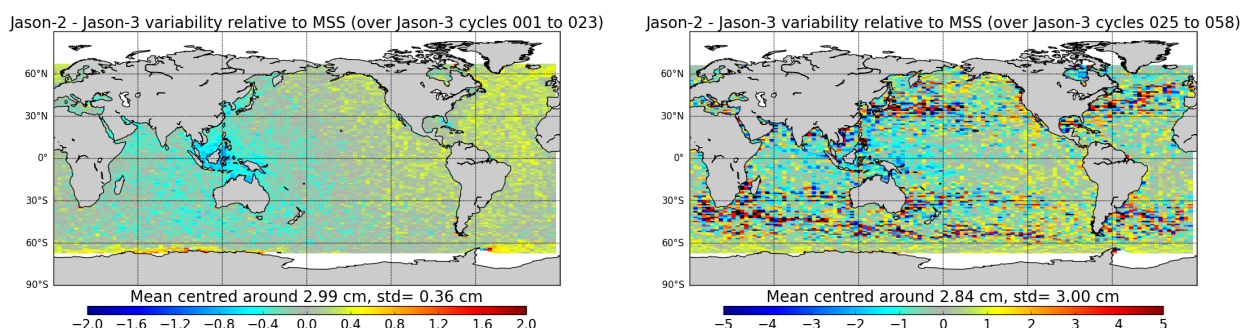


Figure 48 – GDR data. Caution: color map ranges are different between the two figures. **Left:** Map of SLA difference between Jason-2 and Jason-3 over tandem phase **Right:** Map of Jason-2 and Jason-3 SLA differences for Jason-3 cycles 025 to 058

6.3. Standard deviation of SLA differences between Jason-3 and Jason-2

The monitoring of SLA standard deviation has been computed for both missions (figure 49).

Note that this metric is very dependant to the MSS reference solution used to compute SLA. Standard deviation of SLA from L2P products (green and black curves) are lower than with IGDR or GDR thanks to L2P updates that include a change from product MSS referenced on 7 years to a solution referenced on 20 years. In addition, Jason-2 MSS solution in GDR product (red dotted line on right part of figure 49) moved from MSS CNES/CLS 2011 with a 7 years reference to MSS CNES/CLS 2015 (20 years reference) when move to LRO: that explains a better performance on Jason-2 GDR dataset from July 2017 onwards. The change of reference period from 7 years to 20 years integrates the evolution of the sea level in terms of trends, but also in terms of interannual signals at small and large scales (e.g. Niño/Niña) in the additional 13 years: changing from a 7 to 20 years reference period leads to better interannual signals and oceanic anomalies (see [98] for more details about the change on reference period).

Cartography of standard deviation of spatial Jason-3 minus Jason-2 SLA differences (not shown here) does not show any anomaly. It varies indeed in function of noise on measurements, which depends on significant wave height. Therefore, standard deviation of SLA differences is higher in regions with important significant wave heights.

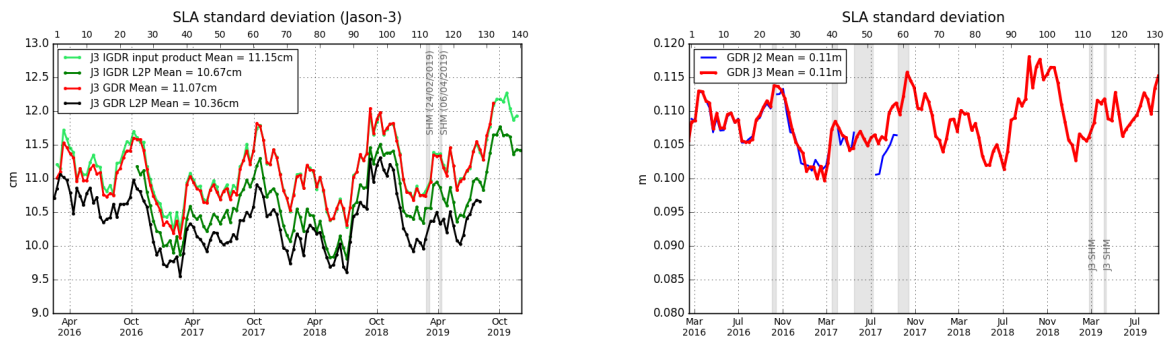
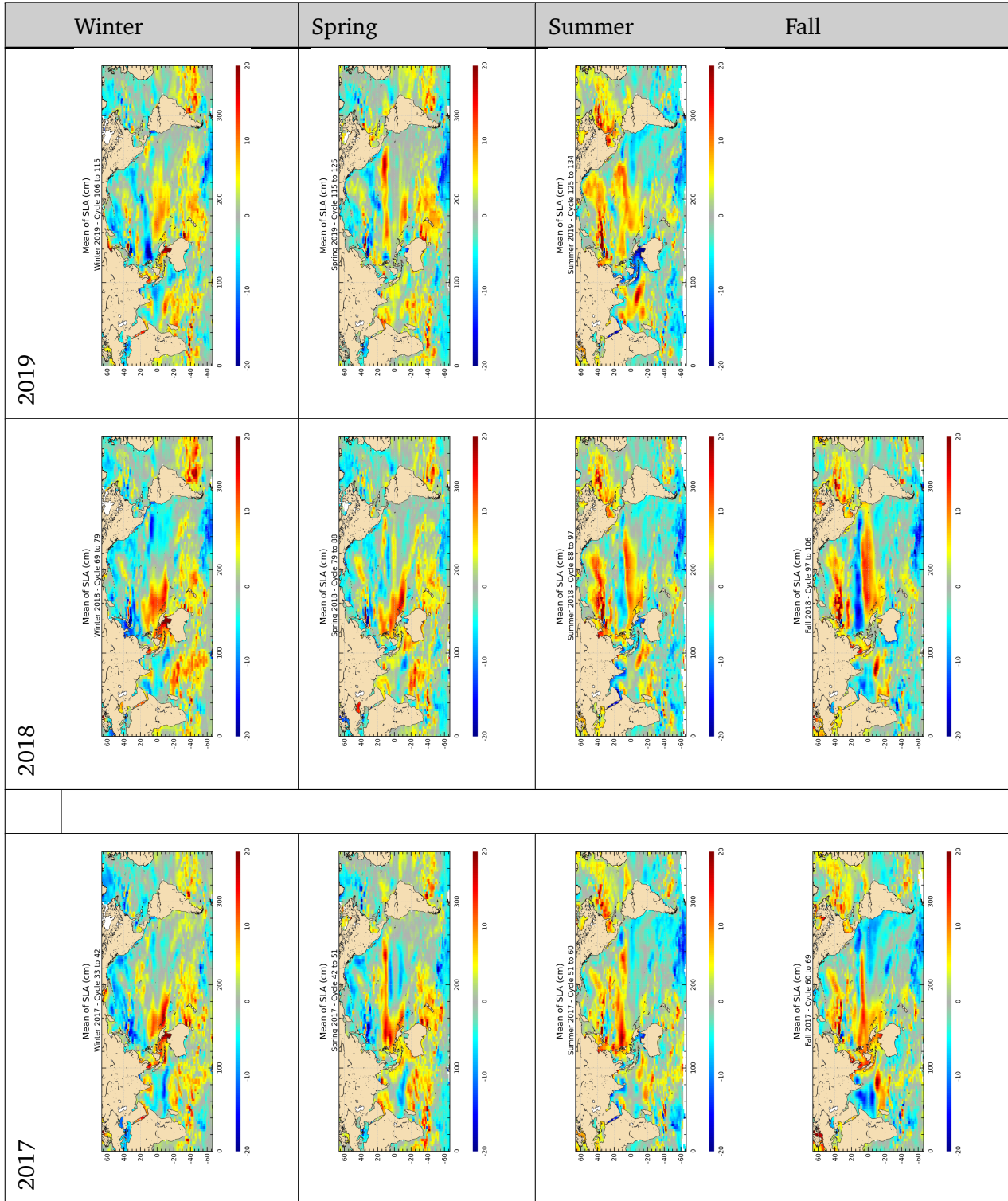


Figure 49 – Cyclic monitoring of along-track SLA standard deviation. Jason-3 OGDRs, IGDRs and GDRs (left). Jason-2 and Jason-3 GDRs (right)

6.4. Sea level seasonal variations

From Sea Level Anomalies computed relative to the Mean Sea Surface CNES-CLS 2011, the surface topography seasonal variations have been mapped in table 7 for the overall Jason-3 data set. Major oceanic signals are shown clearly by these maps: it allow us to assess the data quality for oceanographic applications.



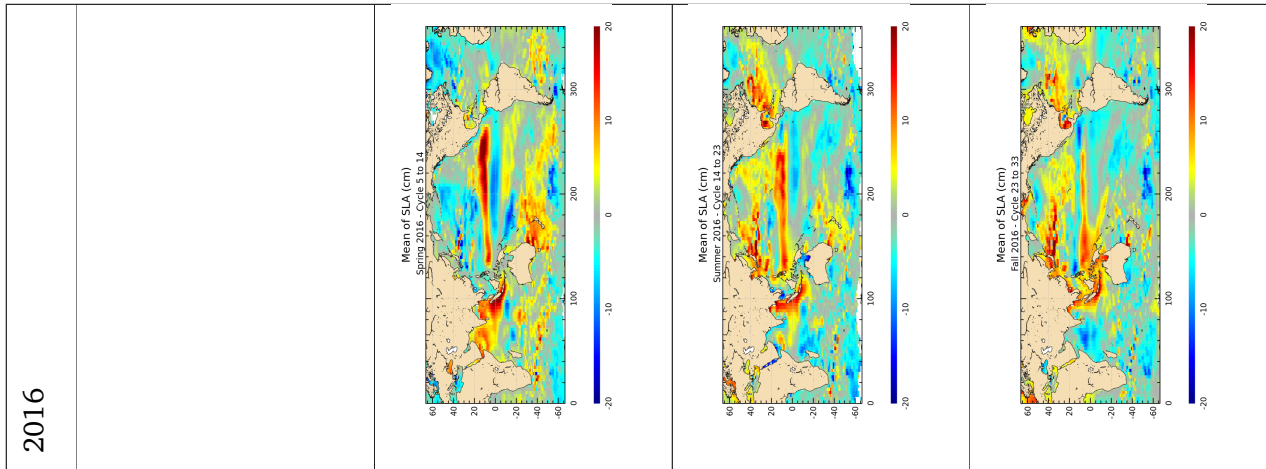
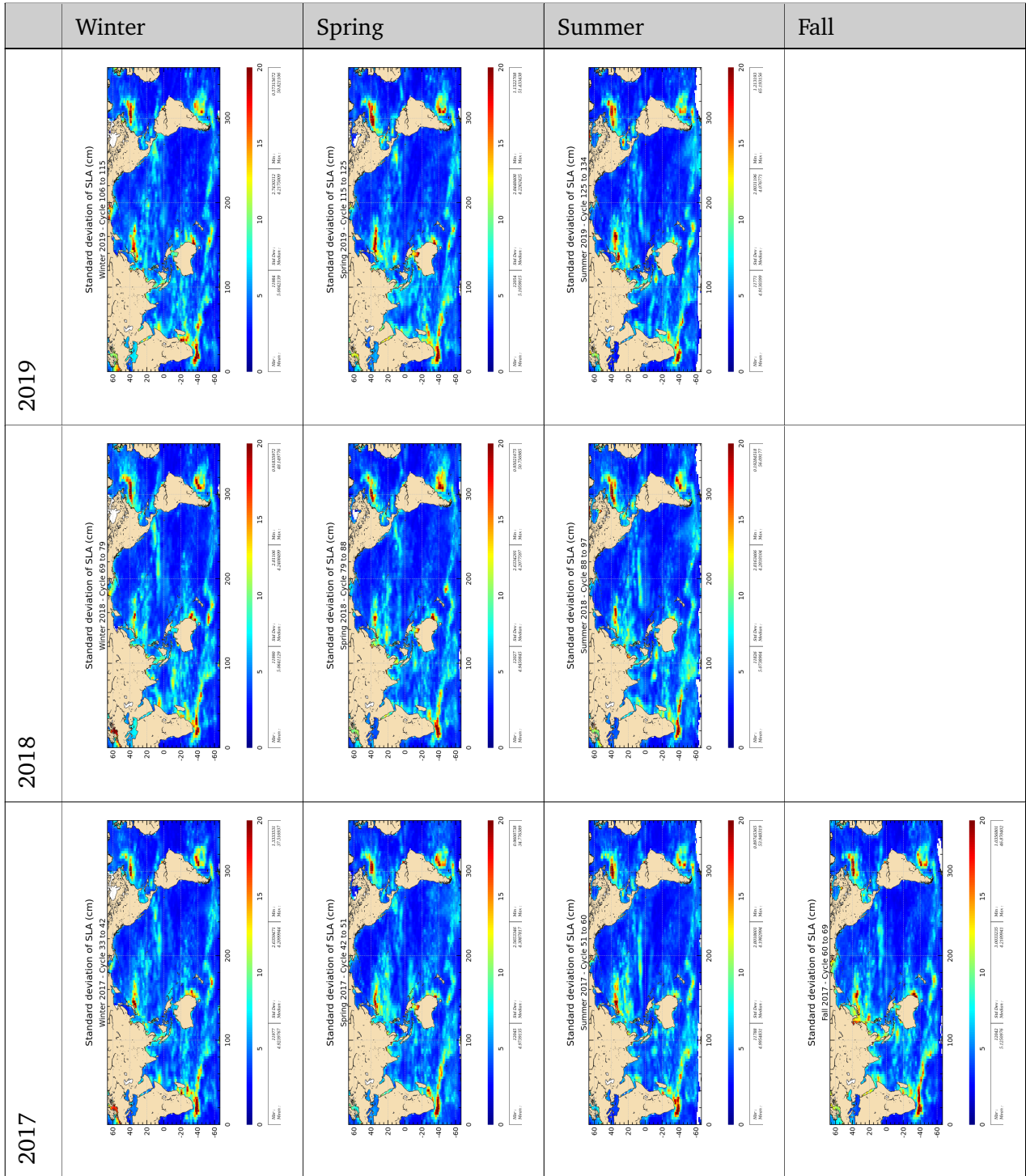


Table 6 – Seasonal variations of Jason SLA (cm) for years 2016 to 2018



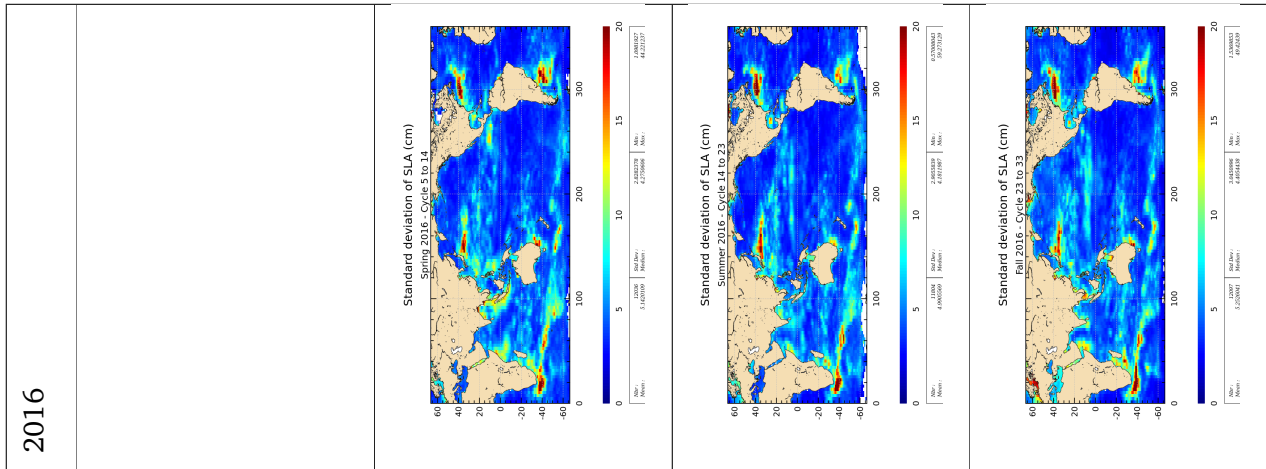


Table 7 – Seasonal variations of Jason SLA standard deviation (cm) for years 2016 to 2018

7. Mean Sea Level (MSL) calculation

For more details about Mean Sea Level studies method, see dedicated annual report of activities [116]. This report includes the description of the Mean Sea Level indicator, the comparisons between altimetry and tide gauges measurements, the comparisons between altimetry and *ARGO+GRACE* measurements and specific studies linked with MSL activities.

7.1. Mean sea level (MSL) calculation of reference time serie and regional MSL trends

Data from Jason-3 mission were introduced in DUACS system end of September 2016 (when Jason-2 moved to its new interleaved orbit). Over the tandem phase of Jason-3 (till cycle 023), both Jason-2 and Jason-3 satellites flew on the same ground track, only 1mn20s apart. They therefore measured the same features, allowing to calibrate Jason-3. This allowed to link precisely the MSL time series of Jason-2 and Jason-3. The uncertainty of the bias value between the two time series is less than 1 mm. The evolution of the ocean mean sea level can therefore be precisely observed on a continual basis since 1993 thanks to the 4 reference missions: TOPEX/Poseidon, Jason-1 (from may 2002 to october 2008), Jason-2 (from october 2008 to may 2016) and now Jason-3 (since june 2016).

Wet troposphere correction, inverse barometer correction, GIA (-0.3 mm/yr) are applied to calculate the MSL and the data series are linked together accurately thanks to the tandem flying phases. The following global bias are applied: -2.260 cm between T/P&Jason-1, 3.900 cm between Jason-1/Jason-2 and 2.880 cm between Jason-2/Jason-3. An exhaustive overview over possible errors impacting the MSL evolution is given in [116]. Furthermore, annual and semi-annual signals are removed from the time serie and a 2-month filter is applied. For more details, see MSL Aviso Website: <http://www.aviso.altimetry.fr/msl>.

Though mean sea level trend is globally positive, it is inhomogeneous distributed over the ocean: locally, sea level rise or decline up to ± 10 mm/yr are observed on right panel of figure 50 (note that this map of regional MSL trends is estimated from multi-mission grids (Ssalto/DUACS products) in order to improve spatial resolution).

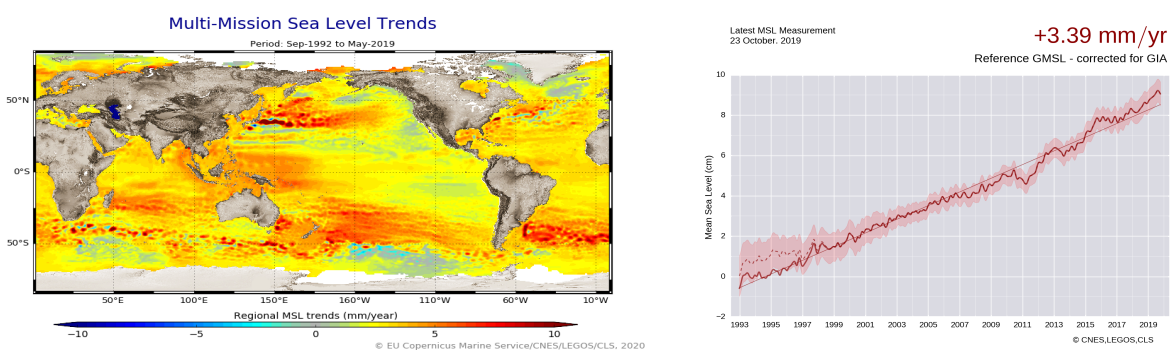


Figure 50 – Global (right) and regional (left) MSL trends from 1993 onwards.

7.2. External data comparisons with tide gauges

In order to assess the global MSL trend, comparisons to independent in-situ datasets are of great interest. Method and data used for MSL comparisons between altimetry and tide gauges measurements are detailed in [116] part 3.

Comparisons of MSL time series between altimetry and Tide Gauges are done from L2P products with CMEMS 2018 standards.

A positive slope of 1.76 mm/year is observed between Jason-3 GMSL timeserie and the GLOSS-CLIVAR tide gauges network. This is of the same order of magnitude as the 2018 results. However, the currently available timeseries spans over 3.5 years (2016.03-2019.09) which is now long enough to start having a fair uncertainty value of 1.96 mm/yr. As compare to the 2018 results, this is a reduction of 1 mm/yr, simply due to the longer time span. Nevertheless, the observed drift between Jason-3 and the Gloss-Clivar network is still not significant.

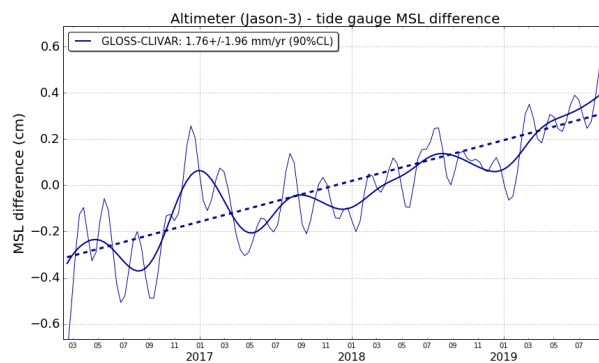


Figure 51 – Evolution of the GMSL differences between the altimeter mission Jason-3 and the GLOSS/CLIVAR tide gauges network. Annual and semi-annual signals have been removed beforehand from each individual timeseries, and a 2-months filter have been applied on the differences (thin blue line). The slope (blue dashed line) is obtained from a generalized least square method applied on the 2-months filtered timeseries. The thick blue line is the 6-months filtered timeseries.

8. Particular points and investigations

8.1. Focus on 2019 Safe Hold Modes [SHM]

During 2019, Jason-3 telemetry stopped by twice due to SHM events. In both cases, daily monitorings of data were done in order to check possible SHM impact on mission performance quality.

8.1.1. 2019 February SHM: cycles 112 and 113

Jason-3 entered Safe Hold Mode (SHM) on 24 February 2019 at 09:57:16 UTC due to an important mispointing (Gyro #1 attitude anomaly). **Due to SHM, there is no data from 24-02-2019 08:41:54 (cycle112) to 06-03-2019 08:44:21 (cycle113).**

Due to SHM, cycle 112 last only two days from 22-02-2019 to 24-02-2019 (last data at 08:41:53, 58 passes processed). Note that there is unusual number of IGDR missing data (over land and sea) from pass 050 onwards:

- 20.30% missing over pass 050,
- 11.03% missing over pass 051,
- 32.67% missing over pass 052,
- 29.41% missing over pass 053,
- 5.43% missing over pass 054,
- 98.59% missing over pass 055,
- 94.53% missing over pass 056,
- 100% missing over pass 057,
- 94.28% missing over pass 058,
- 100% missing from pass 059 onwards.

In addition, anomalies were noticed on available data just before SHM: in IGDR, more than 80% of data are rejected for passes 049 to 052 and all available data are rejected from pass 053 onwards due to altimeter parameters (ionospheric correction, mispointing, sigma0, swl, ...) out of thresholds (left side of figure 52). Pass 053 and 054 have respectively 67.8% and 52.0% of rejected measurements over ocean due to wet tropospheric correction set to 0. For these two parts of passes, brightness temperature for 18.7 GHz channel and brightness temperature for 34.0 GHz channel values are under 5K and brightness temperature for 23.8 GHz channel values are set to default value (right side of figure 52).

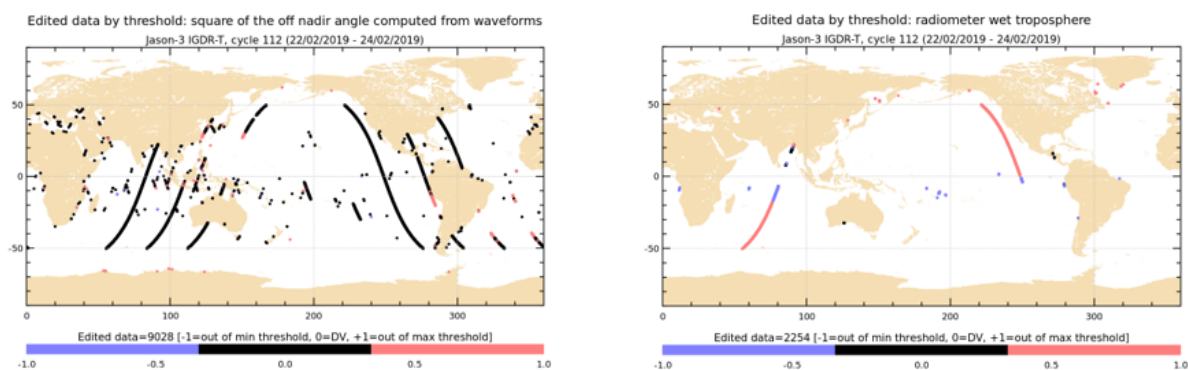


Figure 52 – Rejected measurement on IGDR data for Jason-3 cycle 112 before SHM event for altimeter criteria (*left*) and radiometer wet troposphere correction threshold criterion (*right*)

Note that during SHM recovery procedure, GPS and DORIS software were uploaded:

- On the 2019/02/27 and 2019/02/28 : Upload of the GPS software (version N) on PMB.
- On the 2019/02/29 : Upload of the DORIS patch.

Due to SHM, cycle 113 last from 06-03-2019 to 13-03-2019 (194 passes processed). IGDR analysis reports :

- 100% missing data over passes 001 to 060
- 85.01% missing data over pass 061 (93.14% over ocean)
- Due to GYRO calibration (pass094), 25.06% of rejected data over ocean on thresholds criteria (no altimeter data)
- Note that just after restart MOE orbit was computed using DORIS only (no GPS data used) until pass 077. DORIS + GPS data has been used to compute MOE orbit from 08/03/2019 onwards (IGDR data from cycle 113 pass 078).
- Post-SHM LTM filter has been used from pass 078 onwards. Passes 061 to 077 were produced with pre-SHM LTM filter so that mispointing and wind speed show jump just after restart (wind speed back to pre-SHM levels from pass 078 onwards).

The recovery from SHM on Jason-3 was done on Gyro #2 and Gyro #3. **Jason-3 data quality is not impacted by this SHM event.**

8.1.2. 2019 April SHM: cycle 116

Cycle 116 last from 02-04-2019 to 12-04-2019, but due to SHM, data are missing between 06/04/2019 21:53:38 (C116 P107) and 12/04/2019 07:20:31 (C116 P246), so that 116 passes only were processed for this cycle.

Just after restart, MOE orbit was computed using DORIS only (no GPS data used) until cycle 117 pass 008. DORIS + GPS data has been used to compute MOE orbit from cycle 117 pass 009 onwards.

We only have to note that mispointing is slightly higher than usual just after SHM, which is nominal in case of such an event. **Jason-3 data quality is not impacted by this SHM event.**

8.2. Poster on Jason-3 mission performance towards GDR-F at OSTST

In order to prepare Jason-CS/Sentinel-6 launch, reprocessing of Jason-3 GDR in standard F will begin in 2020. We aim at presenting the overall performance of Jason-3 through different metrics highlighting the high-level accuracy of this mission and we will also focus on the way the future reprocessing would impact Jason-3 dataset.

Jason-3 mission performance towards GDR-F

H. Roinard¹, L. Michaud³, M. Lievin¹,
F. Bignalet-Cazalet², N. Picot², G. Dibarboure²

1. CLS, Toulouse, France
2. CNES, Toulouse, France
Contact: equipe-calval-jason@cls.fr



TOPEX/Poseidon, Jason-1, Jason-2, and then Jason-3 have allowed to build a high-precision ocean altimetry data record on historical ground track and will be followed in few years by Jason-CS/Sentinel-6. A precise knowledge of Jason-3 data quality and errors is a key activity to ensure a reliable service to scientists involved in climate change studies as well as operational oceanography. As Jason-3 is the reference mission used in operational applications or for delayed time studies and especially for monitoring of the Global Mean Sea Level, the assessment of Jason-3 data quality is particularly important and we pay special attention to the long-term stability of Jason Global Mean Sea Level (GMSL). Long-term monitoring of the Jason altimetric system is routinely performed at CLS, as part of the CNES SALP (Système d'Altimétrie et Localisation Précise) project. The main objective of this activity is to provide an estimation of the mission performances for oceanic applications such as mesoscale or climate studies.

The monitoring of all altimeter and radiometer parameters is also routinely performed in order to detect jumps or drifts. After three years in orbit as a precise altimeter mission, two successive Jason-3 Safe Hold Modes occurred at the beginning of 2019. In this presentation we will give an overview of Jason-3 data coverage and data quality concerning altimeter and radiometer parameters, but also the performance of delayed and real time products (GDR, IGDR, OGDG/OSDR) at mono-mission crossovers and along-track. Finally, in order to prepare Jason-CS/Sentinel-6 launch, reprocessing of Jason-3 GDR in standard F will begin in few months. We aim at presenting the overall performance of Jason-3 through different metrics highlighting the high-level accuracy of this mission and we will also focus on the way the future reprocessing would impact Jason-3 dataset.

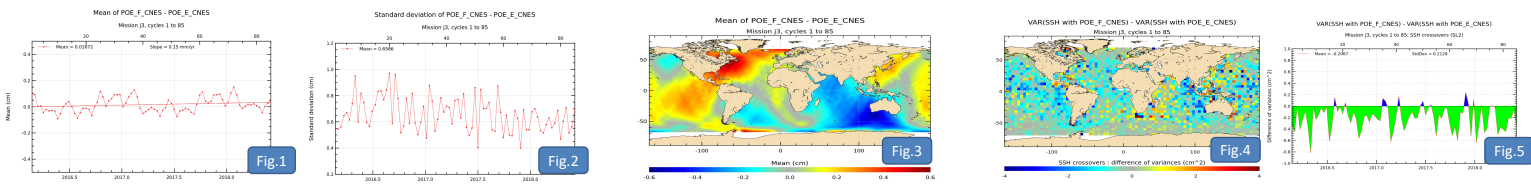
Data used	GDR-D	GDR-F
Orbit	<C01 -> <C94 - POE-E <C95 onwards - POE-F	POE-F
Range	MLE4	MLE4
MSS	2001 (ref. over 7 years)	CNES/CLS 2015
Wet Tropo	JMR	JMR
Dry Tropo	ECMWF OPE	ECMWF OPE
Pole Tide	WAHR85 MPL legacy	DESAI2015/ mpl2017
Solid Earth Tide	Cartwright and Edden [1973]	Cartwright and Edden [1973]
Ocean Tide	GOT4.8	FES14B (34 waves)
InternalTide	N/A	ZARON (M2,K1,S2,O1)
IB/DAC	ECMWF + LEGOS/CLS/CNES	ECMWF + LEGOS/CLS/CNES
SSB	NonParametric fitted on J2 data	NonParametric Tran2018 fitted on J3
Ionospheric correction	Dual Frequency	Filtered solution

POE-F orbit versus POE-E solution [Note that POE-F orbit has been included in GDR product since cycle 095]

Cyclic mean of the differences between the two orbit solutions is stable in time (variations \pm 1mm). POE-E and POE-F are differently computed out of yaw fix period. From mid-2017 onwards, yaw fix periods are longer, so that the impact on the orbit differences is lower (the standard deviation of the difference between the two solutions is slightly lower from mid-2017 onwards).

The map of the differences between the two orbit solutions, computed over 85 cycles shows no global bias (mean <math>< 0.01\text{cm}</math>). This is coherent with Fig.1. Geographically correlated patterns can reach $\pm 0.6\text{cm}$, but are not stable in time (not shown here)

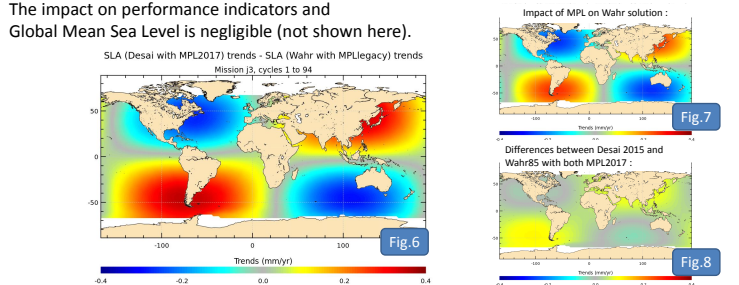
Variance of SSH differences at crossovers are compared using different solutions as a key performance indicator. In our cases, a global gain >math>0.2\text{cm}^2</math> using POE-Fin SSH computation compared to SSH POE-E indicates an improvement.



Pole tide

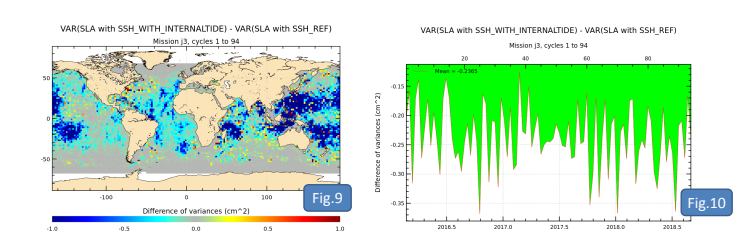
The pole tide altimeter correction is used to correct the response of the solid Earth and Oceans to the polar motion. The Wahr (1985) model has been used for all missions since TOPEX and another model is now available (Desai 2015). Legeais et al. [in 2015] showed the last model has a significant positive impact on the regional mean sea level trends and the comparison with independent in-situ data (Argo profiles) has demonstrated that the use of this model reduces the amplitude of the annual signal of the global mean sea level. A new recommendation for Mean Pole Location equation was done in 2017. This equation has been applied to both Wahr (1985) and Desai (2015) models. The model for the linear mean pole is recommended based on a linear fit to the IERS C01 time series spanning 1900 to 2015: in milliarsec, $X_p = 55.0 + 1.677 \cdot dt$ and $Y_p = 320.5 + 3.460 \cdot dt$ where $dt = (t - t_0)$, $t_0 = 2000.0$ and assuming a year = 365.25 days. The new mean pole location equation has a significant impact on the regional mean sea level trends thanks to the remove of the long term mean pole drift in pole tide computation.

The impact on performance indicators and Global Mean Sea Level is negligible (not shown here).



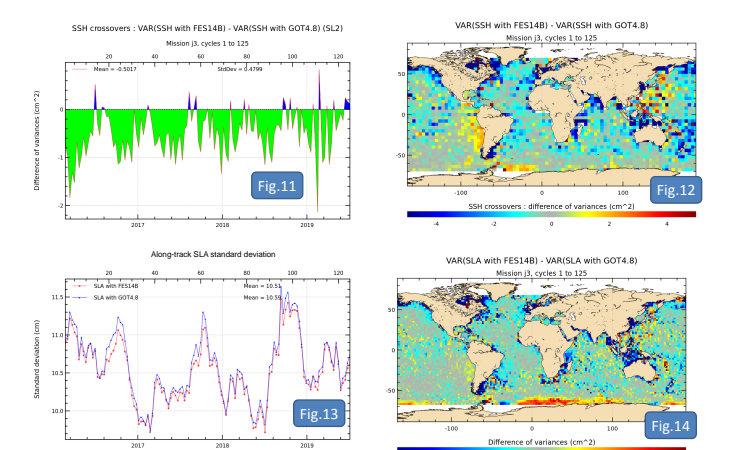
Internal tide

To take into account internal tide corrections improves SSHA performance indicators on along-track Sea Level Anomaly and error at crossover: altimeter performance indicators are computed with or without considering internal tide model as a correction of range. The results presented are computed with Zaron model for M2, K1, O1 and S2 waves. Over Jason-3 period, there is no significant impact on SSH difference at crossover points or on Global Mean Sea Level trend estimation taking into account internal tides or not (not shown here). Variance of SSH differences at crossovers are compared using different solutions as a key performance indicator. In our cases, a global gain close to 0.5cm^2 using internal tides compared to SSH without this correction indicates an improvement, with significant geographically correlated patterns where internal tides areas are defined. In the same way, a reduction is visible in case of global along-track SLA variance ($>0.2\text{cm}^2$), with geographical patterns.



Ocean tide

Using the latest global tide models (GOT4.10 or FES2014b) instead of GOT4.8 or FES2012 improves the coherence between ascending and descending passes. The global variance reduction of SSH crossover variance when using FES2014b instead of GOT4.8 has a value of about 0.5cm^2 (Fig.11). Results are improved in many places, in deep ocean, in shallow waters, and at latitudes $>50^\circ$. Nevertheless, variance at SSH crossovers is slightly lower with GOT4.8 on the western coast of South America. Standard deviation of SLA is slightly lower using FES2014b than with GOT4.8 (Fig.13): the differences are mainly located near coasts. Global Mean Sea Level is equivalent with both solutions (GOT4.10 and FES2014, not shown here). Regional differences between SLA using FES2014 or GOT4.10 is not significant.



CONCLUSIONS

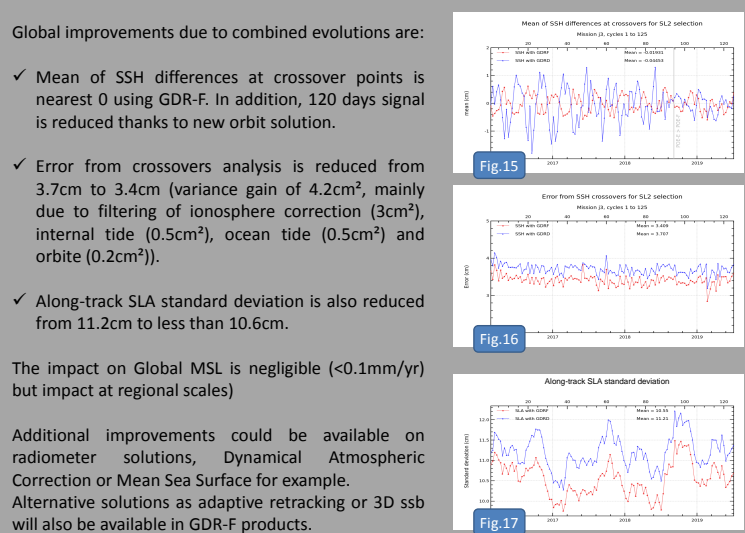
Total impact on SSH differences at crossover points and along-track SLA

Global improvements due to combined evolutions are:

- ✓ Mean of SSH differences at crossover points is nearest 0 using GDR-F. In addition, 120 days signal is reduced thanks to new orbit solution.
- ✓ Error from crossovers analysis is reduced from 3.7cm to 3.4cm (variance gain of 4.2cm^2 , mainly due to filtering of ionosphere correction (3cm^2), internal tide (0.5cm^2), ocean tide (0.5cm^2) and orbite (0.2cm^2)).
- ✓ Along-track SLA standard deviation is also reduced from 11.2cm to less than 10.6cm.

The impact on Global MSL is negligible ($<0.1\text{mm/yr}$) but impact at regional scales)

Additional improvements could be available on radiometer solutions, Dynamical Atmospheric Correction or Mean Sea Surface for example. Alternative solutions as adaptive retracking or 3D sbs will also be available in GDR-F products.



[see also Poster_OSTST19_CVL_005: « Improving Conventional Altimetry, Innovative LRM retracking »].

8.3. Poster on Improving Conventional Altimetry Innovative LRM retracking at OSTST

Since many years, altimetry constellation is delivering relevant measurements to monitor the ocean large scale surface topography. More recently, with our understanding of the oceanic structures, these needs have evolved toward a better characterization of the oceanic mesoscale and sub mesoscales dynamic, over open and coastal areas. To answer this problematic, many progresses were made in the instrumental design domain. Thanks to the new generation of Delay Doppler altimeters (first time onboard on Cryosat-2 mission), the instrumental noise and spectral bump error were significantly reduced. On the other hand, to continue exploiting the recent and past LRM datasets, a lot of work has been dedicated to improve the retracking methods.

This study focuses on the assessment of the adaptive retracker (Thibault et al., OSTST 2018). It aims at reviewing the Sea Surface Height retrieval performances. The assessment will be done with classical metrics at 1 Hz at global scales to assess the improvement compared to the existing MLE4 operational datasets. This will complement the assessment done by Smith et al (OSTST 2017) that focused on performances of several retrackers at small spatial scales.

Improving Conventional Altimetry SSH observability: global assessment of SSH datasets derived from innovative LRM retrackerers

M. Raynal¹, H. Roinard¹, S. Labroue¹, M. Lievin¹,
N. Tran¹, P. Thibaut¹, F. Piras¹, N. Picot², F. Boy²

Contact: equipe-calval-jason@cls.fr

1. CLS, Toulouse, France
2. CNES, Toulouse, France

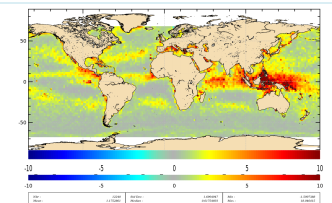
Since many years, altimetry constellation is delivering relevant measurements to monitor the ocean large scale surface topography. More recently, with our understanding of the oceanic structures, these needs have evolved toward a better characterization of the oceanic mesoscale and sub mesoscales dynamic, over open and coastal areas. To answer this problematic, many progresses were made in the instrumental design domain. Thanks to the new generation of Delay Doppler altimeters (first time onboard on Cryosat-2 mission), the instrumental noise and spectral bump error were significantly reduced. On the other hand, to continue exploiting the recent and past LRM datasets, a lot of work has been dedicated to improve the retracking methods.

This study focuses on the assessment of the **adaptive retracker** (Thibaut et al., OSTST 2018). It aims at reviewing the Sea Surface Height retrieval performances. The assessment will be done with classical metrics at 1 Hz at global scales to assess the improvement compared to the existing MLE4 operational datasets. This will complement the assessment done by Smith et al (OSTST 2017) that focused on performances of several retrackerers at small spatial scales.

Data validity and coverage

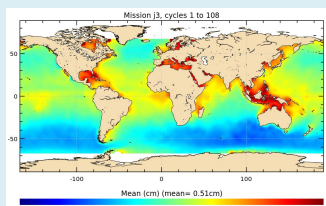
% valid SLA points (ADAPTIVE) – % valid SLA points (MLE4)

There are more valid points with adaptive retracking parameters (yellow and red areas) compared to MLE4, when following the Jason-3 handbook editing procedure. The gain is mainly located over areas affected by rain events and/or sigma bloom where the adaptive retracker is more robust than MLE4 algorithm.

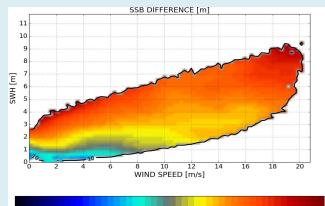


Data Sets Characteristics

The comparison is done at 1 Hz, using specific Adaptive or MLE4 data for retracked parameters and SSB correction. All other geophysical corrections are identical between both data sets. Since adaptive and MLE4 range have different dependency wrt SWH, a new SSB model was estimated for adaptive retracker. Figures show that the difference in range and thus in SSB is close to 0.3% SWH, adaptive SSB being lower compared to MLE4 solution.

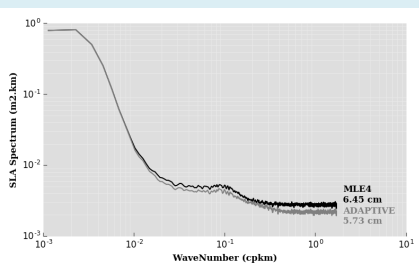


RANGE ADAPTIVE – RANGE MLE4



SSB ADAPTIVE – SSB MLE4

Impact on short spatial scales



As shown by Thibaut et al (OSTST 2018), the adaptive retracker improves the SSH short scale content by reducing the PSD energy below 60 km. The 20 Hz noise reduction is close to 10%. Note that the energy reduction is stronger for adaptive SWH (not shown).

Conclusions

The analysis shows that the adaptive retracker improves SSH data quality compared to MLE4 algorithm.

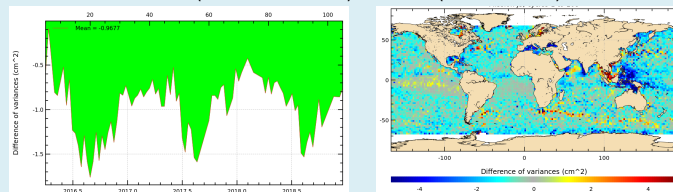
The improvement is present :

- at global scales with improved metrics at crossovers and along track SLA
- over coastal areas with more stable SLA approaching the coast in the last 6km
- at shortest spatial scales thanks to the 20 Hz range noise reduction

The adaptive retracker will be included in the GDR-F Jason-3 reprocessing.

Performances of along-track SLA

variance (SLA with ADAPTIVE) – variance (SLA with MLE4)



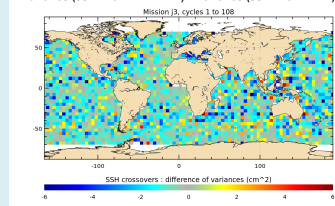
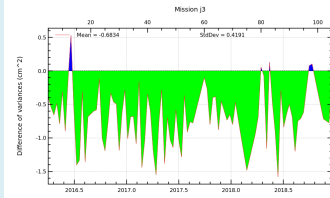
Regarding along track SLA variations, it is confirmed that the adaptive SLA improves data quality with a higher mean impact closer to 1 cm², reducing the mean SLA standard deviation to 1 cm.

The variance improvement shows annual signal while the mean map of the variance gain highlights more contrasted patterns compared to the crossovers. It shows an almost consistent improvement with variance reduction, except over some very specific regions: Malaysia, Baltic Sea, Oman Sea and East Equatorial Pacific. The main currents also exhibit variance increase that need to be further investigated to understand whereas geophysical signal is better retrieved over those high variability regions.

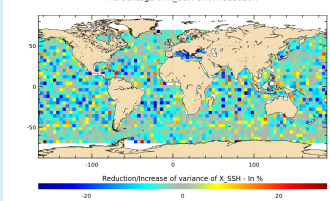
Performance SSH difference at crossovers

Crossover metrics show a global improvement of the adaptive derived SSH close to 0.7 cm² in average. The variance reduction is also quite homogeneous in space, with a constant magnitude over the whole globe. Such an improvement was not expected since this metric mainly checks the consistency between ascending and variance (SSH with ADAPTIVE) – variance (SSH with MLE4)

variance (SSH with ADAPTIVE) – variance (SSH with MLE4)



Percentage of X_SSH error reduction

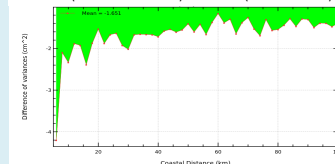


The improvement represents 5 to 10% of the signal variance over equatorial and mid latitude regions.

Performance over coastal areas

The analysis of variance gain at 1 Hz shows an increase in the improvement when approaching the coast. Adaptive retracker reduces the SLA variance in the strip 5 to 20 km.

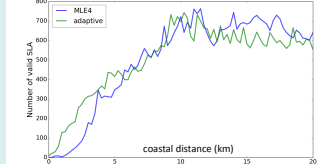
variance (SLA with ADAPTIVE) – variance (SLA with MLE4)



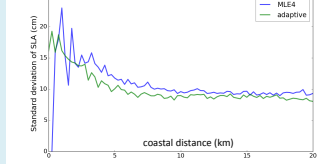
The same analysis is done at 20 Hz focusing on the Mediterranean basin to assess the coastal performances at high resolution. The adaptive retracker is compared to MLE4 with same outliers detection procedure and zoom on the last 20 km confirms excellent performances with:

- Increase of the percentage of valid data in the last 6 km
- Robust mean value of SLA approaching the coast
- Variance reduction of SLA

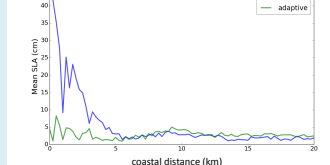
Number of valid SLA vs coastal distance



Standard deviation of valid SLA vs coastal distance



Mean of valid SLA vs coastal distance



9. References

References

- [1] Ablain, M., A. Cazenave, G. Valladeau, and S. Guinehut. 2009 : A new assessment of the error budget of global mean sea level rate estimated by satellite altimetry over 1993-2008. *Ocean Sci*, **5**, 193-201. Available at <http://www.ocean-sci.net/5/193/2009/os-5-193-2009.pdf>
- [2] Ablain, M., S. Philipps, 2006, TOPEX/Poseidon 2005 annual validation report, TOPEX/Poseidon validation activities, 13 years of T/P data (GDR-Ms).
- [3] Ablain, M., S. Philipps, M. Urvoy, N. Tran, and N. Picot (2012) Detection of Long-Term Instabilities on Altimeter Backscattering Coefficient Thanks to Wind Speed Data Comparisons from Altimeters and Models, *Marine Geodesy*, **35:S1**, 258-275. Available at <http://www.tandfonline.com/doi/pdf/10.1080/01490419.2012.718675>
- [4] Ablain, M., G. Larnicol, Y. Faugère, A. Cazenave, B. Meyssignac, N. Picot, J. Benveniste, 2012. Error Characterization of altimetry measurements at Climate Scales. Oral presentation at OSTST meeting, Venice, Italy, 27-28 September 2012. Available at: http://www.aviso.altimetry.fr/fileadmin/documents/OSTST/2012/oral/02_friday_28/04_errors_uncertainties_I/03_EU1_Ablain.pdf
- [5] AVISO and PODAAC User Handbook. IGDR and GDR Jason-1 Products. Edition 4.1, October 2008. SMM-MU-M5-OP-13184-CN (AVISO), JPL D-21352 (PODAAC). Available at http://www.aviso.oceanobs.com/fileadmin/documents/data/tools/hdbk_j1_gdr.pdf.
- [6] Beckley, B. D. , Zelensky, N. P. , Holmes, S. A. , Lemoine, F. G. , Ray, R. D. , Mitchum, G. T. , Desai, S. D. and Brown, S. T. (2010) Assessment of the Jason-2 Extension to the TOPEX/Poseidon, Jason-1 Sea-Surface Height Time Series for Global Mean Sea Level Monitoring, *Marine Geodesy*, **33:1**, 447 - 471. Available at http://pdfserve.informaworld.com/96442__925511460.pdf
- [7] Bertiger, Willy , Desai, Shailen D. , Dorsey, Angie , Haines, Bruce J. , Harvey, Nate , Kuang, Da. , Sibthorpe, Ant and Weiss, Jan P. (2010) Sub-Centimeter Precision Orbit Determination with GPS for Ocean Altimetry. *Marine Geodesy*, **33:1**, 363 - 378. Available at http://pdfserve.informaworld.com/858128__925510150.pdf
- [8] Bertiger, Willy , Desai, Shailen D. , Haines, Bruce J., R. DeCarvalho, and A. Dorsey (2010) Jason-2/OSTM Precision Orbit Determination with GPS *Oral presentation at OSTST meeting, Lisbon, Portugal*, Available at http://www.aviso.oceanobs.com/fileadmin/documents/OSTST/2010/oral/19_Tuesday/bertiger.pdf
- [9] E. Bronner and G. Dibarboure, May 24th, 2012: Technical Note about the Jason-1 Geodetic Mission. *SALP-NT-MA-EA-16267-CNv1.0*. Available at: http://www.aviso.oceanobs.com/fileadmin/documents/data/duacs/Technical_Note_J1_Geodetic_Mission.pdf
- [10] Valladeau, G., S. Philipps. Jason-1 validation and cross calibration activities (Annual report 2009).SALP-RP-MA-EA-21795-CLS, CLS.DOS/NT/10-005.
- [11] Valladeau, G., S. Philipps. Jason-1 validation and cross calibration activities (Annual report 2010).SALP-RP-MA-EA-21903-CLS, CLS.DOS/NT/10-332.

-
- [12] Roinard H., Philipps S., Ablain M., Valladeau G., and Legeais J.-F., Jason-1 validation and cross calibration activities (Annual report 2013). Reference: CLS.DOS/NT/13-226. Nomenclature: SALP-RP-MA-EA-22269-CLS. Available at http://www.avisooceanobs.com/fileadmin/documents/calval/validation_report/J1/annual_report_j1_2013.pdf.
 - [13] Roinard H., Philipps S.: Jason-1 GDR-E release. Global assessment over ocean. SALP-RP-MA-EA-22426-CLS. Available at http://www.avisooceanobs.com/fileadmin/documents/calval/validation_report/J1/Jason1_ReprocessingReport_GDR_E.pdf
 - [14] Philipps, S., M. Ablain, G. Valladeau, and J.-F. Legeais. Jason-2 validation and cross calibration activities (Annual report 2011). Reference: CLS.DOS/NT/12-005. Nomenclature: SALP-RP-MA-EA-22042-CLS. Available at http://www.avisooceanobs.com/fileadmin/documents/calval/validation_report/J2/annual_report_j2_2011.pdf.
 - [15] Philipps, S., M. Ablain, G. Valladeau, and J.-F. Legeais. Jason-2 validation and cross calibration activities (Annual report 2012). Reference: CLS.DOS/NT/12-223. Nomenclature: SALP-RP-MA-EA-22141-CLS. Available at http://www.avisooceanobs.com/fileadmin/documents/calval/validation_report/J2/annual_report_j2_2012.pdf.
 - [16] Roinard, H., Philipps S., Jason-2 reprocessing impact on ocean data (cycles 001 to 020). Comparison of Jason-2 Gdr-D with Gdr-T, as well as with Jason-1 Gdr-C. SALP-RP-MA-EA-22118-CLS. CLS.DOS/NT/12.138. Available at ftp://avisoftp.cnes.fr/AVIS0/pub/jason-2/documentation/gdr_d_calval_report/JA2_GDR_D_validation_report_cycles1to20_V1_1.pdf
 - [17] Roinard, H., S. Philipps. Jason-2 reprocessing impact on ocean data (cycles 001 to 145). Comparison of Jason-2 Gdr-D with Gdr-T, as well as with Jason-1 Gdr-C and Envisat Gdr v2.1. SALP-RP-MA-EA-22140-CLS. CLS.DOS/NT/12.222.
 - [18] Philipps, S., H. Roinard, M. Ablain, G. Valladeau, and J.-F. Legeais. Jason-2 validation and cross calibration activities (Annual report 2013). Reference: CLS.DOS/NT/13-227. Nomenclature: SALP-RP-MA-EA-22270-CLS. Available at http://www.avisooceanobs.com/fileadmin/documents/calval/validation_report/J2/annual_report_j2_2013.pdf.
 - [19] Philipps, S., H. Roinard, M. Ablain, G. Valladeau, and J.-F. Legeais. Jason-2 validation and cross calibration activities (Annual report 2014).
 - [20] Philipps, S., H. Roinard, M. Ablain, G. Valladeau, and J.-F. Legeais. Jason-2 validation and cross calibration activities (Annual report 2015).
 - [21] Lauret O. Jason-3 validation and cross calibration activities (Annual report 2016). SALP-RP-MA-EA-23060-CLS.
 - [22] Roinard H.. Jason-3 validation and cross calibration activities (Annual report 2017). SALP-RP-MA-EA-23187-CLS. https://www.avisooceanobs.com/fileadmin/documents/calval/validation_report/J3/SALP-RP-MA-EA-23187-CLS_Jason-3_AnnualReport2017_v1-2.pdf
 - [23] Roinard H.. Jason-3 validation and cross calibration activities (Annual report 2018). SALP-RP-MA-EA-23248-CLS.
 - [24] Ollivier A., M. Guibbaud. Envisat RA2/MWR ocean data validation and cross-calibration activities. Yearly report 2012. SALP-RP-MA-EA-22163-CLS, CLS.DOS/NT/12-292.
 - [25] A. Ollivier. M. Guibbaud. Envisat RA2/MWR ocean data validation and cross calibration activities (Yearly report 2013). Reference: CLS.DOS/NT/13-290. Nomenclature: SALP-RP-MA-EA-22293-CLS.

-
- [26] M. Guibbaud. A. Ollivier. Envisat RA2/MWR ocean data validation and cross calibration activities (Yearly report 2014). Reference: CLS.DOS/NT/14-253. Nomenclature: SALP-RP-MA-EA-22396-CLS.
 - [27] S. Philipps. Saral/AltiKa validation and cross calibration activities (Annual report 2013). Reference: CLS.DOS/NT/13-228. Nomenclature: SALP-RP-MA-EA-22271-CLS.
 - [28] P. Prandi. Saral/AltiKa validation and cross calibration activities (Annual report 2014). Reference: CLS.DOS/NT/14-234. Nomenclature: SALP-RP-MA-EA-22418-CLS.
 - [29] P. Prandi. Saral/AltiKa validation and cross calibration activities (Annual report 2015). Reference: CLS.DOS/NT/15-064. Nomenclature: SALP-RP-MA-EA-22957-CLS.
 - [30] P. Prandi. Saral/AltiKa validation and cross calibration activities (Annual report 2016). Nomenclature: SALP-RP-MA-EA-23073-CLS.
 - [31] G. Jettou. Saral/AltiKa validation and cross calibration activities (Annual report 2017). Nomenclature: SALP-RP-MA-EA-23188-CLS.
 - [32] A. Ollivier Yearly report 2017 as parts as SALP activities (Annual report 2017).
 - [33] Valladeau, G.. Validation of altimetric data by comparison with tide gauge measurements for TOPEX/Poseidon, Jason-1, Jason-2 and Envisat. SALP-NT-MA-EA-22157-CLS, CLS.DOS/NT/12-259.
 - [34] Legeais J.-F. and S. Dupuy. 2012 annual report: Validation of altimeter data by comparison with in-situ T/S Argo profiles for T/P, Jason-1, Jason-2 and Envisat missions. CLS-DOS/NT/12-261. SALP-RP-MA-EA-22176-CLS.
 - [35] Valladeau G. and Prandi P., 2013:Validation of altimeter data by comparison with tide gauge measurements for TOPEX/Poseidon, Jason-1, Jason-2 and Envisat (Annual report 2013). [CLS.DOS/NT/13-262].
 - [36] Legeais J.F. and Ablain M., 2013: Validation of altimetric data by comparison with in-situ T/S Argo profiles (Annual Report 2013) [SALP-RP-MA-EA-22281-CLS, CLS.DOS/NT/13-256]
 - [37] Prandi P., Valladeau G., 2014:Validation of altimeter data by comparison with tide gauge measurements for TOPEX/Poseidon, Jason-1, Jason-2 and Envisat (Annual report 2014). [SALP-RP-MA-EA-22419-CLS, CLS.DOS/NT/15-020].
 - [38] Prandi P., Legeais J.F. and Ablain M., 2014: Validation of altimetric data by comparison with in-situ T/S Argo profiles (Annual Report 2014) [SALP-RP-MA-EA-22406-CLS, CLS.DOS/NT/15-007]
 - [39] Prandi P., Valladeau G., 2015:Validation of altimeter data by comparison with tide gauge measurements for TOPEX/Poseidon, Jason-1, Jason-2 and Envisat (Annual report 2015). [SALP-RP-MA-EA-22956-CLS, CLS.DOS/NT/15-062].
 - [40] Prandi P., Legeais J.F. and Ablain M., 2015: Validation of altimetric data by comparison with in-situ T/S Argo profiles (Annual Report 2015) [SALP-RP-MA-EA-22966-CLS, CLS.DOS/NT/15-068]
 - [41] Prandi P., Debout V.: Validation of altimeter data by comparison with tide gauges measurements: yearly report 2016 for TOPEX/Poseidon, Jason-1, Jason-2, ERS-2, Envisat and SARAL/AltiKa. SALP-RP-MA-EA-23082-CLS.
 - [42] Zawadzski L., Taburet N.: Validation of altimeter data by comparison with in-situ T/S Argo profiles (Annual Report 2016). SALP-RP-MA-EA-22966-CLS.

-
- [43] Valladeau, G., J.F. Legeais, M. Ablain, S. Guinehut, and N. Picot, 2012: Comparing altimetry with tide gauges and Argo profiling floats for data quality assessment and Mean Sea Level studies. *Marine Geodesy* 2012, DOI: 10.1080/01490419.2012.718226.
- [44] Legeais J.-F., P. Prandi, M. Ablain and S. Guinehut: Analyses of altimetry errors using Argo and GRACE data. *Ocean Science Discussion*, doi:10.5194/os-2015-111, in review, 2016.
- [45] Bond, N. A., M. F. Cronin, H. Freeland, and N. Mantua (2015), Causes and impacts of the 2014 warm anomaly in the NE Pacific. *Geophys. Res. Lett.*, 42, 3414–3420. doi: 10.1002/2015GL063306.
- [46] Boening, C., J. K. Willis, F. W. Landerer, R. S. Nerem, and J. Fasullo (2012), The 2011 La Niña: So Strong, the Oceans Fell, *Geophys. Res. Lett.*, doi:10.1029/2012GL053055, in press.
- [47] John T. Fasullo , C. Boening, F. W. Landerer, R. S. Nerem (2013), Australia’s Unique Influence on Global Sea Level in 2010-2011, doi:10.1002/grl.50834, in press.
- [48] Boy, François and Jean-Damien Desjonquieres. 2010. Note technique datation de l’instant de reflexion des échos altimètres pour POSEIDON2 et POSEIDON3 *Reference: TP3-JPOS3-NT-1616-CNES*
- [49] Brown G.S., “The average impulse response of a rough surface and its application”, *IEEE Transactions on Antenna and Propagation*, Vol. AP 25, N1, pp. 67-74, Jan. 1977.
- [50] Brown S., S. Desai, and W. Lu “Initial on-orbit performance assessment of the advanced microwave radiometer and performance of JMR GDR-C”, *Oral presentation at OSTST meeting, Nice, France, 9-12 november 2008*. Available at http://www.avisooceanobs.com/fileadmin/documents/OSTST/2008/oral/brown_calval.pdf
- [51] Brown, S., S. Desai, W. Lu, and A. Sibthorpe. 2009. Performance Assessment of the Advanced Microwave Radiometer after 1 Year in Orbit. *Oral presentation at OSTST meeting, Seattle, USA*. Available at: <http://www.avisooceanobs.com/fileadmin/documents/OSTST/2009/oral/Brown.pdf>
- [52] S. Brown. 2010. A Novel Near-Land Radiometer Wet Path-Delay Retrieval Algorithm: Application to the Jason-2/OSTM Advanced Microwave radiometer. *IEEE TGRS vol. 48 n°4*. Available at ftp://podaac.jpl.nasa.gov/allData/ostm/preview/L2/AMR/docs/Brown_TGARS_2010.pdf
- [53] Cerri, L. , Berthias, J. P. , Bertiger, W. I. , Haines, B. J. , Lemoine, F. G. , Mercier, F. , Ries, J. C. , Willis, P. , Zelensky, N. P. and Ziebart, M. (2010) Precision Orbit Determination Standards for the Jason Series of Altimeter Missions, *Marine Geodesy*, **33:1**, 379 - 418. Available at http://pdfserve.informaworld.com/816985__925509111.pdf
- [54] Cerri, L., A. Couhert, S. Houry, F. Mercier. 2011. Improving the long-term stability of the GDR orbit solutions. *Oral presentation at OSTST meeting, San Diego, USA*. Available at http://www.avisooceanobs.com/fileadmin/documents/OSTST/2011/oral/02_Thursday/Splinter3POD/05_Cerri.pdf.
- [55] Chambers, D., P., J. Ries, T. Urban, and S. Hayes. 2002. Results of global intercomparison between TOPEX and Jason measurements and models. *Paper presented at the Jason-1 and TOPEX/Poseidon Science Working Team Meeting, Biarritz (France), 10-12 June*.
- [56] Collard, F. (2005). Algorithmes de vent et période moyenne des vagues JASON à base de réseaux de neurones. BO-021-CLS-0407-RF. Boost Technologies.
- [57] Commien, L., S. Philipps, M. Ablain and N. Picot. 2009. SSALTO CALVAL Performance assessment Jason-1 GDR “C”/GDR “b”. *Poster presented at OSTST meeting, Seattle, USA*. Available at: <http://www.avisooceanobs.com/fileadmin/documents/OSTST/2009/poster/commien.pdf>

-
- [58] Couhert, A., L. Cerri, F. Mercier, S. Houry. 2010. Status of Jason-1 and Jason-2 GDR orbits. *Talk presented at OSTST meeting, Lisbon, Portugal*. Available at: <http://www.aviso.oceanobs.com/fileadmin/documents/OSTST/2010/oral/couhert.pdf>
- [59] DeCarvalho, R., S. Brown, B. Haines and S. Desai. 2009. Global cross calibration and validation of the Jason-1 and Jason-2/OSTM data products. *Oral presentation at OSTST meeting, Seattle, USA*. Available at: <http://www.aviso.oceanobs.com/fileadmin/documents/OSTST/2009/oral/deCarvalho.pdf>
- [60] Desjonqueres, J.-D., G. Carayon, J.-L. Courriere, and N. Steunou “POSEIDON-2 In-Flight results”, *Oral presentation at OSTST meeting, Nice, France, 9-12 november 2008*. Available at <http://www.aviso.oceanobs.com/fileadmin/documents/OSTST/2008/oral/desjonqueres.pdf>
- [61] Desjonquères, J. D. , Carayon, G. , Steunou, N. and Lambin, J. (2010) Poseidon-3 Radar Altimeter: New Modes and In-Flight Performances, *Marine Geodesy*, **33:1**, 53 - 79. Available at http://pdfserve.informaworld.com/542982__925503482.pdf
- [62] Dettmering, Denise and Bosch, Wolfgang (2010) Global Calibration of Jason-2 by Multi-Mission Crossover Analysis, *Marine Geodesy*, **33:1**, 150 - 161. Available at http://pdfserve.informaworld.com/315039__925510361.pdf
- [63] - Dibarboure, G., F. Boy, J. D. Desjonqueres, S. Labroue, Y. Lasne, N. Picot, J. C. Poisson, and P. Thibaut, 2014: Investigating short-wavelength correlated errors on low-resolution mode altimetry. *J. Atmos. Oceanic Technol.*, **31**, 1337–1362, doi:10.1175/JTECH-D-13-00081.1
- [64] Dorandeu.,J., M. Ablain, Y. Faugère, F. Mertz, 2004 : Jason-1 global statistical evaluation and performance assessment. Calibration and cross-calibration results. *Marine Geodesy* **27**: 345-372.
- [65] - Dufau, C., M. Orsztynowicz,G. Dibarboure, R. Morrow, and P.-Y. Le Traon (2016), Mesoscale resolution capability of altimetry:Present and future, *J. Geophys. Res.Oceans*, **121**, doi:10.1002/2015JC010904.
- [66] Faugère, Y. et al. 2009. The SLOOP project: preparing the next generation of altimetry products for open ocean. *Poster presented at OSTST meeting, Seattle, USA*. Available at: <http://www.aviso.oceanobs.com/fileadmin/documents/OSTST/2009/poster/Faugere2.pdf>
- [67] Faugère, Y. et al. 2010. CROSS-CALIBRATION between ENVISAT and JASON-1/2. *Oral presentation at OSTST meeting, Lisbon, Portugal*. Available at: http://www.aviso.oceanobs.com/fileadmin/documents/OSTST/2010/oral/19_Tuesday/Tuesday_afternoon/faugere.pdf
- [68] Jason-2 Version “T” Geophysical Data Records : Public Release, August 2009. Available at : http://www.aviso.oceanobs.com/fileadmin/documents/data/products/Jason-2_GDR_T_disclaimer.pdf
- [69] Renaudie C., S. Philipps, 2014: Comparison of the latest GSFC SLR/DORIS std1204 orbits with current orbits for TP,J1 and J2. CLS Ramonville St Agne.
- [70] Gourrion, J., Vandemark, D., Bailey, S., Chapron, B., Gommenginger, G.P., Challenor, P.G. and Srokosz, M.A., 2002: A two-parameter wind speed algorithm for Ku-band altimeters, *Journal of Atmospheric and Oceanic Technology*. **19(12)** 2030-2048.
- [71] http://grgs.obs-mip.fr/grace/variable-models-grace-lageos/mean_fields

-
- [72] Dumont, J.-P., V. Rosmorduc, N. Picot, S. Desai, H. Bonekamp, J. Figa, J. Lillibridge, R. Sharroo, 2011: OSTM/Jason-2 Products Handbook. CNES: SALP-MU-M-OP-15815-CN. EUMETSAT: EUM/OPS-JAS/MAN/08/0041. JPL: OSTM-29-1237. NOAA/NESDIS: Polar Series/OSTM J400. Available at http://www.aviso.oceanobs.com/fileadmin/documents/data/tools/hdbk_j2.pdf
- [73] Hernandez, F. and P. Schaeffer, 2000: Altimetric Mean Sea Surfaces and Gravity Anomaly maps inter-comparisons. AVI-NT-011-5242-CLS, 48 pp. CLS Ramonville St Agne.
- [74] Huffman, G. and D.T.Bolvin, 2009: TRMM and Other Data Precipitation Data Set Documentation. Available at ftp://precip.gsfc.nasa.gov/pub/trmmdocs/3B42_3B43_doc.pdf
- [75] Imel, D.A. 1994. Evaluation of the TOPEX/POSEIDON dual-frequency ionospheric correction. *J. Geophys. Res.*, **99**, 24,895-24,906.
- [76] Jalabert,E., A.Couhert, J. Moyard, F. Mercier, S. Houry, S. Rios-Bergantinos. 2015. JASON-2, SARAL AND CRYOSAT-2 STATUS. *Talk presented at OSTST meeting, Reston, USA, 20-23 October 2015.*http://meetings.aviso.altimetry.fr/fileadmin/user_upload/tx_ausyclsseminar/files/OSTST2015/POD-01-Jalabert.pdf
- [77] Lemoine, F.G., Zelensky N.P., Chinn, D.S., et al. (2010), Towards development of a consistent orbit series for TOPEX, Jason-1, and Jason-2 *Adv. Space Res.*, 46(12), 1513–1540, doi: 10.1016/j.asr.2010.05.007 (updated).
- [78] Lemoine, F., N.P. Zelensky, S. Melachroinos, D.S. Chinn, B.D. Beckley, D.D. Rowlands, and S.B. Luthcke. 2011. GSFC OSTM (Jason-2), Jason-1 & TOPEX POD Update. *Oral presentation at OSTST meeting, San Diego, USA.* Available at http://www.aviso.oceanobs.com/fileadmin/documents/OSTST/2011/oral/02_Thursday/SplinterPOD/03Lemoine_et_al_SWT2011_v01.pdf.
- [79] Lemoine F., N.P. Zelensky, D.S. Chinn, B.D. Beckley, D.E. Pavlis, J. Wimert, O. Bordyugov. 2014 : New GSC POD Standards for TOPEX/Poseidon, Jason-1, Jason-2 (OSTM). *Oral presentation at OSTST meeting, Konstanz, Germany.* Available at <http://www.aviso.altimetry.fr/fr/coin-utilisateur/equipes-scientifiques/sci-teams.html>.
- [80] Le Traon, P.-Y., J. Stum, J. Dorandeu, P. Gaspar, and P. Vincent, 1994: Global statistical analysis of TOPEX and POSEIDON data. *J. Geophys. Res.*, **99**, 24619-24631.
- [81] MSEs (CNES, NASA, NOAA, EUMETSAT). 2011. GDR Status. *Oral presentation (by N. Picot) at OSTST meeting, San Diego, USA.* Available at http://www.aviso.oceanobs.com/fileadmin/documents/OSTST/2011/oral/03_Friday/Plenary/GDRProducts/02PicotGDR_status_2011.pdf.
- [82] Aviso one-satellite-based Mean Sea Level reprocessing, http://www.aviso.altimetry.fr/fileadmin/documents/data/products/indic/msl/MSL_reprocessing_201402.pdf.
- [83] Moyard J., E. Jalabert, A. Couhert, S. Rios-Bergantinos, F. Mercier, S.Houry. 2014 : Jason-2 POD status. *Oral presentation at OSTST meeting, Konstanz, Germany.* Available at <http://www.aviso.altimetry.fr/fr/coin-utilisateur/equipes-scientifiques/sci-teams.html>.
- [84] Obligis, E., L. Eymard, M. Ablain, B. Picard, J.F. Legeais, Y. Faugere and N. Picot, 2010. The wet tropospheric correction for altimetry missions: A mean sea level issue.*Oral presentation at OSTST meeting, Lisbon, Portugal.* Available at http://www.aviso.oceanobs.com/fileadmin/documents/OSTST/2010/oral/19_Tuesday/OBLIGIS.pdf.

-
- [85] Ollivier A., Faugere Y., Granier N., 2008: Envisat RA-2/MWR ocean data validation and cross-calibration activities. Yearly report. Technical Note CLS.DOS/NT/09.10, Contract N° SALP-RP-MA-EA-21633-CLS http://www.avisooceanobs.com/fileadmin/documents/calval/validation_report/EN/annual_report_en_2008.pdf
- [86] Ollivier A., Faugere Y., P. Thibaut, G. Dibarboure, and J.-C. Poisson, 2008: Investigation on the high frequency content of Jason-1 and Jason-2. CLS.DOS/NT/09-027
- [87] Ollivier A., M. Guibbaud, Faugere Y. Envisat RA2/MWR ocean data validation and cross-calibration activities. Yearly report 2011. SALP-RP-MA-EA-22062-CLS, CLS.DOS/NT/12-021.
- [88] Ollivier A., A. Couhert, V. Pignot, C. Renaudie, S. Phillips, N. Picot, 2014 : Assessment of orbit quality through the SSH calculation towards GDR-E standards. *Oral presentation at OSTST meeting, Constance, Germany*. Available at <http://www.avis.altimetry.fr/fr/coin-utilisateur/equipes-scientifiques/sci-teams.html>
- [89] Ollivier A., S. Philipps, M. Ablain, A. Edwell, L. Cerri, N. Picot, 2013 : Assessment of Orbit Quality through the Sea Surface Height calculation, New insight in resolving long term and inter-annual signal for climate studies. *Oral presentation at OSTST meeting, Boulder, USA*. Available at <http://www.avis.altimetry.fr/fr/coin-utilisateur/equipes-scientifiques/sci-teams.html>
- [90] Ollivier A., Dibarboure G., Picard B., Ablain M., OSTST2014, Konstanz - Germany, "Spectral analysis of altimetric signal and errors Towards a spectral error budget of Nadir Altimetric missions" http://meetings.avis.altimetry.fr/fileadmin/user_upload/tx_ausyclsseminar/files/30Ball0900-2_Pres_OSTST2014_J2_ErrorBugdet_Spectra_Ollivier.pdf
- [91] Otten M., C. Flohrer, T. Springer, and W. Enderle. 2011. Generating precise and homogeneous orbits for Jason-1 and Jason-2. *Oral presentation at OSTST meeting, San Diego, USA*. Available at http://www.avisooceanobs.com/fileadmin/documents/OSTST/2011/oral/03_Friday/Splinter6POD/01_Otten.pdf.
- [92] Peltier, 2004, Global Glacial Isostasy And The Surface of The Ice-Age Earth: The ICE-5G (VM2) Model and GRACE. *Annual Review of Earth and Planetary Sciences*, May 2004, **Vol. 32, Pages 111-149**, doi: 10.1146/annurev.earth.32.082503.144359
- [93] Philipps, S., M. Ablain, J. Dorandeu, P. Thibaut, N. Picot and J. Lambin. 2006. SSALTO CALVAL Performance assessment Jason-1 GDR 'B'/GDR 'A'. *Poster presented at OSTST meeting, Hobart, Australia*. Available at: <http://www.avisooceanobs.com/fileadmin/documents/OSTST/2006/ablain1.pdf>
- [94] Picot, N., P. Thibaut, N. Tran, S. Philipps, J.C. Poisson, T. Moreau, and E. Bronner. 2010. New Jason-2 GDR-C standards. *Oral presentation at OSTST meeting, Lisbon, Portugal*. Available at http://www.avisooceanobs.com/fileadmin/documents/OSTST/2010/oral/PThibaut_Jason2.pdf.
- [95] Picot, N., P. Thibaut, N. Tran, S. Philipps, J.C. Poisson, E. Bronner, C. Garcia and many others. 2011. Jason-2 GDR-D standards. *Oral presentation at OSTST meeting, San Diego, USA*. Available at http://www.avisooceanobs.com/fileadmin/documents/OSTST/2011/oral/02_Thursday/Splinter5IP/05NPicot_et_al_OSTST_2011_J2-GDRD-Standards.pdf.
- [96] Schaeffer, P., A. Ollivier, Y. Faugere, E. Bronner, and N. Picot. The new CNES CLS 2010 Mean Sea Surface. *Oral presentation at OSTST meeting, Lisbon, Portugal, 18-20 october 2010*. Available at http://www.avisooceanobs.com/fileadmin/documents/OSTST/2010/oral/19_Tuesday/Schaeffer.pdf.

- [97] Schaeffer, P., Y. Faugere, J.-F. Legeais, A. Ollivier, T. Guinle, and N. Picot (2012). The CNES_CLS11 Global Mean Sea Surface Computed from 16 Years of Satellite Altimeter Data. *Marine Geodesy* **35: sup1, 3-19**. Available at <http://www.tandfonline.com/doi/abs/10.1080/01490419.2012.718231>
- [98] DUACS/Aviso team 'A new version of SSALTO/Duacs products available in April 2014' <http://www.aviso.altimetry.fr/fileadmin/documents/data/duacs/Duacs2014.pdf>
- [99] Scharroo, R., J. Lillibridge, and W.H.F. Smith, 2004: Cross-calibration and long-term monitoring of the Microwave Radiometers of ERS, TOPEX, GFO, Jason-1 and Envisat. *Marine Geodesy*, 97.
- [100] Solar Radio Flux (10.7cm) (daily solar data). Available at http://www.swpc.noaa.gov/ftpmenu/indices/old_indices.html
- [101] Thibaut, P. O.Z. Zanifé, J.P. Dumont, J. Dorandeu, N. Picot, and P. Vincent, 2002. Data editing: The MQE criterion. *Paper presented at the Jason-1 and TOPEX/Poseidon Science Working Team Meeting, New-Orleans (USA), 21-23 October*.
- [102] Thibaut, P., J.-C. Poisson, A. Ollivier, S. Philipps, and M. Ablain: "Jason-2 waveforms, tracking and retracking analysis", *Oral presentation at OSTST meeting, Nice, France, 9-12 november 2008*. Available at <http://www.aviso.oceanobs.com/fileadmin/documents/OSTST/2008/oral/thibaut.pdf>
- [103] Moreau, T., P. Thibaut, 2009. Etude dépointage Poseidon-3: optimisation de l'angle d'ouverture d'antenne. CLS-DOS-NT-09-028. 15 pp, CLS Ramonville St. Agne.
- [104] P. Thibaut. Bilan des activités d'expertise altimétriques menées en 2009 : Lot 2D. SALP-RP-MA-EA-21808-CLS, CLS-DOS-NT-10-029.
- [105] Tran, N. , Labroue, S. , Philipps, S. , Bronner, E. and Picot, N. (2010) Overview and Update of the Sea State Bias Corrections for the Jason-2, Jason-1 and TOPEX Missions, *Marine Geodesy*, **33:1, 348 - 362**. Available at http://pdfserve.informaworld.com/804727__925502357.pdf
- [106] Tran, N., P. Thibaut, J.-C. Poisson, S. Philipps, E. Bronner, and N. Picot. Jason-1, Jason-2 and TOPEX Sea State Bias. Overview and Updates. *Oral presentation at OSTST meeting, Lisbon, Portugal, 18-20 october 2010*. Available at <http://www.aviso.oceanobs.com/fileadmin/documents/OSTST/2010/oral/TRAN.pdf>
- [107] N. Tran, S. Philipps, J.-C. Poisson, S. Urien, E. Bronner, and N. Picot. Impact of GDR_D standards on SSB corrections. *Oral presentation at OSTST meeting, Venice, Italy, 27-28 September 2012*. Available at http://www.aviso.oceanobs.com/fileadmin/documents/OSTST/2012/oral/02_friday_28/01_instr_processing_I/01_IP1_Tran.pdf.
- [108] Zlotnicky, V. 1994. Correlated environmental corrections in TOPEX/POSEIDON, with a note on ionospheric accuracy. *J. Geophys. Res.*, **99, 24,907-24,914**
- [109] Edward D. Zaron , Robert deCarvalho, 2016. Identification and Reduction of Retracker-Related Noise in Altimeter-Derived Sea Surface Height Measurements. *Journal of Atmospheric and Oceanic Technology*, p201-210, doi:10.1175/JTECH-D-15-0164.1
- [110] Zawaszki, L., M. Ablain, A. Cazenave, B. Meyssignac. 2014. Confidence envelop of the Global MSL time-series deduced from Jason-1 and Jason-2 altimetric missions. *Poster presentation at OSTST meeting, Constance, Germany, 28-31 October 2014*, Available at http://meetings.aviso.altimetry.fr/fileadmin/user_upload/tx_ausyclsseminar/files/Poster_OSTST14_GMSLUncertainty.pdf
- [111] World Meteorological Organization, 2010: El Nino/ La Nina Update (30 March 2010). Available at http://www.wmo.ch/pages/prog/wcp/wcasp/documents/El_Nino_Mar10_Eng.pdf.

-
- [112] World Meteorological Organization, 2011: El Nino/ La Nina Update (25 January 2011). Available at http://www.wmo.ch/pages/prog/wcp/wcasp/documents/El-Nino_Jan11_Eng.pdf.
- [113] World Meteorological Organization, 2015: El Nino/ La Nina Update (16 November 2015). Available at http://www.wmo.int/pages/prog/wcp/wcasp/documents/WMO_ENSO_Nov15_Eng.pdf
- [114] Correction Troposphérique Humide pour le radiomètre Jason-3 : approche neuronale. CLS-J3PROTO-15-0002. Projet CNES PEACHI-J3
- [115] H. Roinard, E. Cadier. Jason-2 validation and cross calibration activities (Annual report 2017). Reference: SALP-RP-MA-EA-23186-CLS. Available at https://www.aviso.altimetry.fr/fileadmin/documents/calval/validation_report/J2/SALP-RP-MA-EA-23186-CLS_Jason-2_AnnualReport2017_v1-2.pdf.
- [116] M. Ablain. N. Taburet. L. Zawadzki. R. Jugier. M. Vayre. SALP annual report (2017) of Mean Sea Level Activities. Reference: SALP-RP-MA-EA-23189-CLS. Available at https://www.aviso.altimetry.fr/fileadmin/documents/calval/validation_report/SALP-RP-MA-EA-23189-CLS_AnnualReport_2017_MSL.pdf.
- [117] Uncertainty in Satellite estimate of Global Mean Sea Level changes, trend and acceleration. Michaël Ablain, Benoit Meyssignac, Lionel Zawadzki, Rémi Jugier, Aurélien Ribes, Anny Cazenave, and Nicolas Picot <https://doi.org/10.5194/essd-2019-10>
- [118] Lionel Zawadzki , Michaël Ablain, Loren Carrere, Richard D. Ray, Nikita P. Zelensky, Florent Lyard, Amandine Guillot, and Nicolas Picot. Investigating the 59-Day Error Signal in the Mean Sea Level Derived From TOPEX/Poseidon, Jason-1, and Jason-2 Data With FES and GOT Ocean Tide Models
- [119] Ngan Tran (CLS, France); Doug Vandemark (UNH, USA); Hui Feng (UNH, USA); Fabrice Ardhuin (LOPS,France); Lotfi Aouf (Meteo-France, France); Sophie LeGac (CNES, France); Nicolas Picot (CNES, France) Updated Jason-3 wind speed and SSB solutions (2D and 3D). Abstract: https://cpaess.ucar.edu/sites/default/files/images/abstracts_book-OSTST-2017-2.pdf, Poster number: IPC.001. https://meetings.aviso.altimetry.fr/fileadmin/user_upload/tx_ausyclsseminar/files/Poster_OSTST17_SSB_tran.pdf
- [120] Ngan Tran (CLS, France), Gerald Dibarbouré (CNES, France), Nicolas Picot (CNES, France). Improving the continuity of the Jason SSB time-series. https://meetings.aviso.altimetry.fr/fileadmin/user_upload/tx_ausyclsseminar/files/Poster_OSTST18_SSB_tran.pdf
- [121] https://meetings.aviso.altimetry.fr/fileadmin/user_upload/tx_ausyclsseminar/files/2017-10-25_Le_Gac_Jason-3_DEM_validation_OSTST2017_FINALE_OSTST.pdf
- [122] https://meetings.aviso.altimetry.fr/fileadmin/user_upload/tx_ausyclsseminar/files/Pres_OSTST2017_Jason3_HRoinard.pdf
- [123] <https://www.aviso.altimetry.fr/en/data/product-information/updates-and-reprocessing/ssaltoduacs-product-changes-and-updates.html>
- [124] https://meetings.aviso.altimetry.fr/fileadmin/user_upload/CLOS_10_Ray.pdf
- [125] Wahr JM (1985) Deformation induced by polar motion. J Geophys Res 90(B11):9363–9368. doi:10.1029/JB090iB11p09363
- [126] Revisiting the pole tide for and from satellite altimetry. Desai S., Wahr J., Beckley B., J Geod (2015) 89: 1233. <https://doi.org/10.1007/s00190-015-0848-7>

- [127] Climate Change Initiative conclusions and recommendations about Pole Tide (2015) 1-http://www.esa-sealevel-cci.org/webfm_send/389 2-http://www.esa-sealevel-cci.org/webfm_send/400
3-http://www.esa-sealevel-cci.org/webfm_send/549 4-http://www.esa-sealevel-cci.org/webfm_send/539